2015

Developing novel drug delivery systems for the treatment of epilepsy

Sara Ahmadi
University of Wollongong

UNIVERSITY OF WOLLONGONG

Intelligent Polymer Research Institute, ARC Centre of Excellence for Electromaterials Science

Developing novel drug delivery systems for the treatment of epilepsy

Sara Ahmadi

A thesis submitted in fulfilment of the requirement for the award of the degree

Doctor of Philosophy

August 2015

CERTIFICATION

I, Sara Ahmadi, declare that this thesis, submitted in partial fulfilment of the requirement for the award of Doctor of Philosophy, in the AIIM department, University of Wollongong, is wholly my own work unless otherwise referenced or acknowledged. This document has not been submitted for qualifications at any other academic institution.

Sara Ahmadi

Date: 10th September 2015

ABSTRACT

Epilepsy is characterized by abnormal electrical activity within the brain, which can result in either generalized or partial seizures. In order to control seizure activity a person must take anti-epilepsy medication, normally in the form of a tablet. The goal is to deliver the drug to the brain in quantities sufficient to eliminate seizures without causing adverse effects. In 30% of the cases, sufferers of epilepsy are unable to be medicated due to the dose required to suppress seizures causing adverse side effects. In addition, other anti-epilepsy treatment such as brain surgery or vagus nerve stimulator (VNS) implantation are very expensive treatments and needs high technology and advanced equipment. Therefore there is a need to develop a delivery system for these epilepsy sufferers that is therapeutic but not toxic and also accessible and affordable for every patient all over the world.

Recently there has been much interest in the use of polymeric carriers as localized delivery devices especially for the central nervous system. Bypassing the blood-brain barrier, a polymeric carrier implanted directly into the brain tissue allows the possibility of therapeutic levels of drug being confined to the region of interest, thus eliminating systemic toxicity compared to oral drug administration. Among polymers conducting polymers (CPs) have been shown to act as very effective drug reservoir with the ability to deliver drugs upon electrical stimulation. Polymeric carriers also offer potential advantages, such as partially protecting labile drugs from degradation and releasing multi-drug combinations in a controlled manner from the same implant.

However, one limiting factor for these CP systems is their limited drug loading capacity which restricts the life time of delivery. In order to improve the drug delivery lifetime of the CP device we aimed to develop a CP drug delivery system whereby the drug is encapsulated within a reservoir and release is mitigated by opening and closing a CP "gate". During my research designing and producing of this gate has been done. I have produced a CP gate which is a platinised polyvinylidene difluoride (PVDF) membrane upon which polypyrrole with different counterions including p-Toluenesulfonic acid (*p*TS), polystyrene sulfonates (PSS), chondroitin sulfate (CS), dodecylbenzenesulfonate (DBSA), dextran sulfate (DS) and hyaluronic acid (HA) has been deposited. I have demonstrated that it is possible to

open and close this gate as a function of applied electrical stimulation. Therefore, I have investigated and successfully controlled the transport of lacosamide which is an anti-epilepsy drug (AED) through this gate under non-stimulated, stimulated and pulsed potential conditions. Results of these series of experiments have been presented in chapter 3. Also, in chapter 4, I have been investigating a new gate design that utilizes a PVDF tube which acts as a drug reservoir and transport gate simultaneously. The tubes are platinised and then coated with polypyrrole with different counterions. Drug release from inside of these fibres to outside was investigated at non-stimulated, stimulated and pulsed potential states.

At the next stage of my research I studied the interaction of the drug molecules with the surface of conducting polymer and demonstrated that the affinity of drug molecules to the surface of CP gate can affect the transport behaviour. In chapter 5 the outcomes of these studies have been shown.

Epilepsy is a chronic disease which unfortunately causes so many difficulties in patients' personal life and can impose severe limitations to their life. The current anti-epilepsy treatments have some severe side effects or they are very expensive treatments which is not affordable for all patients everywhere in the world. I hope my research is the beginning of a promising pathway to find a treatment for epileptic patients whom can be treated with a reasonable price and minimum side effects method, and also bring hope and happiness to their life.

ACKNOWLEDGEMENTS

First and foremost, I would like to express my sincere gratitude to Prof Gordon Wallace for the continuous support of my PhD study, for his motivation, patience, and infinite knowledge. His guidance helped me in all the time of research.

My sincere thanks also go to Prof Simon Moulton and I wish to present my special thanks to whose understanding, expertise added considerably to my graduate experience. Who provided me an opportunity to complete my study and develop my ideas.Without his valuable support it would not be possible to accomplish this research.

I would also like to thank my friends who have made each day at IPRI a new experience for me. I would like to thanks all of them for being my bench mate and listening all my future ideas. Thanks to all my friends who spend time with me with their comments.

I would like to express my special appreciation to my lovely family for their love and support during these years. Words cannot express how thankful I am to my mother, father, sister and brother for all of the sacrifices that they have made on my behalf.

My last and most special thank belongs to my beloved husband, Farshad who is my best friend and soul mate. Without his support and encouragement I could have given up thousand times! Thanks for being always by my side.

TABLE OF CONTENTS

LIST OF FIGURES

LIST OF TABLES

1 INTRODUCTION

1.1 Epilepsy and Current Treatments

A deviant electrical activity in the brain represents epilepsy disorder, which can lead to seizures which can happen generally or partially within the brain. In generalized seizures both hemispheres of the brain will are affected. Adversely, a focus or confined area of the brain generates the partial seizure[1, 2]. An epileptic seizure has been defined by the International Bureau of Epilepsy as a "transient occurrence of signs and/or symptoms due to abnormal and excessive neuronal activity in the brain" [3]. A typical Electroencephalography (EEG) signal of a person without epilepsy (a) and an epileptic patient (b) is demonstrated in Figure 1.1.

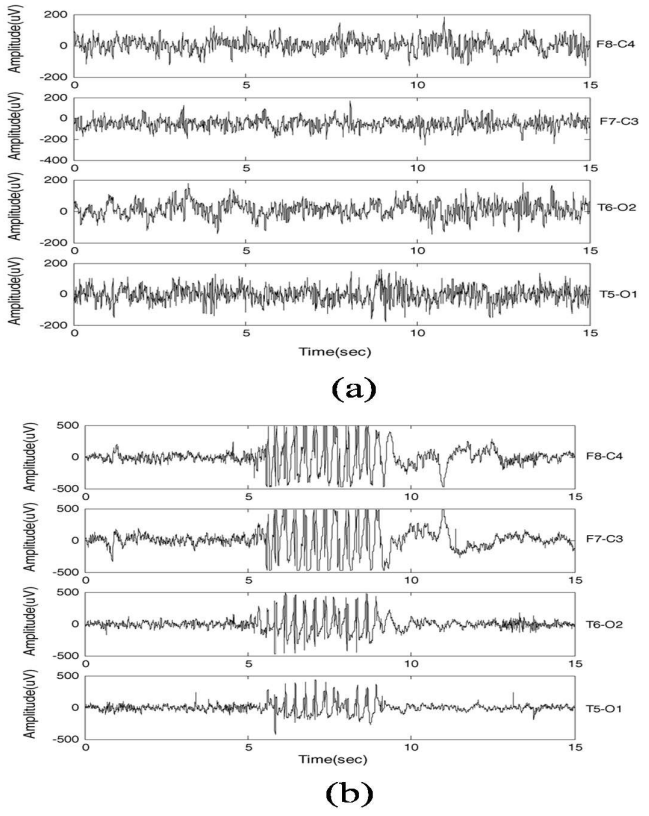

Figure 1.1 (a) EEG signals of a normal person, and (b) EEG signals of an epileptic patient. Adapted from Ref [4].

According to a World health organization (WHO) report published in October 2012 around 50 million people suffers from epilepsy. During a seizure the person's movement, action and consciousness may alter for a short period of time. Approximately three quarters of epilepsy sufferers especially in developing countries remain untreated[5]. In order to control seizure activity a person must take anti-epilepsy drugs (AEDs), normally in the form of a tablet with the goal being to deliver the drug to the brain in quantities sufficient to eliminate seizures without causing adverse effects. In 30% of the cases, sufferers of epilepsy are unable to be medicated due to the dose required to suppress seizures causing adverse side effects. Some patients respond to one specific AED while some patients require a combination of more than one in order to control their epilepsy [6]. Choice of the correct AED is critical as it has been reported that some AEDs can increase the risk of intensifying the seizure occurring condition accompanied with the other adverse side effects [7].

In addition, other anti-epilepsy treatments such as surgical resection of the epileptic region of the brain carry a very high level of risk. Cerebrum is the largest part of the brain which is divided into four paired sections. These sections are frontal, parietal, occipital and temporal lobes. A specific group of human activities are controlled by each lobe. For instance, temporal is responsible to control the brain ability in hearing, language and memory. Unfortunately, the most usual type of epilepsy in confined into the temporal lobe and temporal lobe surgical resection can be performed to control the seizures. By resecting or cutting away the brain tissue in this area, the seizure focused brain tissue will be removed. The most common areas of the temporal lobe which is involved with seizures are anterior and mesial portions. For those epileptic patients whom medication does not control the seizures or the dose causes serious side effects, temporal lobe resection is an option. Vital functions including movement, sensation, language and memory should not be damaged during the surgery [8, 9].

Another non-drug treatment option for treating epilepsy is an implantable device called a vagus nerve stimulator (VNS) (Figure 1.2). In this method a device is implanted in the left side of a patient's chest cavity accompanied with a stimulating lead which wraps around the left vagus nerve in the neck. The device applies electrical stimulation pulses with these mild stimulation signals being transferred to

the brain via the vagus nerve. This approach activates various regions of the brain to prevent electrical irregularities which cause seizures[10].

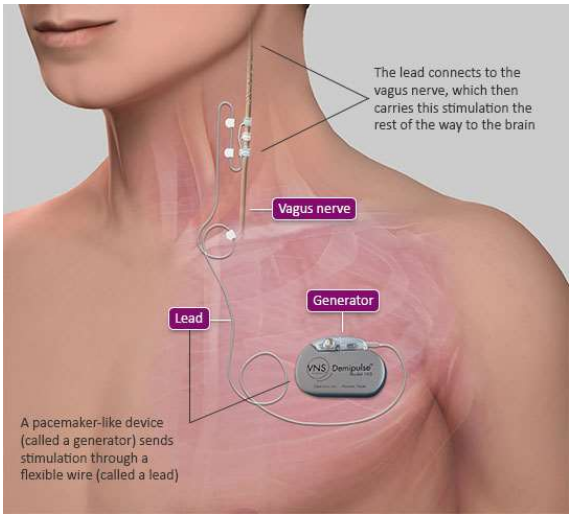

Figure 1.2 Schematic of vagus nerve stimulation (VNS) treatment option for the epilepsy. Adapted from Ref[10].

Another epilepsy treatment option especially for is the ketogenic diet. This special diet includes high fat and low carbohydrate that causes the body to burn fat instead of carbohydrate (such as sugar, bread and etc.,) as a source of energy resulting in the formation of ketones. Higher ketones level has been shown to lead to having more appropriate control of seizure[11]. In some patients a very specific trigger will evoke a seizure and in these infrequent cases avoiding these triggers is helpful with these particular triggers varying from patient to patient. Some possible triggers are lack of sleep, alcohol, flickering lights or patterns, stress, menstruation or significant variation in temperature and overheating[8].

If AED delivery is confined only to the region of interest in the brain, then the unsatisfactory and distractive effects on the other living tissues of the body will be minimised[12]. To feasible this approach two important parameters of an AED has to be considered; (i) the efficiency of the drug (i.e., the minimum level of drug in bloodstream to achieve an appropriate response) and (ii) the therapeutic window of the drug. This window represents the difference between the minimum effective dose and the highest level of drug concentration that causes toxic effects. Hence,

development of a controlled drug delivery device, that takes into consideration these two substantial parameters could increase the number of patients whom can be treated with AEDs without suffering from severe side effects and avoid the more risky and costly surgical and/or implantation treatment options.

1.2 Thesis overview

Giving consideration to all of the advantages and disadvantages of currently available treatment options for the epilepsy, there is a need to develop a drug delivery system for the epilepsy sufferers, especially 30% of them who remained untreated. Most importantly this novel treatment method should be therapeutic but not toxic. Recently, there has been much interest in the use of polymeric carriers as localized delivery devices especially for the central nervous system. Bypassing the blood brain barrier by implanting a polymeric carrier containing an AED directly into the brain tissue would allow the possibility of delivering therapeutic doses directly to the specific region of the brain associated with the epileptic seizures. This targeted approach may overcome the whole body side effects associated with current systemic delivery and therefore offer a treatment option to the 30% untreatable patients as well as the other epilepsy sufferers. Polymeric carriers also offer potential advantages, such as partially protecting labile drugs from degradation and releasing multi-drug combinations in a controlled manner from the same implant.

Conducting polymers (CPs) have been shown to act as very effective drug reservoir with the ability to deliver drugs upon electrical stimulation. However, one limiting factor for these CP systems is their limited drug loading capacity which restricts the life time of delivery. In order to improve the drug delivery lifetime of the CP device the work outlined in this thesis set out to develop a CP drug delivery system whereby the drug is encapsulated within a reservoir and release is mitigated by opening and closing a conducting polymer "gate". This gate has a porous structure and applying an external electrical stimulation will drive drug release. Figure 1.3 demonstrates a schematic of this CP gating system. Application of suitable electrical stimulation to the CP layer will open and close the porous gate and drive drug release from inside of the reservoir into the body tissue.

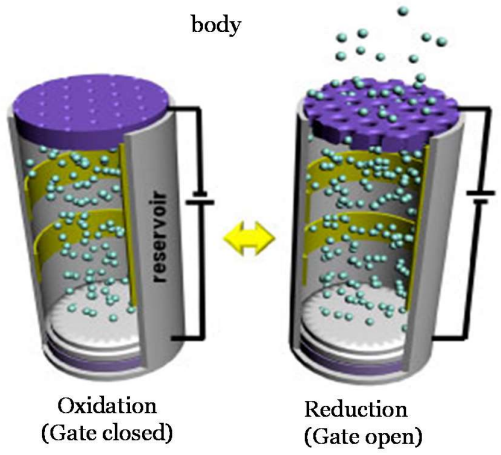

Figure 1.3 Schematic of drug release using a conducting polymer coated gating system.

This thesis aims to design and fabricate this CP coated gating system to develop a prototype of an implantable controlled drug delivery device for the treatment of epilepsy. The preliminary concern of this project was fabrication and characterization of this CP gating system and also the drug reservoir for the intended application. This CP gate (Figure 1.4) is a platinised PVDF membrane which conducting polymer has been deposited on one side of the membrane. This gate will open and close as a function of applied electrical stimulation. Therefore, in this project an electro-responsive polymeric system which can be mitigated by electrical stimulation has been investigated. This device is intended for the treatment of epilepsy.

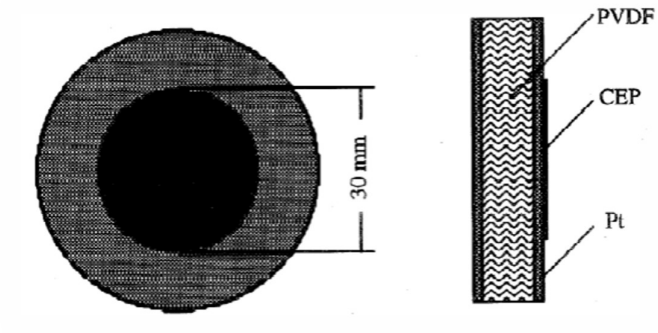

Figure 1.4 Polymer coated Pt/PVDF membrane.

Among all of conducting polymer PPy was chosen to be investigated in this project because this CP is Syntheticesised from aqueous solutions and possess great in vivoand in vitro biocompatibility. Polypyrrole has a low toxicity and, some researches have focused on the use of this polymer for drug delivery application [13]. In the third and fourth chapters, release of anti-epilepsy drug from the conducting polymer coated flat and hollow fibre Pt/PVDF membrane has been investigated. Release studies were carried out at under non-stimulated and stimulated states.

Interaction of AEDs with the surface of CP coated reservoir was also investigated to achieve a more comprehensive understanding of how the CP gating system and reservoir acts as a drug delivery device. Results of this interaction studies has been presented in the fifth chapter.

1.3 Drug delivery methods

1.3.1 Sustained drug release

The most important characteristics of a drug delivery system is providing desirable dosage of drug at regular time interval and also at the region of the body which is confined with a disease. Therefore, by using these drug delivery systems the therapeutic level of drug in blood plasma is provided. Sustained drug delivery

systems have been designed to supply a delivery system with reduced dosing frequency and uniform drug dosage. Sustained drug release system includes drug delivery systems which are not depended on time and release therapeutic levels of a drug over an extended time[14, 15].

Peroral and injection are two common methods for delivering drugs with most drugs developed on the basis of oral or injection delivery routes[16] with oral drug delivery being most preferred delivery method by patients and doctors[17]. However this method has some disadvantages like damaging the hepatic and enzymatic degradation of the drug whilst there is very little control of release in from the per-oral method. In oral administration of drug, effective levels of the drug can be achieved by administration of extra doses which often results in changes in plasma that can be lead to different side effects. A desired peroral drug delivery system has to deliver sufficient levels of drug in a reproducible manner. In addition, the other absorptive tissues have been considered as potential sites for drug delivery such as nasal, rectal, vaginal, ocular and oral cavity[18]. It is well documented that systemic drug delivery results in high level of drugs in the bloodstream and this phenomenon can adversely affect the rest of body because of toxic levels of the drug. Figure 1.5 exhibits an example of therapeutic window of a typical drug and shows the concentration versus time profiles for conventional and sustained controlled drug release[19]. Drug release profile can be optimised by reducing the effective level of administrated drug to the minimum threshold with injecting or ingesting a drug release that follows first-order kinetics. In this form of kinetics profile, there is an initial high blood level of the drug followed by an exponential fall in drug concentration in the bloodstream. When blood drug level reaches more than the therapeutic level (Figure 1.5 (a)) body toxicity occurs. At this state drug kinetics is undesirable, especially for a drug with a narrow therapeutic range. Sustained drug release provide a zero-order release profile if the release is constant and not limited by Fick's diffusion law[20]. The advantage of zero order drug delivery kinetics lies in reducing drug toxicity of the patient and improving drug efficacy (Figure 1.5 (b)).

For AEDs which have been designed to affect the brain tissue, the concentration of penetrated drug through the blood brain barrier (BBB) is much less than the drug concentration in the circulatory system[12, 21]. Therefore, to reach the therapeutic

level of AEDs in the target region of the brain tissue, it is required to deliver daily systemic doses of AEDs[22].

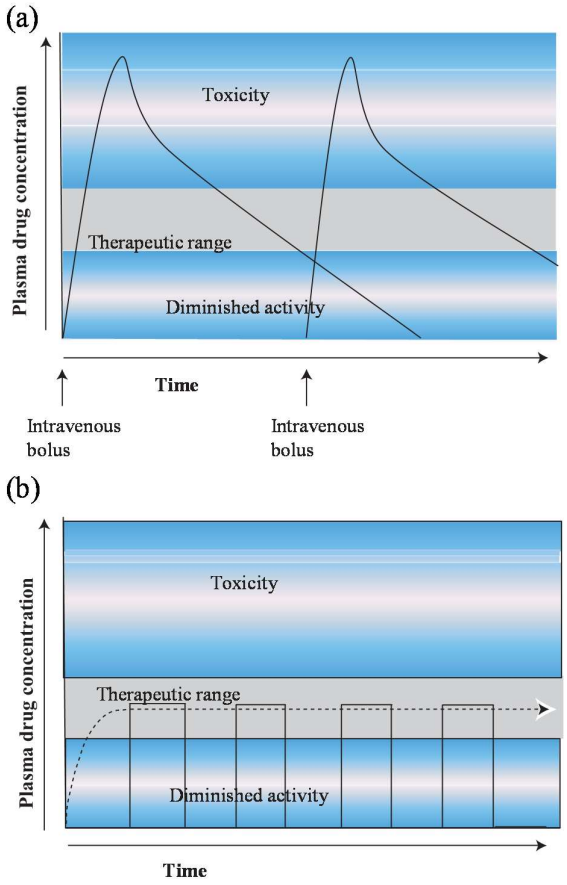

Figure 1.5 Kinetics of first-order (a) versus zero-order (b) in drug delivery systems; First-order kinetics represents plasma concentration versus time curve for intravenous administration of a drug. Zero-order kinetics is represented by sustained or pulsatile release of a drug. Adapted from Ref[23].

The delivery method of a drug plays an important role in how successful the drug is taken up by the body and therefore is therapeutic benefit. As mentioned above systemic drug delivery has a variety of problems and side effects. Therefore, researchers are developing alternative delivery methods such as targeted drug delivery. Drug targeting enables the delivery of drugs directly to the region of interest with decreasing the systemic side effects of the drug being one of the most important advantages of this method. The effectiveness of delivering drug to different parts of the body is also affected by the size of the drug carrier[24] and utilizing targeted drug delivery the efficiency of the drug will be enhanced. Drug

doses used in this method are typically smaller than that used for oral administration of drugs, thus as it has been mentioned before the side effects will be eliminated or reduced. In addition, the patient's acquiescence with this method is higher than using the usual drug delivery systems[25].

There are four different strategies for producing sustained targeted drug delivery systems, namely (1) diffusion controlled and transdermal patches; (2) Water penetration controlled where osmotic drug delivery devices release of the drug is driven by water penetration into the device (3) Chemically controlled where biodegradable reservoir systems used chemically controlled release of encapsulated drug and (4) responsive where mechanical pumps and magnetic systems are examples of some drug delivery systems which release the drug because of the response to the environmental changes[18]. Grimshaw et al.[26] have demonstrated mechanisms of selective controlled transport of protein molecules and neutral solutes through hydrogel membranes.

1.3.2 Controlled release

Delivering a drug directly to a particular diseased tissue or organ is one of the goals of controlled release. By utilizing this system the systemic toxicity will be reduced and provide therapeutic levels of a drug directly at the target organ[27]. Wurster[28] introduced the concept of controlled release in a patent in 1953. There are a wide range of drug delivery mechanisms and Table 1.1 presents some of the commercially available controlled release systems. These systems are classified on the base of therapeutic agent release mechanisms. Recently, various mechanisms by which controlled release can be operated have been reviewed by McCoy et al[29]. These mechanisms include release mitigated by light, heat, magnetism, and ultrasound, mechanical and electrical stimuli[30]. Table 1.1 provides an overview for all of the currently available drug delivery methods.

Table1.1 Different controlled drug delivery systems[42].

Type of delivery system	Mechanism of rate-control
Diffusion Controlled	
- Reservoir devices	- Diffusion through membrane
- Monolithic devices	- Diffusion through bulk polymer.
Water Penetration Controlled	
- Osmotic systems	- Osmotic transport of water through semi-permeable membrane.
- Swelling systems	- Water penetration into glassy polymer.
Chemically Controlled	
- Monolithic systems	- Pure polymer erosion or combination of erosion and diffusion.
- Pendant chain systems	- Combination of hydrolysis of pendant chain groups and diffusion from bulk polymer.
Regulated Systems	
- Magnetic or ultrasound	- External application of magnetic field or ultrasound to device.
- Chemical	- Use of competitive desorption of enzyme-substrate reactions.

In addition to the drug delivery systems presented in Table 1.1 recently there has been an intense interest in developing an advanced intelligent drug delivery systems based on *in vivo* stimuli. These novel systems have been identified as self-regulating[31] or closed-loop systems[32]. For epilepsy treatment using these intelligent delivery systems, an AED can be delivered to the brain tissue in a timely manner upon the response of seizure activity within the brain. According to Figure 1.1 (b) a seizure signal starts very quickly, within one second and these drug delivery devices are capable of initiating drug release in a similar time frame. Therefore, a seizure prediction[33] or detection[4] programmable device is needed to be added to the whole drug delivery system.

There has been much research undertaken in using materials for controlled release systems and the main focus of these studies is on polymers. Furthermore, researches

have used developed novel strategies to make drug release more controllable[34]. These new polymeric systems include polypeptides[13, 35], nucleic acid[36], and polysaccharides functional groups[37-40]. Some researchers have focused on the use of Syntheticetic polymer materials including degradable and non-degradable materials[36].

Hydrogels are cross-linked polymers that have high-water content and possess many advantages for controlled release. One advantage is their ability for localized release of a wide variety of therapeutic agents with a sustained manner. In addition, hydrogels are very sensitive to environmental parameters such as pH, temperature and ionic strength[39]. Recently, Bajpai et al[41] reviewed the different applications of polymeric hydrogels for controllable delivery. Polymeric nanocarriers such as dendrimer, liposoms and micelles also play an important role in the development of controlled release systems due to their ability to encapsulate drug molecules and carry them into the desired body tissue. Using inorganic nanocarriers like nanotubes, nanoshells and mesoporous nanoparticles are also of interest for the progress of therapeutic delivery applications[39].

1.3.2.1 Controlled release devices

Varieties of controlled drug release devices have been developed over recent years. These devices contain; pumps such as osmotic pumps and micropumps, polymeric devices and also systems which are based on microelectromechanical property of the materials and are commonly referred to as MEMS[23]. In 1970s the first controlled drug delivery device was used extensively [43-46] which consisted of a bellows-type pump which was activated by partially liquefied Freon® (DuPont) and provided constant drug administration. This early work inspired many researchers to focus their efforts into this research area and the outcomes of their work provided the opportunity of designing and developing more sophisticated implantable drug delivery devices with the ability to deliver therapeutic levels of drug in a controlled manner.

In 1986 Medtronic Pty. Ltd. developed a novel controlled drug delivery device which worked on the basis of an electronic controllable peristaltic pump[47]. Three years later, MimiMed Technologies revealed an advanced drug delivery device[48] comprising of a combination of a solenoid pump, a reservoir and an advanced electronic control system. A programmable and implantable pump was introduced into the market place by InfusAID Pty. Ltd. [49] Which employed bellows-type pump which was accompanied by a solenoid valve to monitor and control the release of a drug.

Using polymeric materials to fabricate controlled drug delivery devices has been considered. In general, polymeric drug delivery devices can be classified into two different groups [23, 50-56];

I. Non-degradable polymeric reservoirs and matrices,
II. Biodegradable polymeric devices.

An approach that falls into the non-degradable category is devices built by the microfabrication of silicon. Using this approach researchers have developed systems that provide drug release profiles with high precision and control [57-61]. Another novel drug delivery technology has been introduced by MEMS which utilizes microneedle-based chips that provide an alternative to the conventional transdermal drug delivery method [62-68]. Existence of the stratum corneum is the major barrier in transdermal delivery method so by using microneedle-based chips, poor permeability of the skin increases because of creation of micro channels to transport therapeutics across the stratum [67, 69]. Microneedle-based chips can be classified in the following categories;

I. In-plane microneedle,
II. Out-of plane microneedle.

Figure 1.6(a) shows the penetration of two silicon processed microneedle to a porterhouse steak with Figure 1.6(b) showing the injection of an in-plane single crystal silicon microneedle. In this procedure Rhodamin B dye was injected into an anesthetised rabbit[70, 71].

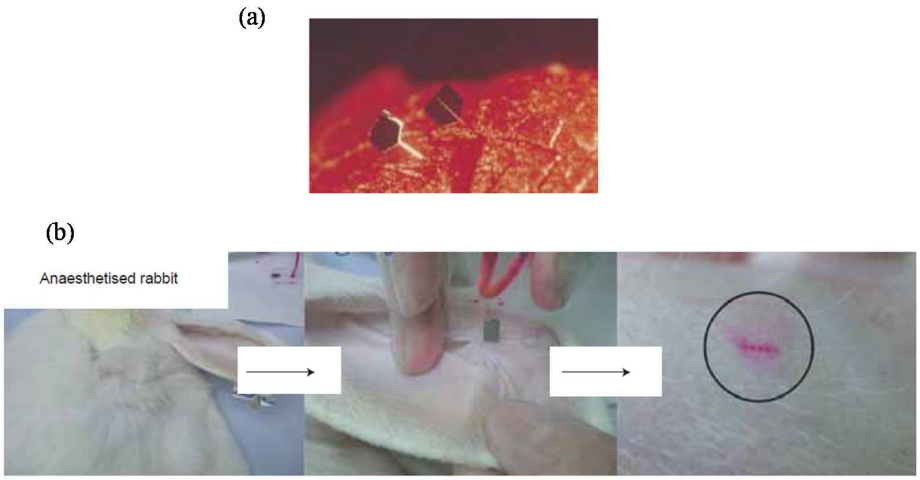

Figure 1.6 Silicon-based microneedle drug delivery chips in use; (a): penetration Of two microneedle into a porterhouse steak; (b): injection of Rhodamin B dye into a rabbit ear using a microneedle.

Silicon microfabrication technology is currently being used by Microchips Biotech Inc. (USA) to develop a device that is capable of delivering proteins, hormones, pain medications and the other drugs or therapeutics[72]. Figure 1.7 demonstrates a section cut of a silicon microchip which has been used for controlled release and highlights the anodes, cathodes and reservoir of this device. The main body of the device is shown in Figure 1.7 (b) that includes a reservoir which is fabricated using a degradable polymer. The truncated conical reservoirs are sealed with polymeric material from the top and a sealant polyester tape layer from the bottom.

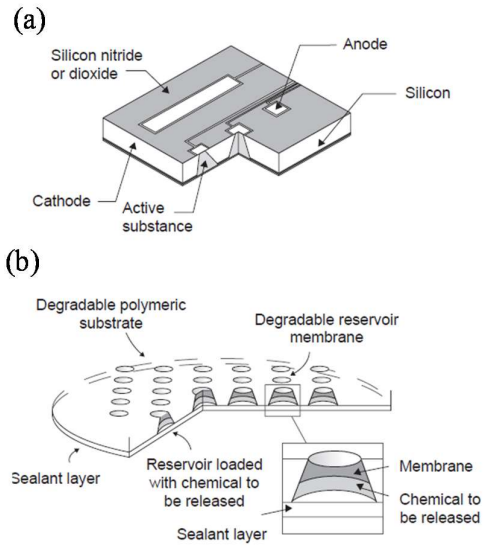

Figure 1.7 Schematic of a Microchips Biotech Inc. silicon microchip used for controlled drug delivery applications. (a): cut off section of the drug delivery device; (b): schematic of the main body[72].

Nano porous and nano channel silicon microchips for drug delivery have also been created by Ferrari and co-workers [73-93] which can also be used as a device for bio-separation and immunoisolation. The device possess a very uniform pore size and very thin thickness which provides sophisticated diffusion and sustained drug release profile [20,62,94,95]. Figure 1.8 presents a microchip which uses the NanoGATE drug delivery implantable device which has been designed by iMEDD Inc. [96]. These nanoporous microchips provide sustained release of drugs for long durations. Therefore the NanoGATE device is an appropriate candidate where a prolonged sustained release of drug is required. One the most unique characteristics of NanoGATE device is its permeability that prevents ingress of fouling agents. Figure 1.8(a) exhibits an implantable device which has been fitted with a nanoporous microchip with the possible diffusion pathway of a drug has been illustrated by dashed arrow. Figure 1.8(b) is a picture of implanted device in the body of a rat[20, 97].

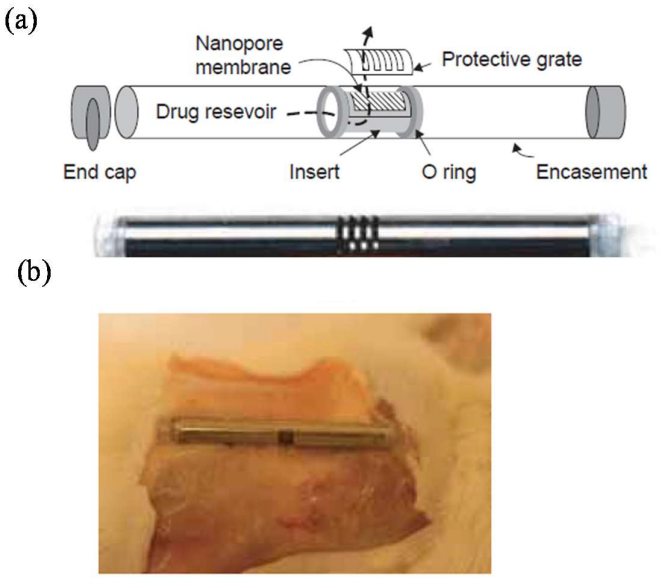

Figure 1.8 NanoGATE microchips drug delivery devices. (a): schematic of NanoGATE microchip; (b): picture of implanted NanoGATE microchip in the body of a rat.

A novel nanochannel drug delivery system called nDS was developed by Ferrari and his colleagues in 2004[98]. The main structure of this nDS device consists of two conjugated wafers. One of them is a filtration wafer which is structured by micromachining and the other one is the cap wafer (Figure 1.9 (a) and (b)). There is a hole in the cap wafer and fluid transfers into the device via this hole where the fluid then flows through the device by horizontal movement and via the filtration channels. At the end of the filtration wafer there is another hole which allows the fluid to exit the device. The nDS drug delivery microchip which has utilized nanochannel technology could be used for sustained release application. For instance, release of IFN-α has been studied using the nDS nanochannel drug delivery device. In this study, IFN-α exhibited a sustained release at the investigated time[99]. Figure 1.9 (a) exhibits the cross section of this device and (b) presents top and cross section view of the nanochannel device.

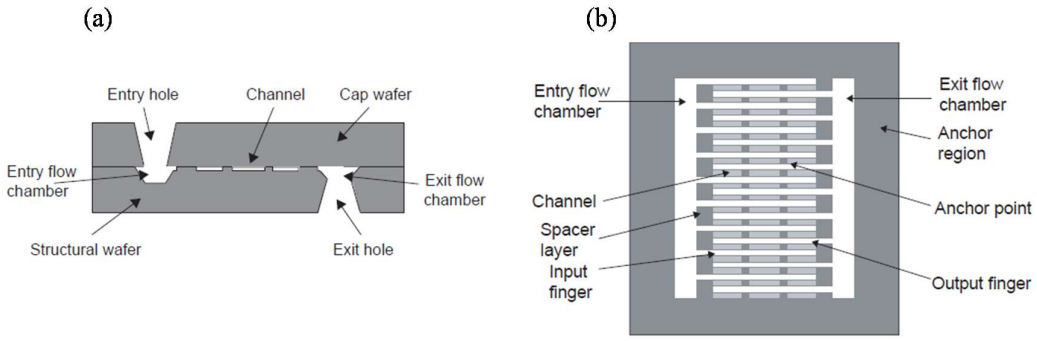

Figure 1.9 Microchip with nanochannel technology; (a) Cross section view; (b) top and cross section view of the device[100].

1.4 Conducting polymers

In 1977 Shirakawa [42], Heeger and MacDiarmid [101] discovered a class of organic polymers and called them conducting polymers (CPs) and in 2000 these researchers won the Noble Prize for Chemistry as a result of their studies in this area. There has been a lot of interest in the use of conducting polymers in wide range of applications such as energy storage [102-106], photovoltaics [107-109], electrochromics [110-113], electromechanical actuation [114-117], separation membranes [118-120], corrosion protection [121, 122] and chemical sensors [123-127]. Conducting polymers are generally biocompatible and non-degradable [128]. Also, this category of polymers are relatively simple to Syntheticesis and demonstrate conductivity as well as "redox switching" which can also be associated with hydrophilic/hydrophobic, colour and mechanical properties changes [129]. The last few decades of research in the CP area has revealed that the most pragmatically applicable and stable conducting polymers are based on polypyrrole (PPy), polythiophene (PTh) and polyaniline (PAn) [129]. The chemical structure of these conducting polymers has been shown in Figure 1.10.

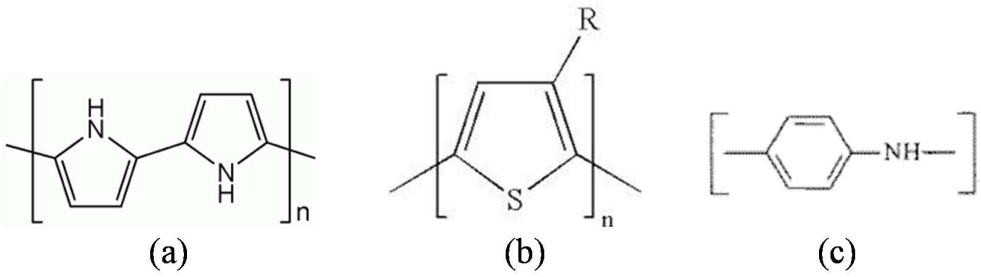

Figure 1.10 chemical structure of (a) polypyrrole (PPy); polythiophene (PTh) and polyaniline (PAn).

The electropolymerized Polypyrrole is widely used in this thesis. Therefore, the electropolymerization mechanism of this conducting polymer is presented in Figure 1.11.

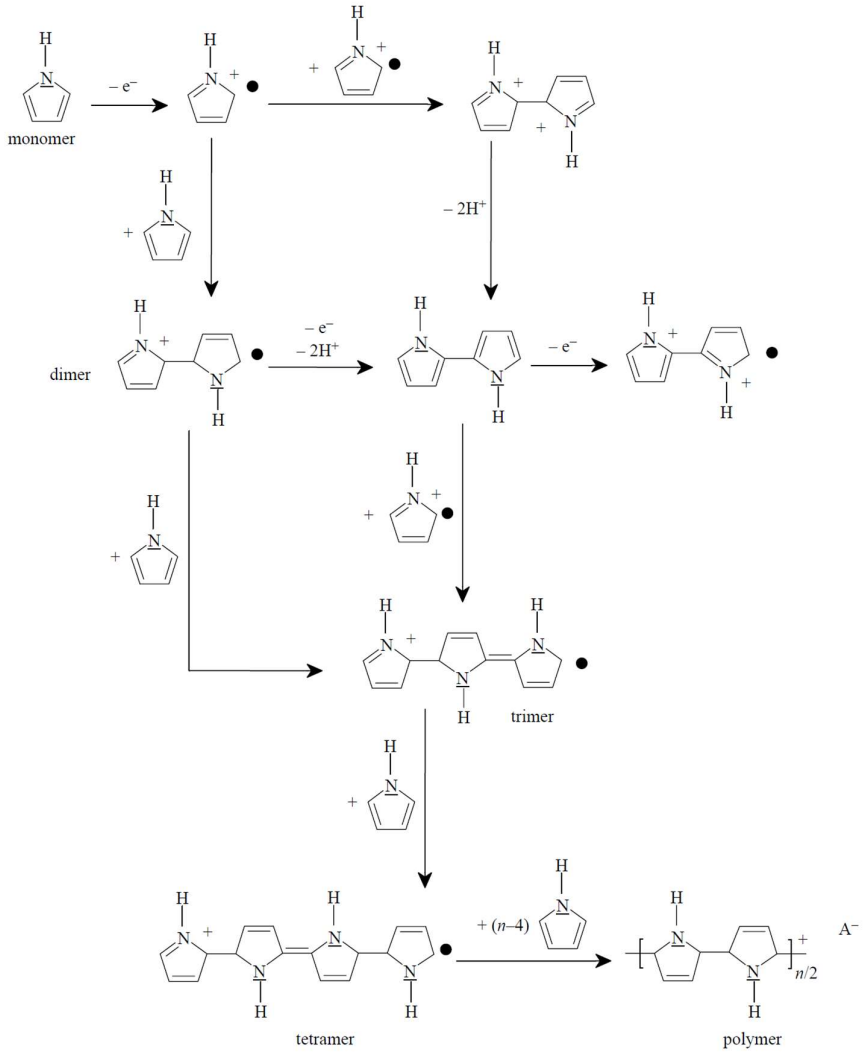

Figure 1.11 Mechanism of electropolymerization of polypyrrole; A^- represents the counterion.

Some advantages of electrochemical polymerization are simplicity, ability to control the thickness, geometry and location [130].

In electropolymerisation method, by absorption of monomers to the surface of working electrode, on-electron oxidation is formed which called as pyrrole cation radical. This cation radical is able to couple with the other cation radicals and also the neutral monomers in the solution. These reactions lead to formation of dimers. Then the polymer chain grows by coupling of dimers with the other dimers or monomers. The role of counterion (A^-) is providing the electroneutrality [130].

When a conducting polymer such as PPy is oxidized or reduced the counterion or

dopant can leave the main structure of the polymer freely and again is incorporated into the polymer matrix [130]. Figure 1.12 shows the redox of PPy where A^- represents a counterion (dopant) molecule.

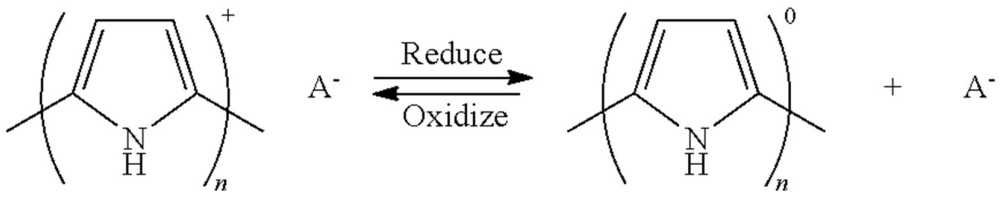

Figure 1.12 Oxidation and reduction process of PPy

Because of the simple redox switching of CPs and the subsequent physical changes, they offer a the possibility of widespread application in actuators, micro-fluidic devices and biomedical science such as controlled drug delivery systems [101].The other great property of conducting polymer is their ability for actuation which has been utilized to produce PPy valves where these valves can control the release of agents from reservoirs [35]. For example, Tsai *et al.* [36] doped PPy with dodecylbenzene sulphate (DBSA) using electrochemical deposition onto a gold layer. During application of a voltage the PPy/DBSA volume changes due to dopant ion moving into and out of the polymer. Therefore, the gate will open and close as a function of electrical stimulation. In similar work, Wang *et al* developed a PPy valve actuator to control release of drug. Figure 1.13 and 1.14 show the photo and schematic of this drug delivery device.

(a) (b)

Figure 1.13 photographs of the actuation of polypyrrole valve in a prototype drug release device; (a) before and (b) after applying voltage to the PPy/DBSA valve [131].

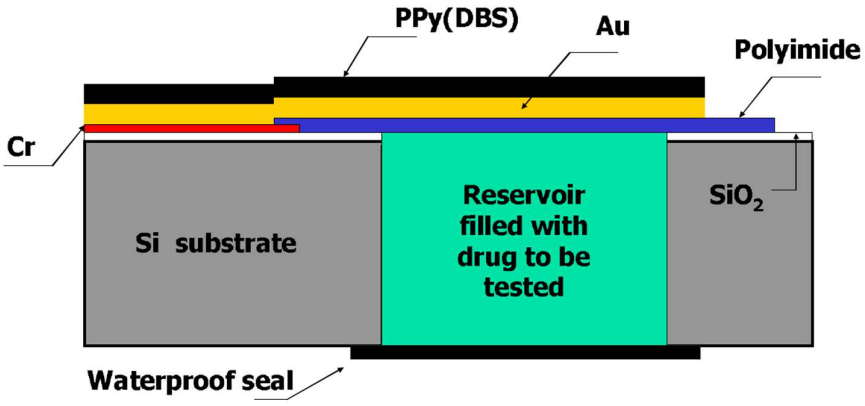

Figure 1.14 Schematic of drug delivery device from the cross section view [131].

Figure 1.13 exhibits the application of +0.3 V to the surface of PPy/DBSA valve leads to actuation of this part and opening the gate of drug delivery reservoir [131]. PPy valves which can actuate using electrical stimulation have been developed by Xu *et al* [37]. These valves have been used over a set drug reservoirs and have demonstrated linear and pulsatile release behaviour.

This thesis focuses only on the use of PPy coated membranes for controlled delivery studies; therefore, PPy has been utilized extensively. Hence, PPy, its polymerization method, and also its structure and characteristics will be introduced through the following sections.

1.5 Polypyrrole for controlled drug delivery

Controlled release using conducting polymers was introduced first by Zinger and Miller in 1984. They had used PPy as the substrate and studied the release of glutamate[35].Therapeutic drugs, pesticides, fungicides, and the other drugs can be released in a controlled manner from conducting polymer structures. These drugs can be used as incorporated dopants (A^- as shown in Figure 1.5). Therefore by applying a desired potential the incorporated drug will release from the structure of the polymer. In the other word, conducting electroactive polymers are able to incorporate biomolecules during their growth and then by using electrical stimulation these molecules will be expelled. These strategies were seen as a novel development of controlled release systems for active ingredients such as anticancer drugs and anti-inflammatories[35].Among all of conducting polymers, PPy and its derivatives have engaged the most of researchers in this area. High electrical conductivity, environmental stability and high mechanical strength are the main reasons of using PPy in most of research. Also this conducting polymer can be easily synthesised using chemical or electrochemical methods [128, 129]. The electropolymerisation can be used to synthesize thin films with awide range of counterions [72-76]. In chemical polymerization method, the pyrrole monomer has to be mixed with an oxidant in a solvent. The advantage of this method is the possibility of conducting the polymerization reaction withoud requiring any special equipment. However, the disadvantage of the chemical polymerization is the availability of the number and limitation of oxidants and counterions. On the other hand, electropolymerisation method is a facil way to vary the properties of polymer by changing the counterions or even the electropolymerisation condition [48].

In addition, PPy is the most widely used conducting polymer because of its low toxicity of the monomer and good biocompatibility of the resulting polymer [132]. Also PPy possesses good stability in various solution such as aqueous environments in vivo and in vitro. In the other word PPy is not biodegradable [132]. Wang *et al.* [133] was atudied the biocompatibility of PPy. In this study PPy did not show any adverse impacts on the lines or animal models's cells. In a study conducted by Georgeet al [134] the neural networks which were grown on PPy elelctrodes and implantedinto rats. These PPy electrodes were compeletely biocompatible. Recentely, Alteh *et al.* [135] concluded based on their research that PPy could provide a new category of

biomaterilas because of its biocompatibility and flexible properties.

1.5.1 Electrochemical polymerization

Conducting polymers can be synthesized by either chemical [136, 137] or electrochemical methods [130, 138, 139]. In both methods, charged specises are incorporated into the polymer structure and this process is termed doping. Figure 1.15 exhibits the polymerisation process of PPy. The A^- is representative of the counterion or dopant being incorporated into the PPy structure during the polymerization process, and also n presents number of pyrrole monomers which is used during Syntheticesis reaction.

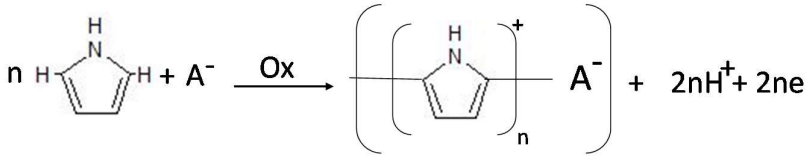

Figure 1.15 Schematic of the Syntheticesis of pyrrole monomer in the presence of a counterion (A^-), and n is pyrrole monomer unit's number per counterion. Ox represents oxidation and can be performed using a suitable chemical oxidant or by applying a suitable electrical stimulation sufficient to initiate oxidation of the pyrrole monomer.

In this thesis only electrochemical polymerization has been used, therefore, this method will be discussed in detail. Using a three-electrode electrochemical cell the electropolymerisation of PPy doped with a wide variety of counterions is possible. This three-electrode system consists of reference, working and auxiliary electrodes (Figure 2.2 in Chapter 2). Polymerization occurs at the working electrode and the process starts with oligomers (several monomer units attached to each other) generation and then when the molecular weight of these oligomers become large enough, the oligomers turn into insoluble large structures and absorb onto the working electrode surface. The polymerization reaction continues by spreading from these active sites until the whole surface of working electrode is covered [140, 141]. The extended explanation regards polymerisation mechanism of PPy has been provided in a review paper by Sadki *et al* [142]. The accurate and exact chemical structure of PPy is not still completely understood. Using X-ray photoelectron

spectroscopy (XPS) [143], UV-photoemission and optical adsorption spectra [144] revealed the linear chains of planar pyrrole rings in PPy structure. These pyrrole rings have been attached to each other in the 2,5-position and roughly two to four (three in average) pyrrole units possess one positive charge. Negative charge from the incorporated counterion balances the positive charge of the PPy during polymerization. A significant number of pyrrole rings have been linked through 2,3-positions. This phenomenon has been introduced as a defect in the hypothetical idea of linear arrangement of PPy chain which leads to decline of PPy conjugation length and the polymer conductivity [138]. Figure 1.16 demonstrates the chemical structure of PPy and also shows some of its structural disorder [138]. Characteristics of the grown PPy can be affected by a number of experimental parameters during synthesis, especially the electropolymerisation method. For instance, concentration of counterion and monomer, temperature of polymerization solution, substrate or working electrode type and growth time can also have an effect [71, 140]. In this study, PPy with different dopants has been deposited on the surface of working electrode under a constant current (i.e., galvanostaticly). During the electropolymerisation process the amount of charge passed (A.s) and potential (V) versus time was monitored. A linear relationship between passing charge through the surface of working electrode and amount of deposited PPy on the surface of working electrode has been shown by Fonner *et al* [140]. Also monitoring the oxidation potential provides some useful data about the degree of PPy oxidation during Syntheticesis process. In conclusion, observing and recording the polymer deposition process parameters is important to adjust and recognize any problem which may occur in the system set up [130].

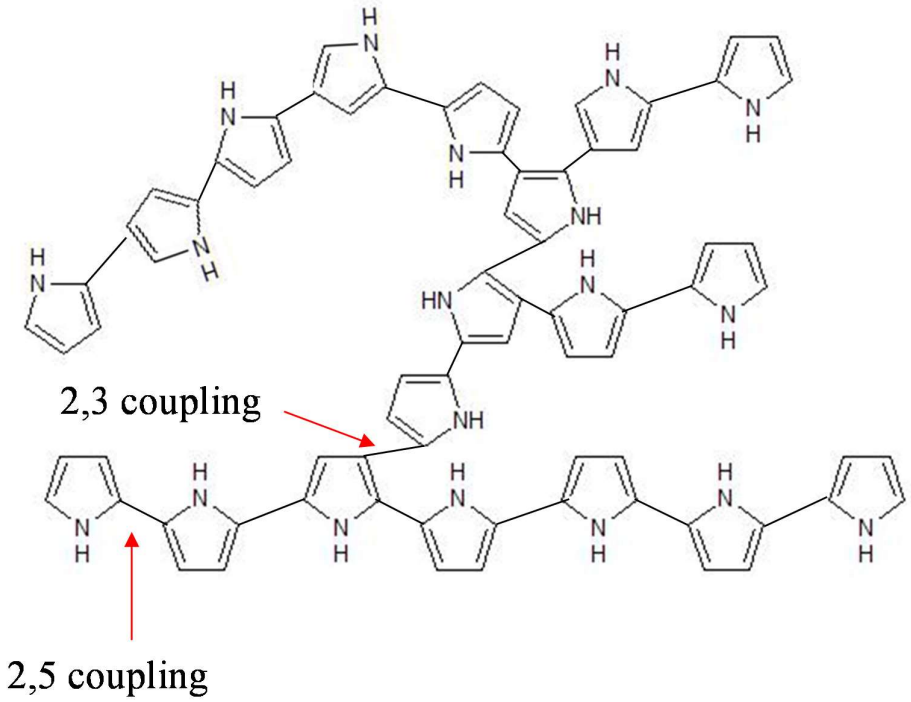

Figure 1.15 Chemical structure of PPy; 2,5 coupling leads to having linear structure while with 2,3 linkage structural disorder is happened into the PPy structure. Adapted from Ref [138].

Pyrrole monomer is an appropriate candidate to use for biomedical and biomaterial applications as this this monomer is relatively soluble in aqueous solvents and most of the biomolecules carry negative charges which can be incorporated into the polymer structure as counter ions, and also these biomolecules are usually water soluble [71, 140].

1.5.2 Properties and characterisation

Electrical property or the ability to transfer electron across the polymer structure is the main and fundamental difference between non-conductive insulating polymers and conducting polymers. Conjugation is the main reason of this phenomenon. Conjugation s defined as the presence of alternate single and double carbon-carbon bonds which are repeated continuously into the structure of conducting polymer chain (Figure 1.17).

Figure 1.16 The chemical structure of PPy.

Conjugation in the structure of conducting polymers such as PPy provides the overlapping opportunity between two sp^2-hybridised orbitals. When these overlapped sp^2 orbitals are full as presented in Figure 1.17, PPy is in its natural state. Figure 1.18 exhibits the band structure evolution upon doping process of PPy.

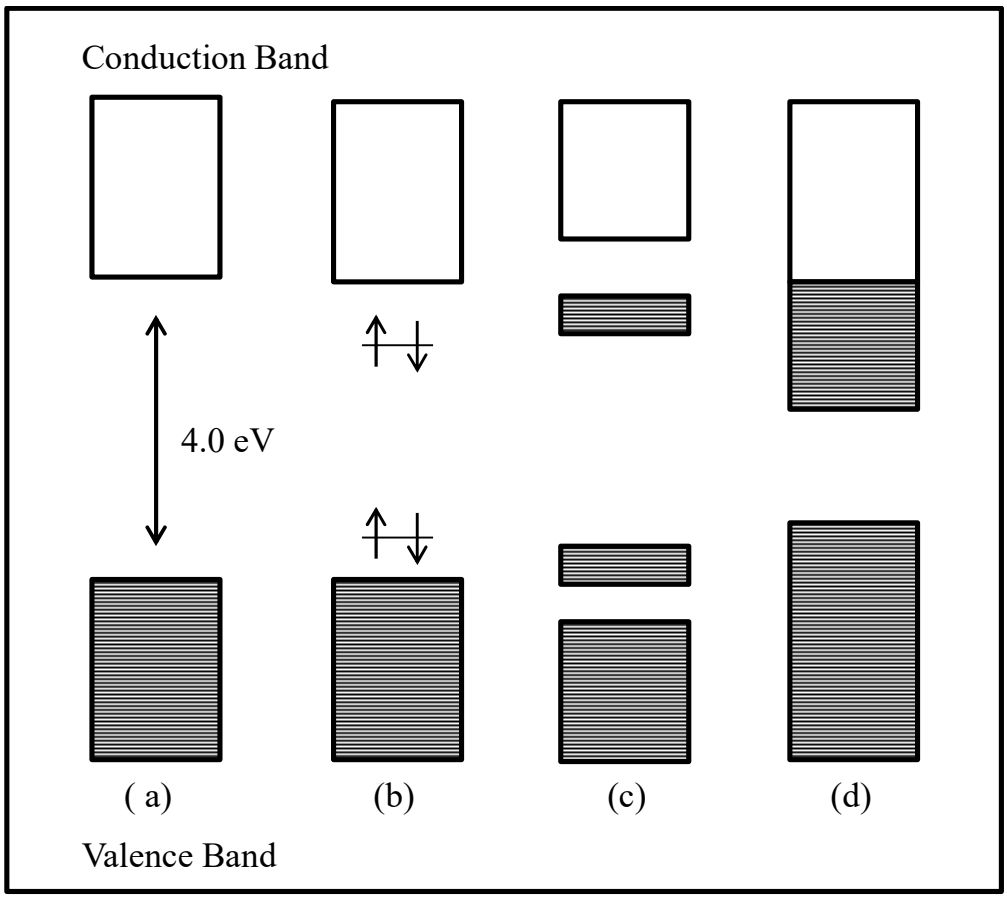

Figure 1.17 Process of band structure of PPy doping; (a) Natural polymer, (b) Polaron, (c) Bipolaron at the intermediate level and (d) Bipolaron band at the high doping levels [145].

At natural state PPy has the lowest electrical activity and acts as a moderate insulator. By polymerization of PPy using doping molecules the sp^2 orbitals will be occupied. The electrical conductivity of PPy will be at the highest level when every three monomers are conjugated by one doping molecule. According to this theory the large band gap for PPy is 4.0eV. The bad gap means the difference between the highest conducting level of a material (highest occupied molecular orbitals, HOMO) and the lowest occupation capacity (lowest occupied molecular orbitals, LUMO). For PPy a molecule need 4.0eV energy to transit across this gap. This amount of energy has been calculated using valence-effective Hamiltonian method [146]. When PPy is syntheticesized in the presence of a doping molecule, the addition or subtraction of charge from the neutral state occurs because of adsorption and desorption of doping molecules. Polymerization of PPy with a counterion molecule ensures occupation of sp^2 orbitals and facilitates electrical conductivity. Oxidation of pyrrole monomer in the presence of an anion molecules (dopant) leads to p-type doping of conducting polymer and balance the PPy polymer chain charge, and also results in a positive charge or polaron formation. On average for every 3 units of pyrrole monomer there is one positive charge in the backbone [147]. Addition of another polaron causes a bipolaron or a pair of polarons formation which is energetically desirable. With the highest level of doping, bipolaron bands blends with conducting band, and also the valence band. At this state the band gap is low enough to classify the material as a conducting material [148].

Measurement of the electrochemical, chemical and physical properties of CPs is the major characterization properties of these materials. A variety of characterization methods have been utilized to study these properties with Table 1.2 presenting some of the most common characterization techniques.

Table1.2 Characterization technique of conducting polymers [130].

Conducting polymer property	**Characterization method**	**Information achieved**
Electrochemical	Cyclic voltammetry Potentiometry Amperometry Impedance analysis	Electrochemical properties and polymerization

		mechanism
Chemical	Elemental analysis NMR XPS Raman spectroscopy FTIR-ATR	Chemical structure of polymer and chemical analysis of incorporated counter ion
Physical	SEM AFM Four point probe conductivity Tensile strength Permeability Porosity analysis	Morphology, porosity structure, mechanical property and conductivity

1.5.3 Controlled drug delivery

Two approaches to drug delivery using PPy are presented in this thesis namely release from a reservoir in (i) flat and (ii) hollow fiber shape, using a CP coated porous membrane, termed "gated release".

1.5.3.1 Direct stimulated release

Release of incorporated therapeutics for PPy can occur under passive conditions (i.e., in aqueous media at room temperature and pressure), as well as under applied electrical stimulation. Through the use of electrical stimulation the rate of release from PPy is significantly altered. Therefore, in comparison with the currently available drug delivery devices on the market, using conducting polymer provides the ability to have fine control over release upon application of electrical stimulation. The ability to have control of the release of therapeutics from PPy is highly desirable, if not essential, for the intended clinical application addressed in this thesis.

The chemical structure of therapeutic drugs which have been chosen for this project is presented in Figure 1.19.

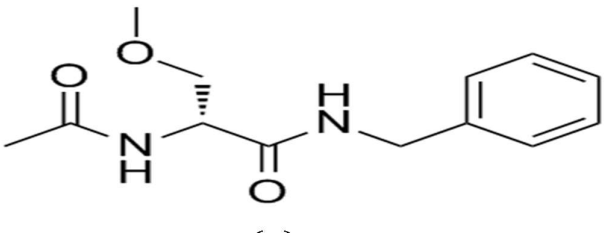

Figure 1.18 Chemical structure of Lacosamide (LCM)

Figure 1.19 exhibits the chemical structure of lacosamide (LCM). Lacosamide or (R)-2acetamido-*N*-benzyl-3-methoxypropionamide, is a functionalized amino acid which is specifically designed and Syntheticesized to act as an anticonvulsive drug. Various animal test of LCM have demonstrates the effectiveness of this drug to control seizures [151].

The first application of PPy as a drug carrier for targeted drug delivery was investigated by Zinger and Miller at 1984 [152]. They studied the release of neurotransmitter from an electrode which was coated by PPy. The neurotransmitter was attached to the backbone of polymer by a covalent bound. Therefore, it was stable on the surface of polymeric electrode until an external pulse from a cathodic current initiate the release of this molecule [153].

Afterwards, PPy was studied as drug release substrate for the treatment of schizophrenia, neural electrode coatings and implantable microchips with controlled drug delivery targets [154-156].Also, PPy coated electrodes were utilized to study the incorporation and release of I-labelled NT-3 growth factor. Release of NT-3 was investigated by applying pulsed voltage, pulsed current and cyclic voltammetry [157, 158].

1.5.3.2 Gated release

In this thesis gated release was mitigated by the use of a PPy coated porous membrane. The choice of the membrane is critical as it is important for it to act selectively in terms of what can pass through. There are many different classification strategies for membranes. For instance, membranes can be classified into two

different categories including Syntheticetic and natural membranes. The structure and functionality of these two groups of membranes are totally different [159, 160].

Biological membranes respond to environmental changes to make the transport process possible. By changing the environment condition such as pH or temperature a biological membrane adjust its permeability on the base of obtained biological data. Then this membrane transfers specific species selectively from one side to the other side. These membranes are made from a great variety of proteins and lipids and assist in chemical transport through the membranes [161].

Syntheticetic membranes can be classified in terms of their application or their physical and chemical dimensions and are composed of ceramic and polymeric materials [162]. Some researchers have divided Syntheticetic membranes in three groups based on the separation mechanism and the application of membranes [163]. According to this classification membranes function with reverse osmosis, ultrafiltration or microfiltration mechanism. In all of these mechanisms the driving force for filtration is pressure. Also, the particle or molecular size of the transition species is important and effective on the transport behavior across the membrane.

The physical dimensions of a membrane is another important aspect which leads to the other classification strategy [164]. In this classification membranes include heterogeneous and homogenous or symmetric and asymmetric. A bulk liquid membrane is a very good example of a homogenous and symmetric membrane. Beside, a supported liquid membrane is called a heterogeneous and symmetric membrane. Figure 1.20 presents classified membranes in a diagram. In this classification the physical dimension and chemical structure of membranes have been combined [161, 165].

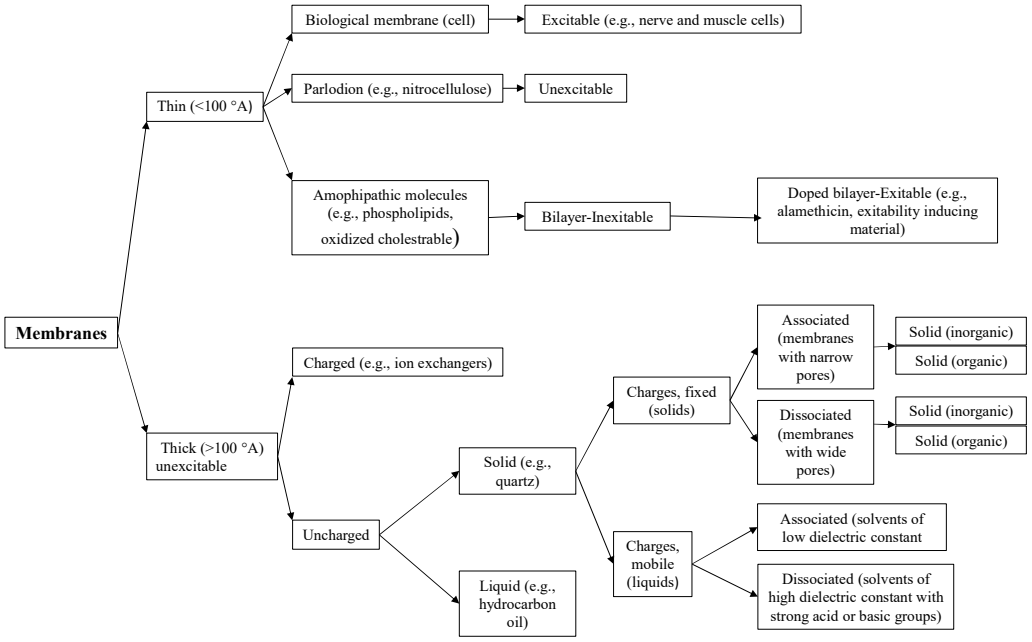

Figure 1.19 Classification of membranes; Adapted from Ref [161].

1.6.1 Membrane separation mechanisms and processes

Different species and chemical reagents transport across the membrane by either active or passive mechanisms with the type of membrane and the transport condition being two effective factors. In active transport an external driving force is needed, while, passive mechanism happens because of a difference in chemical or electrochemical potential between two sides of the membrane. Passive transport is the major transport mechanism which has been employed to develop membranes for industrial uses. Table 1.3 exhibits the classification of membranes which are utilized for different transport mechanisms with employing a variety of driving forces [159, 166].

Table1.3 Classification of membranes processes on the base of membrane transport mechanisms

Pressure difference	Concentration difference	Temperature difference	Electrical potential difference
Microfiltration	Pervaporation	Thermo-osmosis	Electrodialysis

Ultrafiltration	Gas separation	Membrane distillation	Electro-osmosis
Hyperfiltration	Dialysis		
Piezodialysis	Liquid membranes		

1.6.1.1 Osmosis transport mechanism across a membrane

When a membrane is placed between two solutions which have different concentrations, an osmotic pressure is the driving force of transport mechanism through the membrane. In addition, in some case which the membrane possesses selective permeability the osmotic pressure occurs. However, for microfiltration and ultrafiltration membranes which have porous structure the osmotic pressure is negligible. Osmotic pressure of a non-porous membrane is a function of solute concentration, molar weight of immigrant species and the experiment temperature [159, 167, 168].

1.6.1.2 Pressure driven transport mechanism across a membrane

When an external pressure is a driven force to initiate transport through a membrane, differences between membrane pore sizes and the particle size of the immigrant solute are two effective factors. In addition, solubility of the solute and diffusion power of this solute in the membrane matrix is significant. These types of membranes can be divided into three different classes as it has been presented in Table 1.4.

Table1.4 Classification of membrane on the base of pressure driven mechanism

Type of membrane	Microfiltration	Ultrafiltration	Hyperfiltration
Immigrant particle size range (nm)	>100	1-100	0.1-1 nm

Applied pressure (bar)	<2	1-10	0.1-1
Separation mechanism	Separation based on particle size	Separation based on particle size	Separation based on difference in solubility and diffusivity

1.6.1.3 Concentration gradient driven transport across a membrane

In general, concentration gradient as a transport mechanism happens for non-porous membranes. These type of membranes includes, gas separation, evaporation, liquid and dialysis membranes. For separation of gas a pressure from upstream to downstream with the value of 100 bar is required. Evaporation membranes utilized the vapor pressure the activity difference as a driving force for transport across the membrane. In liquid and dialysis membranes the difference between concentrations in two sided of the membrane initiated transport through these membranes. Affinity between m species and the membrane or diffusion is two effective factors in transition mechanism.

1.6.1.4 Thermally driven transport mechanism across the membrane

In some separation or transport systems which utilized a non-porous membrane, the temperature between two sides of the membrane in different. Mass flow induction across the membrane occurs due to temperature gradient across the membrane which is called Soret effect. Fourier's law can explain this phenomenon [159]. In membrane distillation process two liquids with different temperature are separated by a porous membrane. In this process the membrane is not directly involved in the separation mechanism. The transport driving force is vapor-liquid equilibrium. Different industrial areas such as, water purification in semiconductor industries, feeding boiler water for power plants and seawater desalination are using these type of membranes [169].

1.6.1.5 Electrically driven transport across a membrane

Ion-exchange membranes are classified in this category. A different between electrical potential mitigates the transport of charged species through the membrane. Donnan exclusion mechanism explains the principle of this transport mechanism. For instance, this separation mechanism is being used for desalination of either water or food and also in pharmaceutical industries. In addition, for producing of sulfuric acid and sodium hydroxide these membranes are being applied [170]. It has to be noted that the chemical nature of the membrane is an effective factor. The other significant factor is the member morphology.

1.6.2 Conducting polymer coated membranes

1.6.2.1 Development of conducting polymer coated membranes

Movement of conducting polymers as a result of redox switching has been used to develop a new strategy for producing smart membranes. These membranes have been coated with a CP such as PPy and stimulated by applying the oxidation and reduction potentials of the CP. By using these electrical pulses redox switching will occur, so the counterion will move between the electrolyte and the coated membrane *in situ* or *ex situ*. This property of conducting polymers enables them to be applicable in ion separation such as K^+ and Na^+, transition metal ions (i.e., sulfonated aromatics) and large molecules such as proteins[101]. Previously researches have studied the fabrication and application of these smart membranes which has been shown in Figure 1.20 [171-176].

The mechanical strength of PPy films are not sufficient to be used as free standing membrane, therefore, most research has been performed using a supporting substrate. For instance a gold mini grid membrane was used to support PPy membrane for ion transition studies by Burgmayer *et al* [175,176]. According to their study alteration the redox state of PPy can change the ion permeability of PPy. Also, they reported that when PPy was at its oxidized state the ion transition rate was much higher than the permeation rate at reduced state. Wang and co-workers [177] developed the first free standing PPy membrane to study the transport of

monovalent cation such as H^+, K^+, Na^+ and NH_4^+. Ion permeability through this free-standing PPy membrane was investigated by applying an external electrical field to the surface of PPy film. Size and charge of the cations and also the surface property of the PPy membrane had significant effects on the permeation rate of cations between two electrolyte solutions.

Polypyrrole free-standing membranes were also used by Zhao *et al* [178-181] to study the transport of metal ions. In these studies metal ion transport initiation and control was carried out by using electrochemical stimulation such as applying pulse potentials. The on/off metal ion transport profile was achieved by varying the external electrical stimulation of the PPy membranes. As a consequence of this research, transport of small organic molecules through PPy membranes, as a result of applying electrical stimulation to the surface of the membrane, was investigated by Mirmohseni *et al* [182].

Research was also undertaken to study the permeation of gaseous and volatile reagents across PPy coated membranes [183] and it was revealed that the redox status of PPy had a significant effect on the conducting polymer permeation properties. Higher transition rate was achieved at reduced state of conducting polymer compared to the oxidizing state [175,176]. Another conducting polymer called polyaniline (PAni) as well as PPy free-standing membranes were fabricated to study the separation of gas [184-186]. A novel technique to improve gas separation using a PAni coated membrane was reported that involved subsequent dedoping/doping processes which caused permanent morphological structural changes in the surface of conducting polymer membranes.

1.6.2.2 Fabrication and characterization of conducting polymer membranes

Fabrication of conducting polymer coated membranes is the same as Syntheticesise process of conducting polymer films. Either chemical or electrochemical methods can be utilized to prepare these membranes. However, some effective factors such as uniformity, mechanical property, electrical conductivity and electroactivity must be monitored and considered while the polymerization process is being held. Also

characterization of conducting polymer coated membranes is similar to characterization methods of conducting polymer films.

1.6.2.3 Electrochemically controlled transport through conducting polymer coated membranes

Permeability changes of the polymer coated membrane occur due to differences in densities and charges of the CP in oxidation and reduction state [187]. *In situ* electrochemical stimulation of these membranes has been carried out to evoke their appropriate chemical and physical responses such as ion-exchange that result in the desired physical responses such as changes in their hydrophobic/hydrophilic properties. These particular properties are very useful in terms of designing, fabricating and operating the intelligent electrodynamic membranes for a variety of applications, and especially controlled drug delivery systems (the main focus of this thesis). An electrical field can cause swelling, shrinking or bending in CPs [188].

The transition of biomolecules and charged species through electroactive CP coated membranes is influenced by a range of different processes with the redox state of CP being a major contributing factor. The redox switching property of a CP coated membrane largely depends on the nature of the incorporated counterion. Other influencing factors are diffusion phenomenon which occurs in the solution and across the membrane. Ion insertion/expulsion during the transport experiment happens as a result of diffusion and electrochemical properties of the conducting polymer membrane. There are some effective factors which dictate the diffusion such as diffusion coefficient, density and chemical potential of the ion, velocity of the fluid, mass density, pressure and viscosity of the fluid. Also, osmotic, magnetic and electrostatic forces as well as antiparticle interactions can control the diffusion process [189]. In addition, empirical studies about polymer base membranes have revealed that permeability of a membrane is a function of the selectivity of that membrane [190, 191].

Whilst the membrane type and the CP growth conditions all have an influence of ion transport through the membrane another influencing factor is the application of an

electrical stimulation to the CP membrane. As discussed above electrical stimulation evokes a wide range of changes within the CP that in turn has a profound effect on the transport kinetics. Figure 1.21 presents a diagram of different electrostimulation methods that can be utilized to stimulate the surface of conducting polymer coated intelligent membranes. In addition to the stimulation properties other factors such as the electrochemical cell set up and design need to be considered. The combination of all of these elements and circumstances contributes to the final performance of the transport through the intelligent membrane system [179].

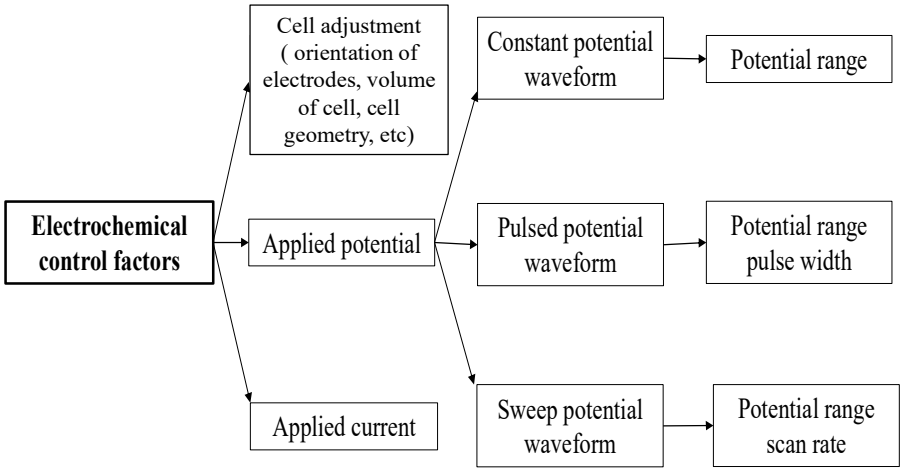

Figure 1.20 Effective factors on electrochemically transport across intelligent conducting polymer coated membrane

1.7 References

1. M.F Bennewitz, W.M Saltzman, Neurotherapeutics, 2009. **6**(2): 323-336.

2. X.D Tiege, H laufos, S.G Boyd, W Harkness, P.J Allen, C.A Clark, A Connelly, J.H Cross, Epilepsia, 2007. **48**: 385-389.
3. R.S Fisher, B.W van Emde, W Blume, C Elger, P Genton, P Lee, J Enge, Epilepsia, 2005. **46**(4): 470-472.
4. A Alkan, E Koklukay, A Subasi, J NeuroSci Meth, 2005. **148**(2): 76-167.
5. *Epilepsy*. 2012 [cited 2012; Fact Sheet No 999]; http://www.who.int/mediacentre/factsheets/fs999/en/ .
6. C.D Ferrie, J.H Livingston, EJPN, 1997. **1**(5-6): 139-147.
7. O Dulac, Epilepsia, 2001. 42(3): 23-26.
8. *Avoiding triggers for epileptic seizures*. 2014 [cited 2014 12.8.2014]; http://www.betterhealth.vic.gov.au/bhcv2/bhcarticles.nsf/pages/epilepsy].
9. A.K Sharma, E Rani, A Waheed, S.K Rajput, J Epilepsy Res, 2015. **5**(1): 1-8.
10. *How VNS Therapy works*. 2014 [cited 2014 12.8.14]; http://us.cyberonics.com/vns-therapy/how-vns-therapy-works].
11. *Ketogenic Diet*. 2014 [cited 2014 12.8.2014]; http://www.epilepsy.com/learn/treating-seizures-and-epilepsy/dietary therapies/ketogenic-diet].
12. A.J Hlliday, G.G Wallace, M.J Cook, Adv. Drug Delive. Rev, 2012. **64**(10): 953-964.
13. T.J Cook, V.C Yang, IJP, 1997. **159**(2): 197-206.
14. M.P Ratnaparkhi, J.P Gupta, IJPR, 2013. **2**(3): 11-21.
15. N Dixit, S.D Maurya, B.P.S Sagar, IRPB, 2013. **1**(3): 305-310.
16. A.G Hughes, Nanomedicine, 2005. **1**: 22-30.
17. A.H Shojaei, J. Pharmacy and Pharmaceutical Sci, 1998. **1**(1): 5-30.
18. R.J Tamargo, J.I Epstein, M.B Yang, M Chasin, H Brem, Cancer Res, 1993. **53**: 329-333.
19. R Langer, J.T Santini, A.C Richards, R Scheidt, Chem. Int. Ed, 2000. **39**: 2396-2407.
20. F Martin, A Boiarski, JCR, 2005. **102**: 123-133.
21. E Oby, D Janigro, Epilepsia, 2006. **47**(11): 1761-1774.
22. A Nayak, D.B Das, Biotechnol Lett, 2013. **35**:1351–1363.
23. S Sharma, P.M Sinha, R.J Walczak, X Liu, M.C Cheng, M Ferrari, Expert Opin. Drug Deliv., 2006. **3**(3): 379-394.
24. R.K Verma, S Garg, J Pharm Pharmacol, 2001. **25**(2): 1-14.

25. N Rajgor, M Patel, V.H Bhaskar, Syst. Rev. Pharm, 2011. **2**(2): 91-95.
26. P.E Grimshaw, M.L Yarmush, 1992: Oxford University Press, New York, NY, USA.
27. R.L Juliano, 1980: Oxford University Press, New York, NY, USA.
28. D.E Wurster, *Wurster Air Diverter*. 1953: US.
29. C.P Mc Coy, J.F Cowley, S.M Mcglinchey, N Mcgoldrick, D.J Kinnear, G.P Andrews, D.S Jones, Expert Opin. Drug Deliv, 2010. **7**(5): 605-616.
30. T.M Allen, P.R Cullis, Drug. Deliv. Sys, 2004. **303**(5665): 1818-1822.
31. P Broz, J Ziegler, Nano Letters, 2006. **6**(10): 2349-2353.
32. T Traite, R Goldbart, J Kost, J. Biomater. Sci. Polymer Edn, 2008. **19**(6): 755-767.
33. D.R Freestone, D.B Grayden, E & B, 2011. **22**(S): 110-118.
34. N Bhattarai, M.Q Zhang, Adv. Drug Deliv. Rev, 2010. **62**(1): 83-99.
35. Y Zhong, L Zhang, D.T Haynie, Nanomed. Nanotech. Biol. Med, 2007. **3**(2): 154-160.
36. W.K Wan, D.T Padavan, NanoMed, 2007. **2**(4): 483-509.
37. C.K Kim, E.J Lee, IJP, 1992. **79**(1-3): 11-19.
38. M.T Maeda, A Sano, K Fujioka, JCR, 1999. **62**(3): 313-324.
39. R Herrero-Vanrell, M Alonso, V Reboto, I.T Molina-Martinez, J.C Rodriguez-Cabello, JCR, 2005. **102**(1): 113-122.
40. H Eroglu, L Oner, Drug. Dev. Ind. Pharm, 2007. **33**(3): 265-271.
41. A.K Bajpai, S Bhanu, S Kankane, Prog. Plym. Sci, 2008. **33**(11): 1088-1118.
42. H Shirakawa, A.G Macdiarmid, C.K Chiang, A.J Heeger, Chem. Soc, Chemical comunications, 1977. **16**: 578-580.
43. W Greatbatch, C.F Holmes, IEEE. Eng. Med. Biol. Mag. , 1991. **10**(3): 38-49.
44. P.J Blackshear, P.L Blackshear, R.L Varco, H Buchwald H, Surg. Forum 1970. **21**: 136-137.
45. P.J Blachshear, F Prosl, H Buchwald, Med. Prog. Tech, 1979. **6**:149-161.
46. W.M Rupp, P.J Blackshear, H.B Mccarthy, T.D Rohde, Engl. J. Med, 1982. **307**: 265-270.
47. A.J Salkind, B.V Berkovits, B.B Owens, K.B Stokes, M Bilitch, 1986: Plenum Press, New York, NY, USA.

48. C.D Saudek, H.A Pitt, K Waxman, M Rubio, Engl. J. Med., 1989. **321**: 574-579.
49. H Fogel, P.R Eaton, P Micossi, J.L Selami, Rev. Euro. Technol. Biomedicale 1990. **12**: 196.
50. M Danckwerts,A Fassihi, Drug Dev. Ind. Pharm, 1991. **17**(11): 1465-1502.
51. E.A.H Hall, EMT, 1986. **8**(11): 651-658.
52. M.B Yang, R.J Tamargo, H Brem, Cancer Res, 1989. **49**: 5103-5107.
53. S.W Kim, Y.H Bae, T Okano, Pharm Res, 1992. **9**(3): 283-290.
54. A.D Emanuele, J.N Staniforth, Pharm. Res, 1991. **8**: 913-918.
55. K.F Lawrence, W.M Saltzman, Adv. Drug Del. Rev, 1997. **26**: 209-230.
56. S Sershen, J West, Adv. Drug Del. Rev, 2002. **54**: 1225-1235.
57. M.J Schoening, R Otto, F Johnen, Electroanalysis, 2000. **12**(9): 703-715.
58. J Wang, Talanta, 2002. **56**: 223-231.
59. P.C Simpson, A.T Woolley, R.A Mathies, Biomed Microdevices, 1998. **11**: 7-26.

60. Sh Liu, A Guttman, Trends Analyt. Chem, 2004. **23**(6): 422-431.
61. A.T Woolley, A.N Glazer, R.A Mathies, Anal. Chem. , 1998. **70**: 684-688.
62. J.R Lewis, Oosterbroek. 2003: Elsevier, New York, NY, USA.
63. D.L Polla, A.G Erdman, W.P Robbins, D.T Markus, J Diaz-Diaz, R Rizq, Y Nam, H.T Brickner, Annu. Rev. Biomed. Eng, 2000. **2**:551–576.
64. R.G.J Hadgraft. 1989: , New York, NY, USA.
65. H.M Smith. 1995: CRC Press, Boca Raton, FL, USA.
66. B.G Amsden, M.F.A Goosen, AIChE J, 1995. 41(8): 1972-1997.
67. S Henry S, M.G Allen, M.R Prausnitz MR, J. Pharm. Sci. , 1998. **87**: 922-925.
68. Sh Kaushik, A.H Hord, D.D Denson, D.V McAllister, S Smitra, M.G Allen, M.R Prausnitz, Anesth Analg. , 2001. **92**: 502-504.

69. D.V McAllister, M.G Allen, M.R Prausnitz, Annu. Rev. Biomed. Eng, 2000. 2:289–313.

70. L Lin , A.P Pisano, J. Microelectromech. Syst. , 1999. **8**(1): 78-84.

71. T Patois, B Lakard, N Martin, P Fievet, Synt Met, 2010. 160(19-20): 2180-2185.

72. S Sharma, A.J Nijdam, P.M Sinha, R Walczak, X Liu, M M-C Cheng, M Ferrari, Expert Opin. Drug Deliv, 2006. 3(3): 379-394.

73. J.T Santini, M. J. Cima, R Langer, Nature, 1999. **397**: 335-338.

74. T.A Desai, D.J Hansford, M Ferrari, Biomol. Eng, 2000. **17**: 23-36.

75. W Chu, T Huen, J Tu, M Ferari, SPIE, 1996. **2978**: 111-122.

76. W.H Chu, T Huen, M Ferrari, J. Microelectromech. Syst, 1999. **8**: 34-42.

77. J.K Tu , R Szema, M Ferrari, Biomed. Microdev, 1999. **1**(2): 113-120.

78. T.A Desai, D.J Hansford, L Kulinsky, A.H Nashat, G Rasi, J Tu, Y Wang, M Zhang, M Ferrari, Biomed Microdevices, 1999. **2**(1): 11-40.

79. M Ferrari, W.H Chu, T Desai, D Hansford, T Huen, G Mazzoni,M Zhang, Proc. MRS, 1996. 414: 101-106.

80. T.A Desai, D.J Hansford, L Leoni, M Essenpreis, M Ferrari, Biosens. Bioelectron, 2000. **15**: 453-462.

81. R Walczak, A Boiarski, T West, J Shapiro, S Sharma, M Ferrari, Nanobiotech, 2005. **1**(1): 35.

82. K.R Kidd, D.P Dal Ponte, R.S Kellar, S.K Williams, J. Biomed.Mater. Res, 2002. **59**(4): 682-689.

83. P.M Sinha, G Valco, S Sharma, X Lui, M Ferrari, Nanotechnology, 2004. **15**: 585-589.

84. Global drug delivery: Industry profile. Datamonitor, 2003. Available at http://www.datamonitor.com.

85. L.A Clark, G.T Ye, R.Q Snurr, Phys. Rev. Letter, 2000. **84**: 2893-2896.

86. Q Wei, C Bechinger, P Leiderer, Science, 2000. **287**: 625-627.

87. B Lin, J Yu, S Rice, Phys. Rev. E Stat. Phys. Plasmas Fluids Relat. Interdiscip. Topics, 2000. **62**(3 Pt B): 3909-3919.

88. C Consentino, F Amato, R Walczak, A Boiarski, M Ferrari, J. Phys. Chem. B. 2005. **109**(15): 7358-7364.

89. J.K Tu, T Huen, R Szema, M Ferrari, Biomed. Microdev, 1999. **1**(2): 113-120.

90. V.V Ranade, M.A Hollinger, CRC Press, Inc., Boca Raton, FL, USA, 1996.

91. G.B Lesinski, S Sharma, K Varker, P Sinha, M Ferrari, W.E Carson, Biomed. Microdev, 2004. **6**(3): 183-190.
92. T.A Desai, D Hansford, M Ferrari, J. Memb. Sci, 1999. **159**: 221-231.
93. F Martin, R Walczak, A Boiarski, J. Control. Release, 2005. **102**: 123-133.
94. F.J Martin, C Grove, Biomed Microdevices, 2001. **3**(2): 97-108.
95. G.B Lesinski, K Varker, P Sinha, M Ferrari, W.E Carson, Biomed Microdev, 2004. **6**(3): 183-190.
96. S Sharma, P.M Sinha, R.J Walczak, X Liu, M M-C Cheng, M Ferrari, Expert Opin. Drug Deliv, 2006. **3**(3): 379-394.
97. R Walczak, T West, J Shapiro, S Sharma, M Ferrari, Nano. Bio. Tech, 2005. **1**(1): 35.
98. P.M Sinha, S Sharmam, X Lui, M Ferrari, NanoTech, 2004. **15**(S): 585-589.
99. G.B Lesinski, K Varker, P Sinha, M Ferrari, W. E Carson, Biomed Microdev, 2004. **6**(3): 183-190.
100. F Martin, R Walczak, A Boiarski, M Cohen, T West, C Cosentino, M Ferrari, JCR, 2005. **120**: 123-133.
101. C.K Chiang, Y.W Park , A.J Heeger, H Shirakawa, E.J Louis, S.C Gau, A.G MacDiarmid, Phys. Rev. Letters, 1977. **39**(17): 1098-1101.
102. P.R Teasdale, M.J Spencer, G.G Wallace, Electroanal, 1989. 1:541.
103. W Zheng, A.G MacDiarmid, M Angelopoulos, Y Liao, A.J Epstein, Synthetic.Met, 1997. **84**: 63.
104. J Stejskal, J Prokes, J Zemek, Synt Met, 1999. **105**: 195.
105. Z Huang, A.G MacDiarmid, Y Xia, G Whitesides, Langmuir, 1997. **13**: 6480.
106. L.A.P Kane-Maguire, I.D Norris, G.G Wallace, W Zheng, Synt Met, 1999. **106**: 171.
107. R.V Gregory, W.C Kimbrell, H.H Kuhn, Synt Met, 1989. **28**(C): 823.
108. S.P Armes, J.G Beery, F Garzon, C Mombourquette, M Hawley, H.H Kuhn, J. Mater. Chem, 1991. **1**: 525.
109. S.W Byun, S.S Im, Polymer, 1998. **39**(2): 485-489.
110. D.S Kelkar, N.V Bhat, Polymer, 1993. **34**(5): 986-989.
111. B Zinger, D Kijel, Synt Met, 1991. **41-43**: 1013-1023.
112. S Pouzet, A Richard, F Jousse, Synt Met, 1993. **55**: 1079.
113. Sh Yang, E Ruckenstein, Synt Met, 1993. **60**: 249-254.

114. A Mohammadi, O Inganas, J.O Nilsson, I Lundstrom, J. Polym. Sci. Part A. Polym. Chem, 1994. **32**: 495.
115. T Iyoda, K Honda, T Simidzu, Macromol, 1990. **23**: 1971.
116. N.S Sariciftci, D Braun, C Zhang, V.I Srdanov, A.J Heeger, G Stucky, F Wudl, Appt. Phys. Lett, 1993. **62** (6): 585-587.
117. Y.A Dubitsky, B.A Zhubanov, Synt Met, 1993. **53**: 303.
118. U Geibler, M.L Hallensleben, L Toppare, Adv. Mater, 1991. **3**: 104.
119. S Dogan, U Akbulut, L Toppare, Synt. Met, 1992. **53**: 29-35.
120. Y.H Park, J. Appl. Polym.Sci, 1973. **45**: 992.
121. H Okuzaki, T Kira, T Kunugi, J.Appl. Polym.Sci, 2000. **75**: 566-571.
122. S.J Pomfret, N.P Comfort, A.P Monkman, Polymer, 2000. **41**: 2265.
123. H Sirringhaus, R.H Friend, T Shimida, M Inbasekaran, W Wu, E.P Woo, Science, 2000. **290**: 2123.
124. Y Yoshioka, G.E Jabbour Synt Met, 2006. **156**: 779.
125. O Ngamna, A.J Killard, S.E Moulton, M.R Smyth, G.G Wallace, Langmuir, 2007. **23**: 8569.
126. B Winther-Jensen, P Subramanian, R Helmer, S Ashraf, G.G Wallace, L Spiccia, D MacFarlane, J.Appl. Polym.Sci, 2007. **104**: 3938.
127. W.R Small, G.G Wallace, M in het Panhuis, J. Mat. Chem, 2007. **17**: 4359.
128. B Guo, L Glavas, A.C Albertsson, *Prog. Polym. Sci,* 2013. **38** (9): 1263-1286.
129. G.G Wallace, M.J Higgins, R.M.I Kapsa, *Organic Bionics*. 2012.
130. G.G Wallace, L.A.P Kane-Maguire, P.R Teasdale, ed. third. 2009: CRC Press.
131. C.H Wang, C.L Wang, J Zoval, M Madou, Electroactive Plym. Actu. Dev, 2004. **5385**: 468-474.
132. A.F Diaz, K.K Kanazawa, G.P Gardini, J.C.S. Chem. Comm, 1979 : 635-636.
133. K Kontturi, P Pentti, G Sundholm, J. Electroanal. Chem, 1998. **453**(1-2): 231-238.
134. X.D Wang, X.S Gu, C.W Yuan, S.J Chen, P.Y Zhang, T.Y ZhangJ Yao, F Chen, G Chen, J. Biomed. Mater. Res, 2004. **68A** (3): 411-422.
135. P.M George, A.W Lyckman, D.A Lavan, A Hegde, Y Leung, R Avasare, C Testa, P.M Alexander, R Langer, M Sur. Biomater, 2005. **26** (17): 3511-3519.

136. D.D Ateh, H.A Navsaria, P Vadgama, J. R. Soc. Interface, 2006. **3** (11): 741-752.
137. K.K Kanazawa, R.H Geiss, W.D Gill, J.F Wak, J.A Logan, J.F Rabolt, G.B Street, J.C.S. Chem. Comm, 1979: 854-855.
138. K.J Kim, D.E Whiley, A.G Fane, J. Membr. Sci, 1993. **80**: 241-249.
139. W.R Bowen, R.S Kingdon, H.A.M Sabuni, J. Membr. Sci, 1989. 40: 219-229.
140. J.M Fonner, L Forciniti, H Nguyen, J.D Byrne,Y.F Kou, J Syeda-Nawaz, C.E Schmidt, Biomed. Mater, 2008. 3(3): 034124.
141. T.V Vernitskaya, O.N Efimov, Russ. Chem. Rev, 1997. 66(5): 443-457.
142. S Sadki, N Brodie, G Sabouraud, Chem. Soc. Rev, 2000. **29**(5): 283-293.
143. W.R Salaneck, Synt Met, 1983. 5(2): 125-139.
144. W.K Ford, C.B Duke, W.R Salaneck, J. Chem. Phys, 1982. 77(10): 5030-5039.
145. J.L Brédas, B Thémans, J.M André, Phys. Rev-B, 1983. 27(12): 7827-7830.
146. J.M Andre, J.L Bredas, Phys. Rev-B, 1983. 27(12): 7827-7830.
147. J.L BrLdas, G.B Street , Acc. Chem. Res, 1985. 18(4): 309-315.
148. A.G MacDiarmid, Angew. Chem. Int. Ed, 2001. 40:2581-2590, 2001.
149. K Kontturi, P Pentti, G Sundholm, Electroanal. Chem, 1998. 453(1-2): 231-238.
150. N.K Guimard, N Gomez, C.E Schmidt, Prog. Polym. Sci, 2007. 32(8-9): 876-921.
151. B.K Beyreuther, C Heers, N Krebsfanger, U Scharfenecker, T Stohr, CNS Drug Rev, 2007. **13**(1): 21-42.
152. B Zinger, L.L Miller, J. Am. Chem. Soc, 1984. 106(22): 6861-6863.
153. L.E Guselnikov, N.S Nametkin, Chem. Rev, 1979. 79(6): 529-577.
154. N Gomez, C.E Schmidt, BJP, 2006. 81A(1): 135-149.
155. D Gea, X Tian, R Qi, S Huang, J Mu, Sh Hong, Sh Ye, X Zhang, D Li, W Shi, Electrochemica Acta, 2009. 55: 271-275.
156. D Svirskis, J Travas-Sejdic, S Garg, J. Chromatogr. Sci, 2011. 49(10): 780-785.
157. B.C Thompson, S.E Moulton, J Ding, R Richardson, A Cameron, S O'Leary, G. G Wallace, G.M Clark, JCR, 2006. **116**: 285-294.

158. R.T Richardson, B.C Thompson, B.O Flynn, P. J Atkinson, N.J Fretwell, J.B Fallon, G.G Wallace, R.K Shepherd, G.M Clark, S.J O'leary, Biomat, 2009. **30**: 2614-2624.
159. M Mulder, 1991: Kluwer Academic Publishers, Dordrecht, Boston, London.
160. J.E Shriver, D.P Dikhhaut, 1987: John Whiley and sons Inc., New York.
161. N Lakshminarayanaiah, 1984: Academic Press, U.S.A.
162. K.C Khulbe, T Matsuura, Syn. Plym Memb. 2008: Springer.
163. K.T Chen, Bull. Amer. Math. Soc,1977. 83:831-879.
164. W Pusch, A Walch, J. Membr. Sci, 1982. 10(2-3): 325-360.
165. N Lakshminarayanaiah, 1969: Academic Press, New York.
166. D.W Van Krevelen, K.T Nijenhuis, 1987: John Whiley and sons Inc., New York.
167. J Jabs, C.M Devine, J Sobal, 1991: Plenum press, New York, USA.
168. H Budka, C.A Wiley, P Kleihues, J Artigas, 1991: John Wiley, New York, USA.
169. R.H Fish, J.J Komlenic, Anal.Chem, 1984. 56(3): 510-517.
170. A Diaz, *Handbook ofconducting polymer*, ed. E.T. Kotheim S. 1986.
171. W Erkang, D Shaojun, D Jie, J. Chemm. Soc. Faraday Trans, 1990. **86**: 2243-2247.
172. E Wang, Y Liu, Z Samec, C Dvorak, Electroanalysis, 1990. 2(8): 623-629.
173. I.H Loh, R.A Moody, J.C Huang, J. Membr. Sci, 1990. 50(1): 31-49.
174. T Shimidzu, A Ohtani, T Iyoda, K Honda, J. Electroanal.Chem, 1987. 224:123–135.
175. P Burgmayer, R.W Murray, J. Am. Chem. Soc, 1982. 104(22): 6140-6142.
176. P Burgmayer, R.W Murray, J. Phys. Chem, 1984. 88(12): 2515-2521.
177. Y.C Liu, B.J Hwang, Thin Solid Films, 1999. 339(1-2): 233-239.
178. H Zhao, P.R Teasdale, G.G Wallace, Reactive Plym, 1994. **23**: 213.
179. A Mirmohseni, W.E Price, G.G Wallace, H Zhao, J. Intell. Mater. Syst. Struct, 1993. 4: 43-49.
180. D Zhou, W.E Price, G.G Wallace, J. Membr. Sci, 1995. **98**: 173-176.
181. H Zhao, C.O Too, G.G Wallace, D Zhou, J. Membr. Sci, 1996. **119**: 199-212.
182. A Mirmohseni, W.E Price, G.G Wallac, H Zhao, J. Intell. Mater. Syst. Struct, 1993. 4(1): 43-49.
183. V.M Schmidt, J Heitbaum, Synt Met, 1991. 41-43: 425-428.

184. M.R Anderson, B.R Mattes, H Reiss, R.B Kaner, Synt Met, 1991. 41(1151):41-43.
185. M.R Anderson, B.R Mattes, H Reiss, R.B Kaner, Sicence, 1991. 252(5011): 1412-1415.
186. K Kamada, A Motonaga, T Iwasaki, H Hosokawa, J. Polymer, 1994. **26**(2): 141-149.
187. G Inzelt, *Conducting Polymers, Monographs in Electrochemistry*, 2012: Springer-Verlag Berlin Heidelberg.
188. F.C Carvalho, M.L Bruschi, R.C Evangelista, M.P.D Gremio, Braz. J. Pharm. Sci, 2010. 46(1):1-17.
189. M Tagliazucchi, I Szleifer, Materials. Today, 2015. 18(3): 131-142.
190. A.I Skoulidas, D.S Sholl, J.K Johnson, J. Chem. Phys, 2006. 124(054708): 1-7.
191. L.M Robeson, J. Membr.Sci, 1991. 62:165.

2 GENERAL EXPERIMENTAL

2.1 Chapter aims

The aim of this chapter is to outline the experimental techniques, characterization methods and materials which have been utilized throughout this thesis.

2.2 Materials

2.2.1 Pyrrole

Pyrrole monomer was purchased from Merck with >99% purification. The distillation process was performed out in the organic laboratory of Intelligent Polymer Research Institute (IPRI), and then stored under nitrogen at -18º C. Solutions of 0.2 and 0.1 M aqueous pyrrole with different dopants were prepared to perform all of the electropolymerization experiments. The concentration of dopant molecules and electropolymerization condition were different and are be present in the respective chapters. Paratoluene sulfonic acid sodium salt (*p*TS), chondroitin 4-sulphate sodium salt (CS), poly (4-styrene sulfonic acid) sodium salt (PSS), doddecylbenzeneslfonic acid sodium salt (DBSA), hyaluronic acid (HA) and dextran sulphate sodium salt (DS), were used as dopants to grow polypyrrole galvanostatistically. All of these chemicals were purchased from Sigma-Aldrich Pty. Ltd.

2.2.2 Lacosamide

Lacosamide with the generic name of Vimpat (SPM 927, (R)-2-acetamido-N-benzyl-3-methoxypropionamide) is a functionalized amino acid which has been synthesized to be used as anticonvulsive drug. This drug has demonstrates a significant effect on reducing seizure in animal models. Also, safety pharmacology and toxicity experiments conducted to examine lacosamide. Results showed that this drug in rats,

mice, rabbits and dogs was well tolerated[1]. The chemical structure of lacosamide with abbreviation of LCM is shown in Figure 2.1. To make a solution of this drug, artificial cerebrospinal fluid (ASCF) was prepared as media [2]. The preparation and dissolving of LCM in ACSF is explained in more detail in Chapter 3.

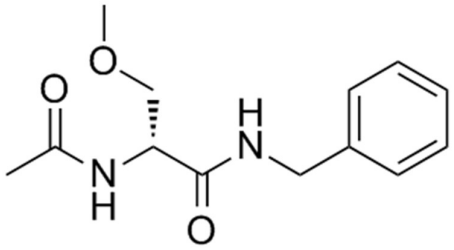

Figure 2.1 The chemical structure of Lacosamide (LCM) molecule.

2.3 Polymer Polymerisation

Several different growth cells were used to synthesis PPy throughout this thesis and all are based on the standard 3 electrode cell design. Figure 2.2 shows a typical 3 electrode polymerisation cell incorporating the working electrode (upon which PPy is deposited), counter electrode and the reference electrode.

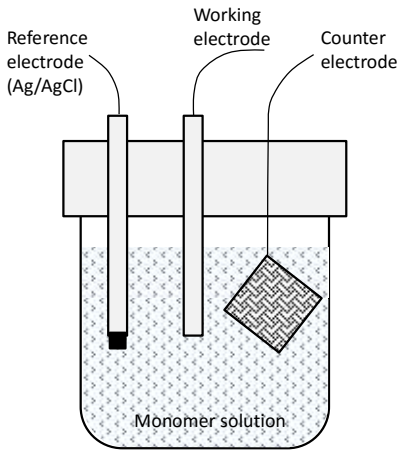

Figure 2.2 Three electrode cell used in the electropolymerisation of polypyrrole. The 3 electrode cell comprises of a working electrode, Pt mesh as auxiliary electrode and the Ag/AgCl reference electrode.

The growth cells and procedures used to polymerise PPy on the Pt/PVDF membranes described in Chapters 3 and 4 are detailed in the respective chapters.

All of the conducting polymer films were rinsed with excess amounts of Milli-Q water to remove oligomers, monomers and loosely bounded dopants. After that, these composite membranes were dried at room temperature.

2.4 Characterization techniques

2.4.1 Scanning electron microscopy (SEM)

Scanning Electron Microscopy (SEM) images of conducting polymer film surfaces were taken using a field emission SEM (JOEL JSM-7500FA). Figure 2.3 presents an image of this instrument. For flat PPy coated platinized PVDF membranes, SEM images from the surface and cross section were taken. Scanning electron microscopy (SEM) was used to observe the cross-sectional morphology of the membranes. The conducting polymer coated membranes were freeze fractured to expose the cross-section. Briefly, the membranes were immersed in liquid nitrogen and then cut using a sharp blade along their cross-sections. The membranes specimens were sputter coated with gold layer before observation using a field emission SEM (JOEL JSM-7500FA). X1,000, X6,000, X20,000 and X75,000 were used as magnification and also 5.0, 10 and 15 KV energy were utilized. The working condition of every SEM images have been taken is indicated inside of every images.

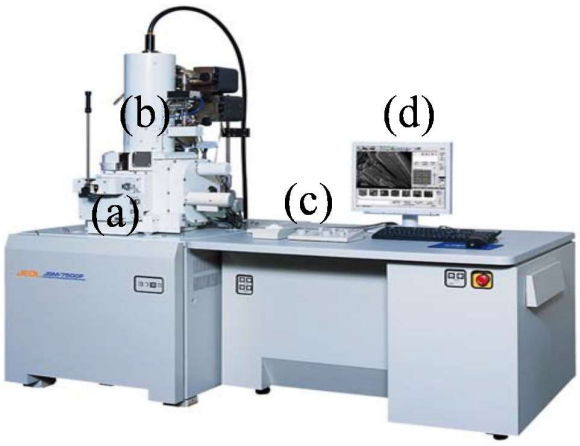

Figure 2.3 Scanning Electron Microscopy (SEM) instrument; (a) sample holder, (b) electron transmitter beam, (c) controller key pad, (d) accompanied PC which provides appropriate software.

2.4.2 Cyclic voltammetry

Cyclic voltammetry (CV) was used to investigate the electrochemical properties of the conducting polymer films which were grown on the surface of Pt/PVDF membranes. A three electrode electrochemical set up was used that contained a platinum mesh counter electrode, a Ag/AgCl reference electrode, and the conducting polymer films on the surface of platinized PVDF membranes as the working electrode. ACSF was utilized as the electrolyte and five cyclic voltammograms (CVs) were measured using an eDAQ e-recorder (v5.5.11) and potentiostat shown in Figure 2.4.

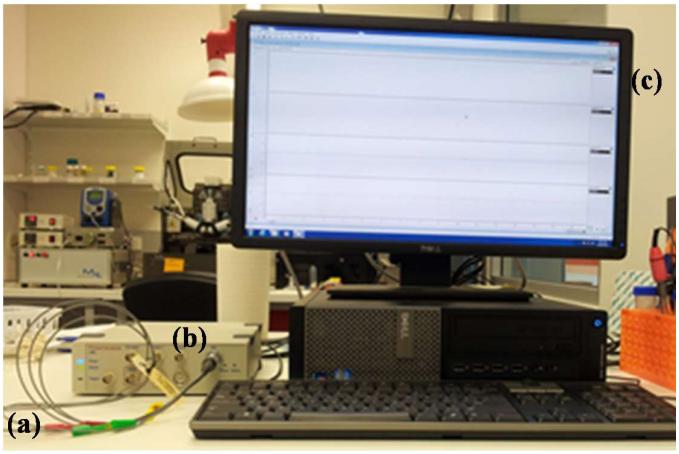

Figure 2.4 An eDAQ system; (a) electrode leads, (b) potentiostat box, (c) PC provides the required software.

When an applied potential is swept between an upper and lower potential at a constant rate, the generated current can be measured. This technique is called cyclic voltammetry (CV). Some other techniques including staircase voltammetry (SV) and differential pulse voltammetry (DPV) can be used to investigate the electrochemical experiment[2, 3]. However, CV is most extensively used. CV can provide some useful data such as number of oxidation states and the reversibility of them. This technique has been widely utilized to study the electroactivity of conducting polymers.

A rectangular generated current is observed for a non-faradaic experiment. Non-faradaic experiment happens when no electrode neither solution is associated with redox active species. For this experiment the CV curve shows sharp charging and discharging behaviour which is demonstrated in Figure 2.5. In Figure 2.5 arrows indicate the scan directions.

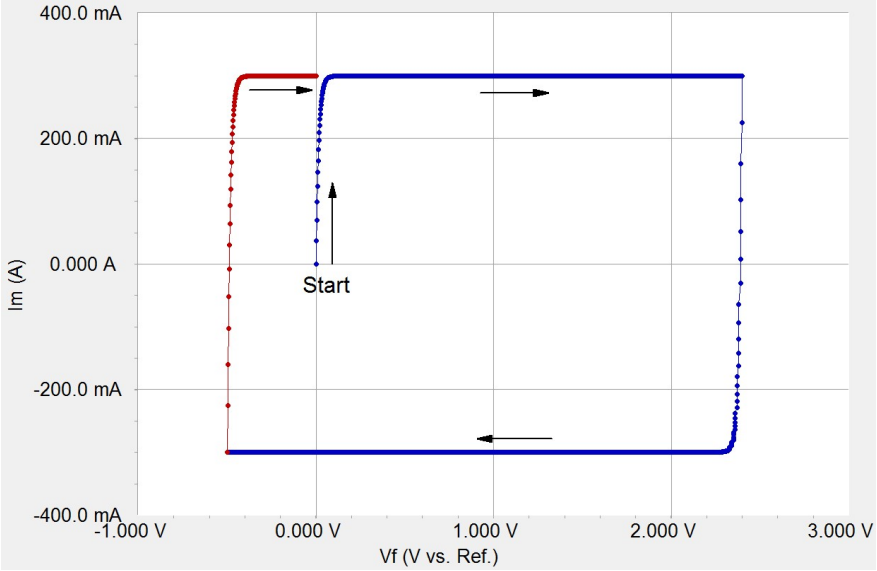

Figure 2.5 typical cyclic voltammograms of a non-faradaic response[4].

Figure 2.6 presents the typical CV of $Fe(CN)_6$. The redox reaction of this reagent is shown in the following equation[5];

$$Fe(CN)_6^{3-} + e^- \longrightarrow Fe(CN)_6^{4-} \qquad (2.1)$$

At point 1 in Figure 2.6 the initial applying potential is more negative than the required potential for the oxidation reaction to occur. By scanning the potential in the positive potential direction oxidation of the $Fe(CN)_6$ redox pieces in solution occurs at the electrode surface (point 3).. As the oxidising species becomes depleted at the electrode surface the oxidation current decrease as the potentials is continued to be scanned positively. The scan process is reversed at point 4and at a specific potential the oxidised redox species in the vicinity of the electrode surface is reduced and as the reducing species is depleted the current decreases.

For a completely reversible system which is shown in equation (2.1) the CV possesses identical oxidation and reduction peaks characteristics (i.e., amount of charge passed). Therefore, the ratio of reduction to oxidation (*i/i'*) peak current is 1 for fully electrokinetically reversible redox reaction. In this case the difference between reduction potential (*Ep*) and oxidation potential (*Ep'*) which is indicated by

ΔE in Figure 2.6 is 59.2 mV/n at room temperature. n is the number of transferred electrons in the redox reaction.

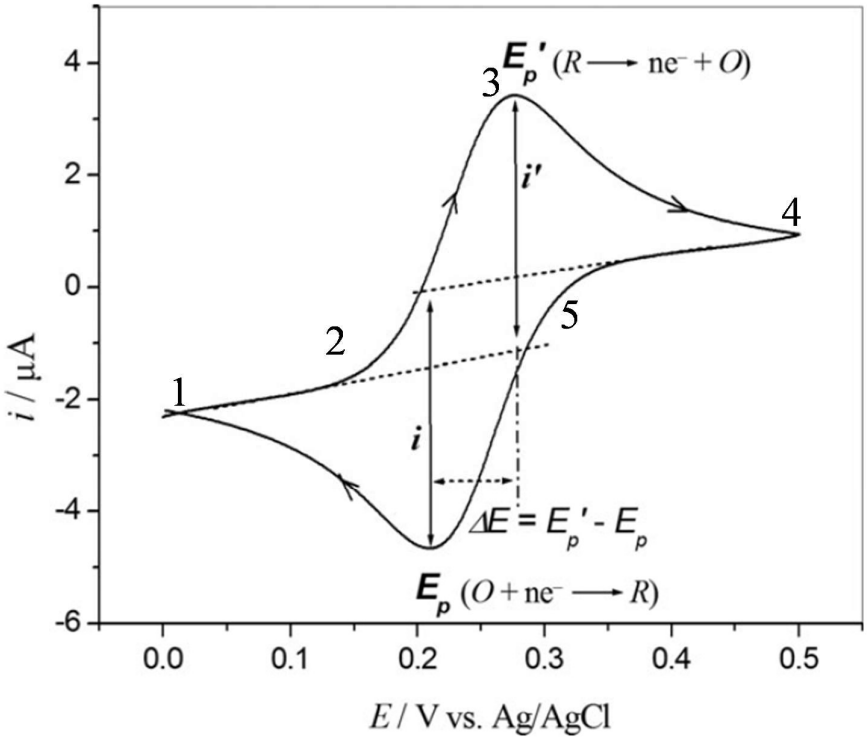

Figure 2.6 Typical cyclic voltammograms of a completely reversible redox reaction; *Ep* represents the reduction potential and *i* is the created current at this potential. *Ep'* is the oxidation potential and *i'* presents the created current through the oxidation process [5].

The capacitive behaviour of electrode can affect the CV[6]. The following equation presents the capacitive charging current;

$$i_c = dQ_c/dt = C_{dl}\, dE/dt = C_{dl}V \qquad (2.2)$$

Where i_c is the capacitive charging current, Q_c presents the amount of dielectric charge, the capacitance of double layer is C_{dl}, dE/dt (V) indicates the applied potential scan rate. C_{dl} can be change throughout the experiment. Therefore, i_c is not constant.

2.4.3 Goniometry

Measurement of solid-liquid (γ_{sl}) interfacial tensions is the consideration of a wide variety of issues in applied science[7]. Direct measurement of surface tension accompanied with some difficulties. Therefore, some indirect approaches have been utilized to estimate the tension between the liquid and solid phase [8-16]. Among all of the techniques, measurement of contact angle seems to be the simplest one.
The base of this method is measurement of the angle of a liquid droplet with a solid surface. In 1805 Yong[17] recognized a relation which makes it possible to estimate the estimating the solid surface tension from contact angle.

The mechanical equilibrium of the droplet with three interfacial tensions is the base of contact angle measurement. These three tensions are solid-vapour, γ_{sv}, solid-liquid, γ_{sl}, and liquid-vapour, γ_{lv} tensions. Figure 2.7 exhibits the schematic of a droplet contact angle.

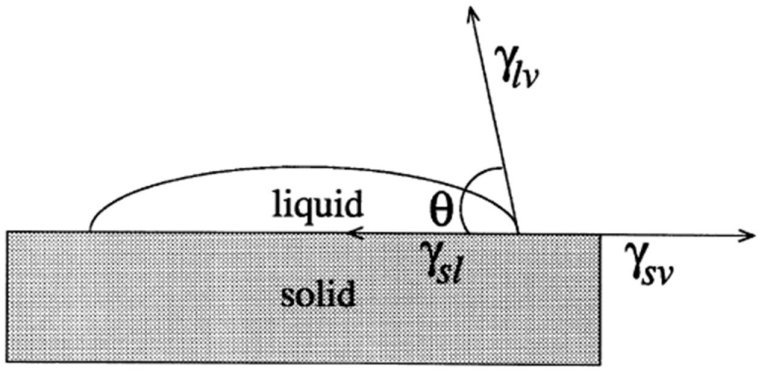

Figure 2.7 Droplet contact angle schematic; γsv is solid-vapour, γsl is solid-liquid, and, γlv is liquid-vapour tensions. θ presents the Yung contact angle.

The following equation is known as Young's equation and presents the equilibrium relation between three interfacial tensions;

$$\gamma_{lv}\cos\theta_Y = \gamma_{sv} - \gamma_{sl} \tag{2.3}$$

where θ_Y presents the Yung contact angle.

A Dataphysics optical contact angle goniometer was used to measure the mean static contact angle of the conducting polymer films. The volume of deionised water droplets of 1 µl for each reported value. Figure 2.8 (a) exhibits a schematic of contact angle.

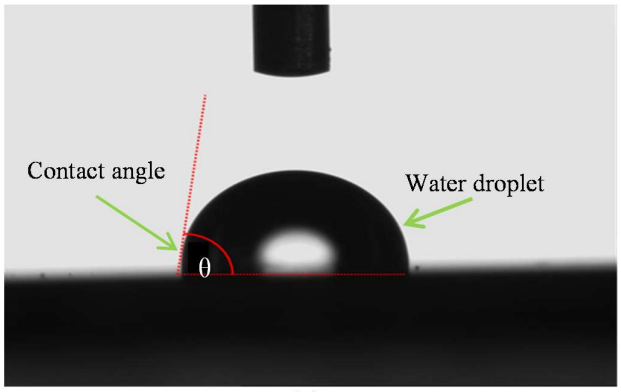

(a)

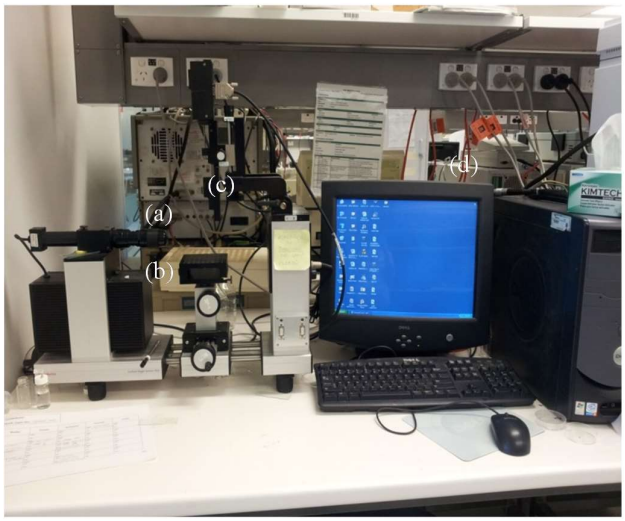

(a')

Figure 2.8 (a) schematic of measured angle of droplet on the OCP surface; (a') Dataphysics optical contact angle goniometer; (a) camera, (b) sample holder, (c) syringe, (d) PC provides the required software.

Figure 2.8 (a') shows the Dataphysics optical contact angle goniometer which has been used in thesis. Measuring the contact angles reveals any differences in wettability of the surface of OCPs.

2.5 High Pressure Liquid Chromatography (HPLC)

Chromatography is one of the most common methods which can be used in chemical analysis whereby different components of a mixture separate and the quantitative values of each component can be determined. The basis of separation is the variation in movement of each component through a column. HPLC relies on the pressure of mechanical pumps on a liquid solvent to carry a sample mixture into a column where separation occurs. A HPLC separation column is filled with solid particles such as silica, polymers, or sorbents. The sample mixture is separated into compounds as it interacts with the column particles. HPLC separation is influenced by the liquid solvent's condition like pressure and temperature and also chemical interactions between the sample mixture and the liquid solvent. Chemical interactions between the sample mixture and the solid particles packed inside of the separation column are the main reason of component separation. The chemical interaction occurs because of differences between the molecule polarity or affinity and ion exchange. Every HPLC instrument needs a digital microprocessor for controlling the HPLC components and user software. Figure 2.9 shows the Agilent HPLC system which has been used in this thesis. The concentration of transported and released lacosamide across the conducting polymer coated flat PVDF membranes and also PVDF tubes were measured using HPLC.

The mobile phase consisted of 65% distilled water, 26.2% acenotirile and 8.8% methanol. A C18 column was used as separation column with the flow rate of mobile phase set at 0.8 ml/min and detection wavelength was 210 nm.

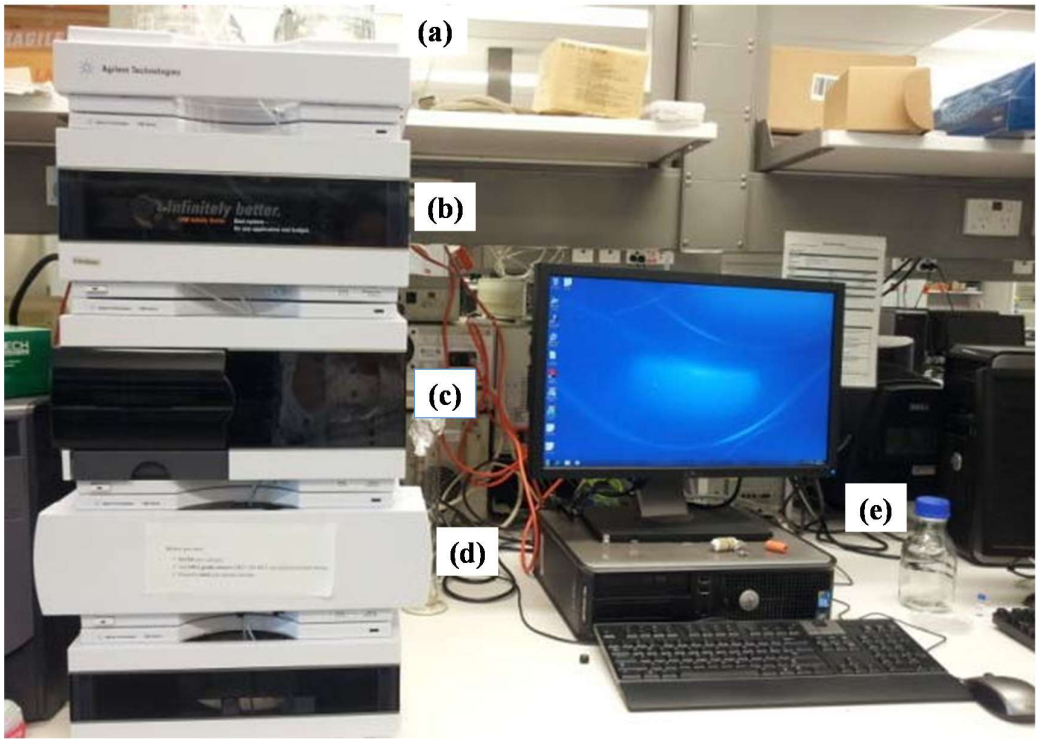

Figure 2.9 HPLC instrument; (a) Pump, (b) UV-VIS detector, (c) auto sampler, (d) column and (e) PC.

2.6 Quartz Crystal Microbalance (QCM)

The signal transition in quartz crystal microbalance (QCM) works on the basis of piezoelectric effect of a quartz crustal[18]. In 1880 the Curie brothers discovered the piezoelectric effect in quartz crystal via application of pressure on quartz[19]. Later Lord Rayleigh utilized the changes of the vibrating crystal inertia to shift the frequency (f) of its resonant[20]. Subsequently, some researches have been developed an appropriate stability of crystal while applying electric resonators[21] and also the stability of AT-cut crystals at room temperature[22]. Mostly for QCM applications, the thickness of quartz crystal is a few tenths of mm and cut with AT form by 35º 10′ angle with the Z-axis. With this geometry a stable oscillation without any frequency vibration at room temperature is provided. picture schematic of AT-cut quartz crystal is presented in Figure 2.10[23-25].

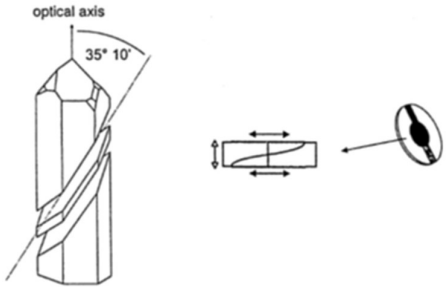

Figure 2.10 At-cut quartz crystal which is used to produce metal coated QCM sensor[18].

The QCM technique is an efficient and economical technique capable of sensing mass change at interface with very high resolution. QCM has sensitive solution-surface measurement ability suitable for analytical chemistry and electrochemistry applications. The detection range of this technique is much extended. For instance, a monolayer surface coverage which has been generated by very small molecules such as drug molecules or polymer films can be detectable using QCM instrument. Bounding of much bigger molecules such as protein molecules or biopolymers to the surface is also detectable by this technique. Furthermore, the energy dissipation properties of the adlayer are available using QCM. One of the special and unique characteristics of the QCM technique is the capability of mass measurement while conducting electrochemistry on the solution or upon the QCM crystal adlayer. These capabilities provide the feasibility of electropolymerization of an electroactive film or can enable ion or solute exchange between the adlayer and environment as a result of electrical stimulation which can be driven by the underlying surface potential.

In-situ polymerisation of conducting polymer films using the Q-Sense electrochemical cell provides physical and mechanical properties analyses by using QCM-D measurement parameters. Absorption of a material to the surface of the sensor electrode leads to a decrease in the sensor oscillating frequency. Where a pure elastic mass added to the surface, an explicit linear equation which known as Sauerbrey equation is utilized to accurately quantify the mass of added layer to the surface with ng sensitivity[26].

$$\Delta f = -2\Delta m f^2 / A(\mu\rho_q)^{0.5} = -C_f \Delta m \qquad (2.4)$$

Where Δf indicates the decrease in resonant frequency (Hz), f is the inherent frequency of quartz crystal, Δm shows the changes in elastic mass (g), A suggests the electrode area which equals to 0.196 cm^2 in many applications, ρ_q demonstrate the quartz crystal density (i.e. 2.65 g cm^{-3}), and finally μ represents the shear modulus which equals to 2.95×10^{11} dyn cm^{-2}. Putting all of these values results is C_f which is the integrated QCM sensitivity to have a value of 0.903 Hz/ng by having a ~ 9 MHz frequency of crystal. Therefore, QCM has a mass sensitivity which is 1000 times greater than an electronic mass balance. The electronic mass balance sensitivity is 0.1 µg. According to this unique mass sensitivity of QCM it can be called as a nano-balance. The Sauerbrey equation is just applicable for small molecules which form an elastic adlayer at the interface. Larger molecules generate a soft and viscoelastic adlayer with the mass which is more than 2% greater than quartz crystal mass. In these cases the Sauerbrey equation is not accurate. In this case more complicate models are required to calculate the amount of absorbed mass on the sensor surface.
The first use of QCM as a sensing mode was in 1959 when a linear relationship between f changes of oscillating quartz crystal and the mass of deposited metal was reported by Sauerbrey[26]. The mass binding of a gas to the surface of quartz crystal was the very early application of QCM for chemical analyses. For instance, this technique was utilized to study chemical sensors for moisture and volatile organic compounds [27, 28], environmentally pollutant reagents[29], and gas detectors[30]. An advanced QCM technique to measure frequency alterations of damping liquid media was developed in 1980s. In this case frequency changes were related to changes of viscosity and density of the liquid[31, 32].

Using QCM as a sensor for liquid phase measurements is not as simple as its other applications, such utilizing QCM as a gas phase sensor. However, utilizing QCM technique for this application provides important data regarding interactions and reactions which may occur at the liquid-solid interface. Despite its difficulties researchers have used the QCM technique to study depositing polymeric films; electrochemically generating polymeric films; creating biomacromolecular films incorporating protein molecules and nucleic acids as well as investigating biosensors including living cells[18, 33-43]. In all of these studies the adlayer does not behave as an elastic mass on the QCM sensor surface, therefore, as it has been mentioned

before, the Sauerbrey equation is not applicable. The versatility of the QCM technique is demonstrated in Figure 2.11 where the QCM is used to study cell attachment by placing the QCM system in a cell culture [44]. In this case, frequency (*f*) and yielding the motional resistance (*R*) at the interface of quartz crystal-solution were measured.

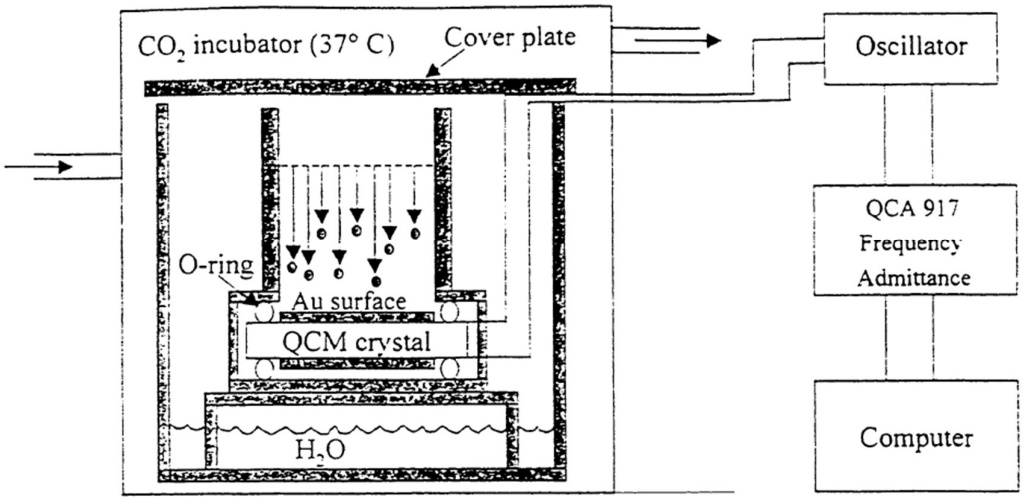

Figure 2.11 Schematic of a QCM crystal for investigating of cell attachment to the surface of QCM gold coated crystal in a cell culture incubator[44].

In developed and advanced QCM systems where samples are immersed in liquid the QCM system delivers the fluid to the QCM electrode surface via automated flow injection. This automated flow injection delivers very small volumes (i.e. μL) with constant flow rate to the QCM crystal surface with minimal effect on the QCM performance[45]. This capability has provided an opportunity for researchers to utilize the QCM technique to undertake the following biomedical studies: (a) generate and investigate biomimetic systems; (b) study a wide area of fundamental biochemical processes; (c) form biosensors by encapsulating of nucleic acids and proteins or even cells upon the quartz crystal surface or incorporated with a polymeric films which have been deposited on the QCM sensor; (d) study the interaction of drug molecules with the target surface for drug discovery applications[46-51].

QCM or quartz crystal microbalance technique has been utilized in this thesis to calculate the mass of absorbed lacosamide molecules to the surface of conducting

polymers. The Q-tools software package v.3.0.10.286 (Biolin Sci, AB) was utilized to apply Sauerbrey model to determine layer thickness of the conducting polymer and also absorbed mass layer.
Frequency responses of quartz crystal can be because of one of these following reasons or a combination of them such as firm bounding of an elastic mass to the Q-sense surface; or changing of viscosity-density of the aqueous solution and bounding mass in inelastic and dissipates the energy.

The *f* decrease changes due to dried mass absorption will be used to calculate the amount of mass with the assumption of dried mass density is used to calculate film thickness.

Interaction of an elastic mass with surface of oscillating quartz crystal leads to *f* decreasing changes and developed Sauerbrey model is utilized to calculate the amount of bounded mass to the surface which is the base of absorbed mass calculation in this thesis. The experimental protocol and detail of these experiments will be presented in chapter 5.

2.7 Profilometry Topography

Optical profilometry has been developed during last decades. This technique is utilized for surface roughness measurements. There are two types of profilometer; a stylus and laser type. Application of optical devices has some advantages such as, contact less scanning of the material which leads to avoiding any possible damage especially for the soft surface materials[52].

The surface roughness of the polymer films were examined by using a Veeko Wyko NT9100 optical profilometer (Figure 2.12). For each sample at least three measurements were carried out. To measure surface roughness of conducting polymer films Q-sense sensors were used since optical profilometer does not damage the quartz crystal.

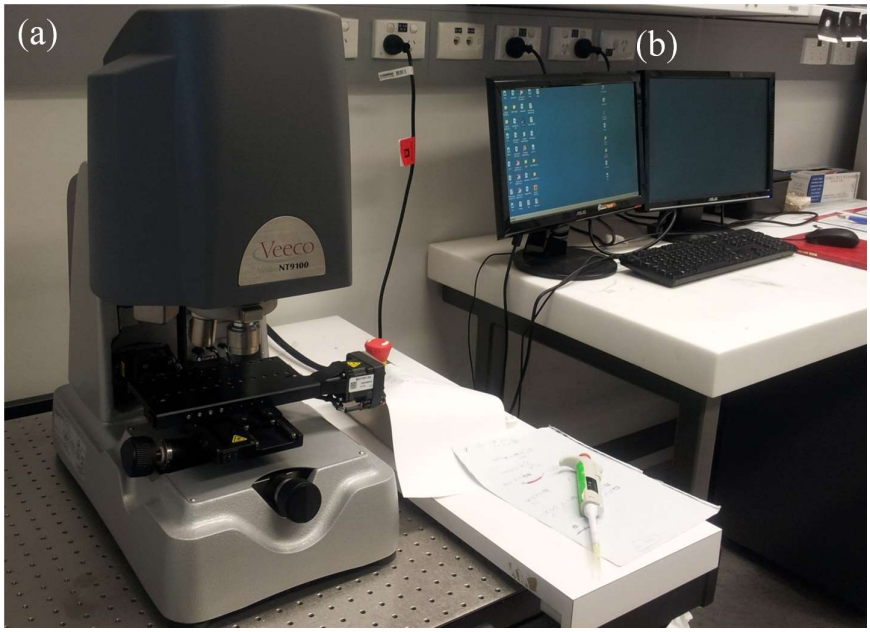

Figure 2.12 (a) optical profilometer; (b) PC provides the Veeco's Vision® analysis software.

2.8 References

1. B.K Beyreuther,C Heers, N Krebsf˙anger, U Scharfenecker,T St¨ohr, CNS Drug Rev, 2007. **13**(1): 21–42.
2. N.A Ralph, *Electrochemistry at soid electrodes*. 1969: New York.
3. A.W Bott, Current Sep., 1993. **12**(1).
4. B.E Conway, B.E., *Electrochemical Supercapacitors: Scientific Fundamentals and Technological Applications*. 1999: New York: Kluwer Academic Press/Plenum Publishers.
5. F Zhao, R.C.T Slade, J.R Varcoe, Chem. Soc.Rev, 2009. **38**: 1926-1939.
6. H.I Loh, J.C Haung, J. Membr. Sci. 1990 . **50**: 31-49.
7. D.Y Kwok, Adv. Colloid Interface Sci, 1999. **81**: 167-249.
8. B.V Derjaguin, Y.P Toporov, J. Colloid Interface Sci, 1980. **73**.
9. K.L Johnson, K. Kendall, A.D Roberts, Proc. R. Soc. Lond-A, 1971. **324**: 301-313.
10. V.M Muller, B.V Derjaguin, J. Colloid Interface Sci, 1983. **92**.
11. A Fogden, J. Colloid Interface Sci, 1990. **138**.
12. R.M Pashley, R.G Horn, B.W Ninham, J. Colloid Interface Sci, 1988. **126**.
13. H.K Christenson, J. Phys. Chem, 1986. **90**.
14. P.M Claesson, P.C Horn, B.W Ninham, J. Colloid Interface Sci, 1986. **14**.
15. P.M Pashley, Colloids Surf, 1987. **27**.
16. R.M Pashley, B.W Ninham, D.F Evans, Science, 1985. **229**.
17. T Young. Vol. 95. 1805: Philos. Trans. R. Soc. London.
18. K.A Marx, Bio Macromol, 2003. **4**(5):1109-1120.
19. J.C Curie, P Comput. Rend. Acad. Sci. Paris, 1880. **91**: 294-297.
20. P.T Buttry, J. Phys. Chem, 1987. **91** : 1292-1295.
21. W.G Cady, Phys. Rev, 1921. **17**:531-533.
22. F.R Lack, G.W Fair, Bell Syst. Technol, 1934. **13**: 453-455.
23. A.G Janshoff, H.J Steinem, C Angew. Chem., Int. Ed, 2000. **39**: 4004-4032.
24. C.K.G O'Sullivan, Biosens. Bioelectron, 1999. **14**:663-670.
25. K.D Pavey, Expert Rev. Mol. Diag, 2002. **2**:173-186.
26. G.Z Sauerbray, Phys, 1959. **155**: 206-222.
27. G.G Guilbault, Anal. Chem, 1983. **55**: 1682-1984.

28. W.H King, Jr. Anal. Chem, 1964. **36**:1735-1741.
29. G.G Guilbault, CRC Rev, 1988. **19**:1-28.
30. P.L Konash, Anal. Chem, 1980. **52**:1929-1935.
31. K.T Kurosawa, E Kamo, N Kobatake, Anal. Chim. Acta, 1990. **230**: 41-49.
32. T.O Nomura, Anal. Chim. Acta, 1982. **142**: 281-284.
33. J Wang, F Lu, J. Electroanal. Chem, 1998. **444**:127-133.
34. W Koh, D.D Kutner, M.T Jones, K.M Kadish, J. Phys. chem, 1992. **96**: 4163-4168.
35. K Takada, H.D Abruna, I Cuadrado, C Casado, B Alonso, M Moran, J Losada, J. Am. Chem. Soc, 1997. **119**:10763-10768.
36. J Tanguy, G Zalczer, G Lecayon, J. Electroanal. Chem, 1996. **417**: 175-184.
37. K.A Marx, R Sarma R, Biotechnol. Prog, 1999. **15**: 522-528.
38. D.D Long, T Zhou, J. Electroanal. Chem, 2001. **501**:107-113.
39. K.A Marx, T Sarma, J. Electroanal. Chem, 2002. **521**:53-60.
40. C.K Baker, J. Electroanal. Chem, 1988. **251**:307-312.
41. H Muramatsu, M Suda, T Sakuhara, T Ataka, J. Electroanal. Chem, 1992. **322**: 311-323.
42. N lasalle, T Livache, P Maillley, E Vieil, Talanta 2001. **55**: 993-1004.
43. G Bidan, K Galasso, T Livache, G Mathis, A Roget, L Torres-Rodriguez, E Vieil, Appl. Biochem. Biotechnol, 2000. **89**:183-193.
44. T Zhou, M Warren, H Schulz, S Braunhut, J. Biotechnol. Prog, 2000. **16**: 268-277.
45. M.M Tanaka, A Motomura, T Shimura, K Onishi, M Okahata, Colloids. Surf-A, 2001. **193**:145-152.
46. S Nakata, M Hayashi, M Hara, H Sasaba, T Sugawara, T Matsuda, Biophys. Chem, 1996. **62**:63-72.
47. F Hook, P Brzezinski, B Kasemo, Langmuir, 1998. **14**: 729-734.
48. O Sadik, Talanta, 2001. **55**: 929-941.
49. A.L Briseno, A.J Baca, F Zhou, J. Electroanal. Chem, 2001. **513**:16-24.
50. A Kobayashi, F Mizutani, Biotechnol. Biochem., 2001. **65**:2392-2396.
51. H Kaneda, T Kobayakawa, S Saiton, Y Okakata, J. Inst. Brew, 2000. **106**: 305-309.
52. M Visscher, K.G Struik, Precis Eng, 1994. **16**(3):192-198.

3 DRUG TRANSPORT STUDIES THROUGH CONDUCTING POLYMER COATED PLATINIZED PVDF FLAT MEMBRANE

3.1 Chapter aims

In this chapter we investigated the transport of the anti-epilepsy drug, lacosamide through polyvinylidene fluoride (PVDF) membranes. The aim is to develop a system whereby the membrane acts as a "gate" to mediate the transport of drug upon the application of an appropriate electrical stimulation protocol. The membranes used in this study have been coated in platinum and subsequently coated electrochemically with the conducting polymer, PPy using a range of dopants.

3.2 Introduction

The OCP polypyrrole (PPy) is routinely used in controlled drug delivery [1] due to its ease of synthesis from aqueous solutions and demonstrated [2]. There have been many reports published detailing the use of organic conducting polymers (OCPs) as novel drug delivery devices [3-8]. It is the ability for the OCP to incorporate a drug during synthesis and undergo subsequent reduction-oxidation (RedOx) process that facilitates the use of OCPs as drug delivery devices. In addition to drug delivery this simple redox switching facilitate the use of OCPs in application in actuators [9-11], electrochromics [12] and micro fluidic devices [13].

Whilst OCPs have shown to be suitable materials for drug delivery they also suffer from some limitations such as;

(i) inherently low drug loading levels,
(ii) passive loss of loaded drug molecules by diffusion,
(iii) poor control and unpredictability of the release kinetics and,
(iv) incomplete delivery of all incorporated drug.

Hence, One approach to overcome these limitation is by utilizing the OCP as a membrane in which drug can pass through from a drug loaded reservoir (Figure 3.1).

This membrane approach utilizes the OCP as a "gate" upon which drug can pass through. In this way the reservoir can be loaded with higher amounts of drug that can be otherwise be attained within the OCP film.

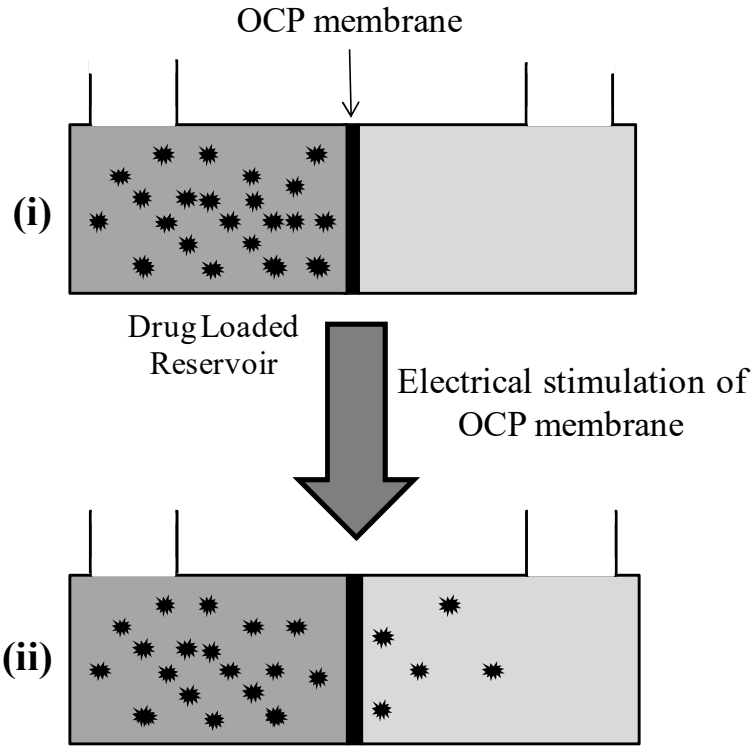

Figure 3.1 Schematic of drug transport through an OCP coated membrane via electrical stimulation of OCP membrane surface

Conducting polymer membranes have been reported previously [1, 2]. Most of these membranes were supported membranes due to the limited mechanical properties of the polymer. Burgmayer et al [1, 2] reported that the ionic resistance or ion permeability of a PPy membrane can be varied by changing the redox state of the membranes. The permeation rate through a PPy membrane in an oxidised state was found to be much higher than when in the reduced state. The use of OCP membranes to control the movement of a range of molecules has been reported previously [14-16]. Whilst the use of a polypyrrole (PPy) coated membrane was used to electrochemically control the transport of metal ions. Fan et al [1] demonstrated the use of an OCP membrane (Polyaniline) as a drug delivery system.

3.3 Experimental

3.3.1 Materials

Polypyrrole was purchased from Merck, purified by distillation, and stored at -18°C. Parra toluene sulfonic acid sodium salt (*p*TS) was purchased from BOH Chem. Chondroitin 4-sulphate sodium salt form bovine trachea (CS) was purchased from Fluka. Poly (4-styrene sulfonic acid) sodium salt (PSS), dodecylbenzenesulfonic acid sodium salt (DBSA), dextran sulphate sodium salt (DS) and hyaluronic acid (HA) had been supplied by Aldrich chemistry. Lacosamide (LCM) with the generic name of Vimpat was provided form St. Vincent Hospital in Melbourne. Figure 3 shows the chemical structure of *p*TS, CS, PSS, DBSA, DS and HA dopants and also LCM molecules.

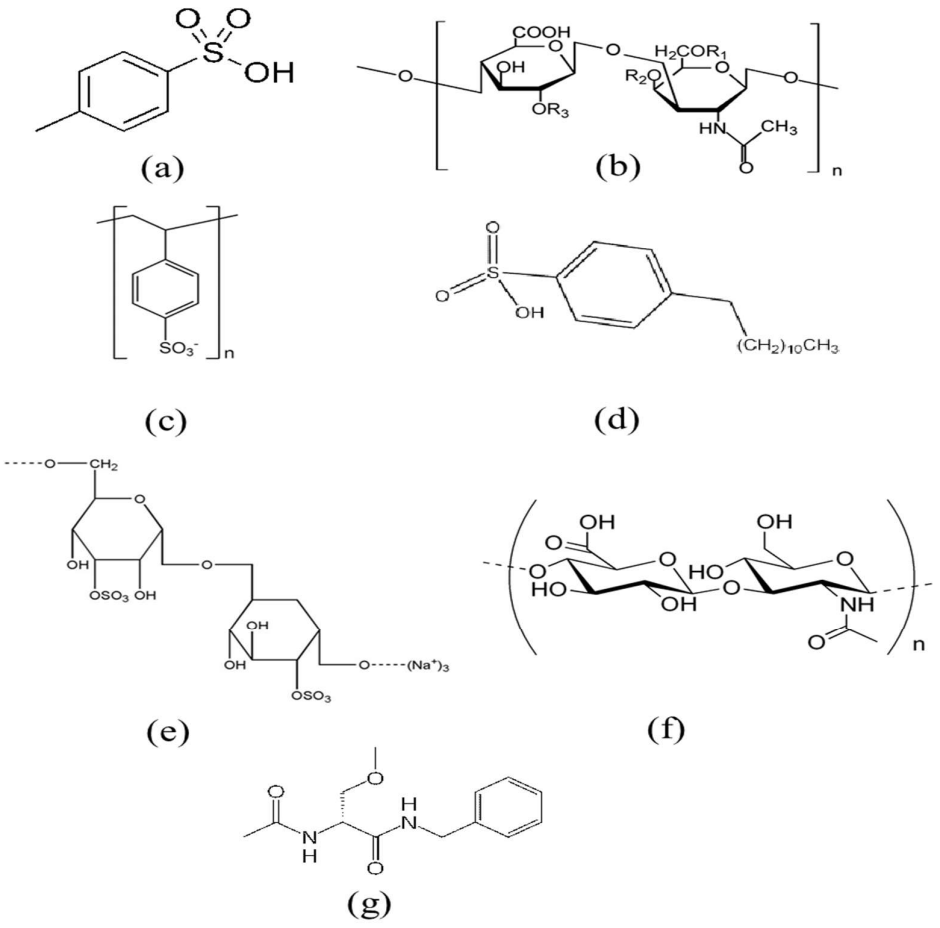

Figure 3.2 Chemical structure of; (a) Parra toluene sulfonic acid sodium salt (*p*TS), (b) Chondroitin 4-sulphate sodium salt form bovine trachea (CS), (c) Poly (4-styrene

sulfonic acid) sodium salt (PSS), (d) Dodecylbenzenesulfonic acid sodium salt (DBSA), (e) dextran sulphate sodium salt(DS), (f) hyaluronic acid (HA) and (g) lacosamide (LCM) molecules.

Artificial cerebrospinal fluid of the brain (ACSF) was prepared from two solutions with the proportion of 50:50 v/v; solution A was made from NaCl (8.66 g), KCl (0.224 g), $CaCl_2.2H_2O$ (0.206 g), $MgCl_2.6H_2O$ (0.163 g) which has been dissolved in 500 ml pyrogen-free water. Solution B was made of $Na_2HPO_4.7H_2O$ (0.214 g), $NaH_2PO_4.H_2O$ (0.027 g) which has been dissolve in 500 ml pyrogen-free water. ACSF was stored at 4^{o} C prior to use. All of the ingredients to make ACSF were purchased from BASF.

Polyvinylidene fluoride (PVDF) flat membranes (type HVHP) were purchased from Millipore and utilized as substrate membranes. The nominal pores size of these membranes is 0.22 μm. The surface of these substrate PVDF membranes was coated with a layer of platinum (Pt) using Edwards sputter coater 302 Auto instrument with four different thickness of Pt layer. Sputtering coating has been carried out under 2.5×10^{-3} Pa vacuum. Desired thickness of Pt layer was achieved through instrument set up with a sputtering power for Pt of 40 W.

3.3.2 Electrochemical Polymerization of Polymer Films

Polypyrrole coated platinised PVDF membranes (PPy/Pt/PVDF) were electrochemically synthesized. The electrochemical polymerisation of PPy composite membranes process was carried out using a cell which will be called the growth cell which was designed using the software Solidworks 2013 (X64)(Figure 3.3(E)) . Objet Connex 350 printer was utilized to fabricate this growth cell. Using photocurable Acralate Fullcure720 material supplied by Objet Pty. Ltd. Figure 3.3 demonstrates the growth cell for electropolymerization of the conducting polymer on the surface of the Pt/PVDF membrane. Region (a) in Figure 3.3(A) shows the cell opening where the reference (Ag/AgCl) and auxiliary (Pt mesh) electrodes are placed. The volume of the growth cell is approximately 10 ml. A platinized PVDF membrane (the working electrode) is placed between the two parts of the cell which has been shown in figure 3.3 (C) and (D) (indicated by a red arrow). Then these two

parts of the cell which is presented in Figure 3.3 (B) are screwed together to form a sealed unit.

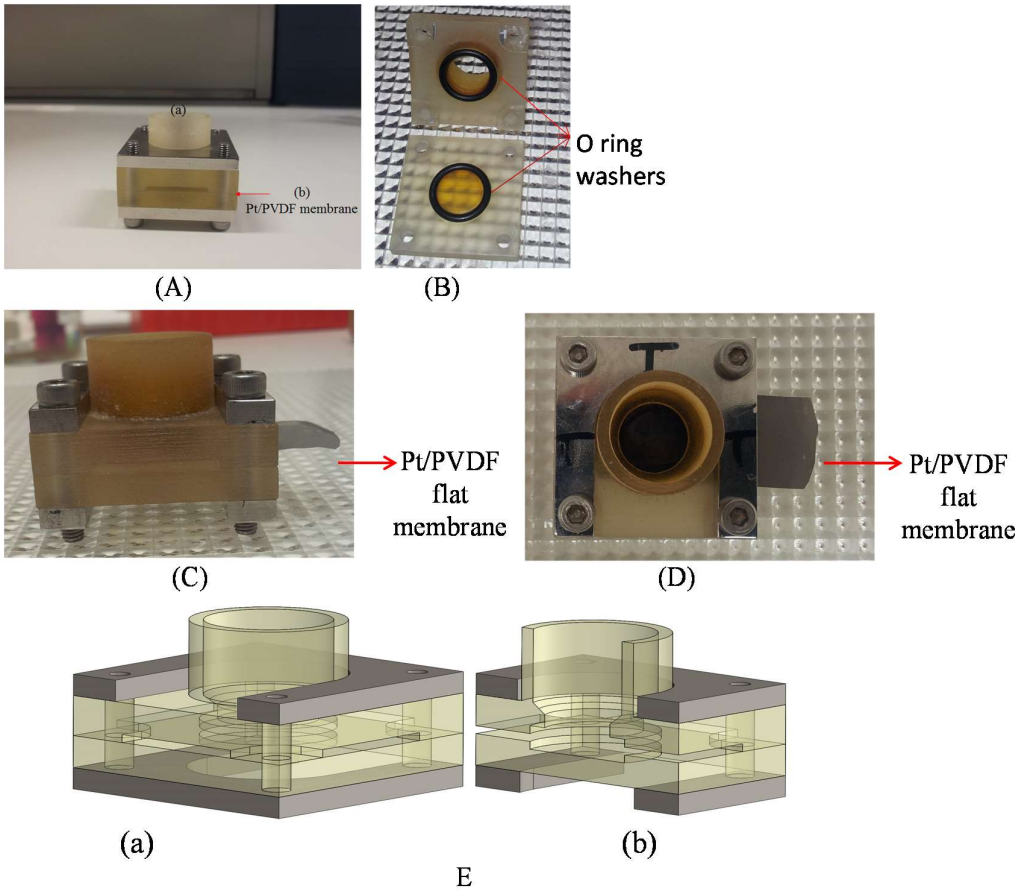

Figure 3.3 (A) Picture of growth cell which has been used to prepare composite PPy/Pt/PVDF membranes. Region (a) shows where the reference and auxiliary electrodes go into the cell; and (b) indicates where a Pt/PVDF membrane is placed; (B) presents two parts of the cell and O ring washers; (C) is a picture of the cell from side view; and (D) is a top view of the cell; (E) Schematic of growth cell; (a) overall view and (b) cross section view.

The dopants, current density and polymerisation time used to form the PPy polymers are presented in Table 3.1.

Table3.1 Electropolymerisation conditions used for form the PPy polymers on the Pt/PVDF membrane. The polymerisation area is defined by the O-ring of the growth cell (1.8 cm^2) (Figure 3.3).

Dopants	**Current Density (mA/cm^2)**	**Applied Currents (mA)**	**Polymerisation time (min)**
*p*TS	0.5,1, 2, 3	0.9, 1.8, 3.6, 5.4	1, 1.5, 2, 5 and 10
CS	0.25	0.45	1.5
DBSA	2	3.6	1.5
PSS	1	1.8	6
HA	0.25	0.45	12
DS	0.5	0.9	15

Each solution was deoxygenated with nitrogen gas bubbling for 10 min prior to commencing polymerisation. Conducting polymer films were grown galvanostaticly on the surface of Pt/PVDF membranes using an eDAQ e-corder 410 recorders and EA163 potentiostat which is connected to the growth cell. Three electrode growth cell set up and connection to the potentiostat have been shown in figure 3.4. During galvanostatic growth the voltage was recorded, which provides information on the oxidation voltage generated during conducting polymer growth.

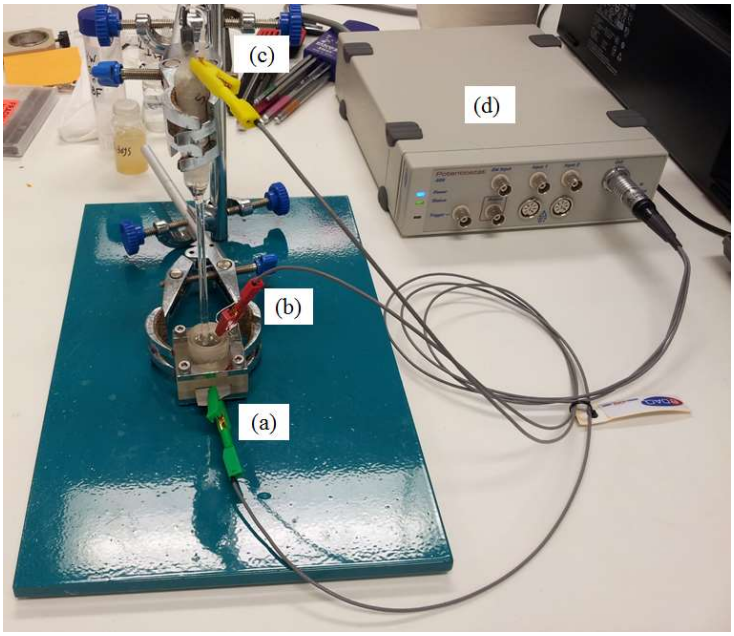

Figure 3.4 Growth cell set up and connection to the potentiostat; (a) platinised surface of PVDF membrane as the working electrode, (b) platinum mesh as auxiliary electrode, (c) Ag/AgCl reference electrode all connecting to the (d) EA163 potentiostat.

Electropolymerisation experiments were carried out at room temperature. Subsequently, at the end of the electropolymerisation processes the conducting polymer coated Pt/PVDF membranes were removed from the growth cell and rinsed with distilled water and dried using a stream of nitrogen gas. These membranes were stored at room temperature and then used for drug transport studies.

3.3.3 Polypyrrole coated PVDF membrane characterization

3.3.3.1 Water flux measurements

Water flux is the volume of water which passes through the PPy coated flat membrane per second and is measured in mL/sec. Water flux measurements provides information of the deposited coatings influence on the ability of a solution to transfer through the membrane. A very thick coating my decrease the porosity and hence decrease the ability of solution (in particular solution containing drug) to pass through the membrane. A Pt/PPy coating that does not impede flow but can be stimulated to control flow is ideal. For flat conducting polymer coated membranes

water flux was measured using the transport cell (Figure 3.5). However, in this experiment the reservoir side contained water and the receiving side was left empty.

The PPy coated flat Pt/PVDF membrane was placed between the two halves of the transport cell. The feed side of the cell (Figure 3.5B-(b)) was filled with Milli-Q water with the transported water passing into the receiving side (Figure 3.5B-(c)) collected every min for 10 min with the volume plotted against time. The water flux measurement experiment was repeated 3 times for every sample.

3.3.3.2 Cyclic voltammetry

In order to investigate the electrochemical properties of the conducting polymer films grown on the surface of Pt/PVDF flat membranes, the PPy/Pt/membrane was placed in a three electrode electrochemical set up containing a platinum mesh counter electrode, Ag/AgCl reference electrode, with the conducting polymer films being the working electrode. ACSF was utilized as the electrolyte and five cyclic voltammograms (CVs) were measured using an eDAQ e-recorder (v5.5.11) and potentiostat shown in Figure 3.4. The potential ranges and voltage scanned rates of have been presented in the caption of every CVs. In all of the Figures showing the CVs it is the 5^{th} CV of each PPy that is shown.

In addition, to study the electroactivity of lacosamide, four solution of lacosamide in PBS with concentration of 12.5, 25, 50 and 100 µg/ml were prepared. Cyclic voltammograms of this solution in the presence of glassy carbon electrode (GCE) working electrode was then measured. Cyclic voltammograms were run from -600 mV to +600 mV at a scan rate of 50mV/sec.

3.3.4 Anti-epilepsy drug transport through flat polypyrrole coated Pt/PVDF membrane

3.3.4.1 Non-stimulated state

The controlled transport of an anti-epilepsy drug across PPy coated Pt/PVDF flat membranes was carried out at non-stimulated state using a "transport cell" shown in Figure 3.5.

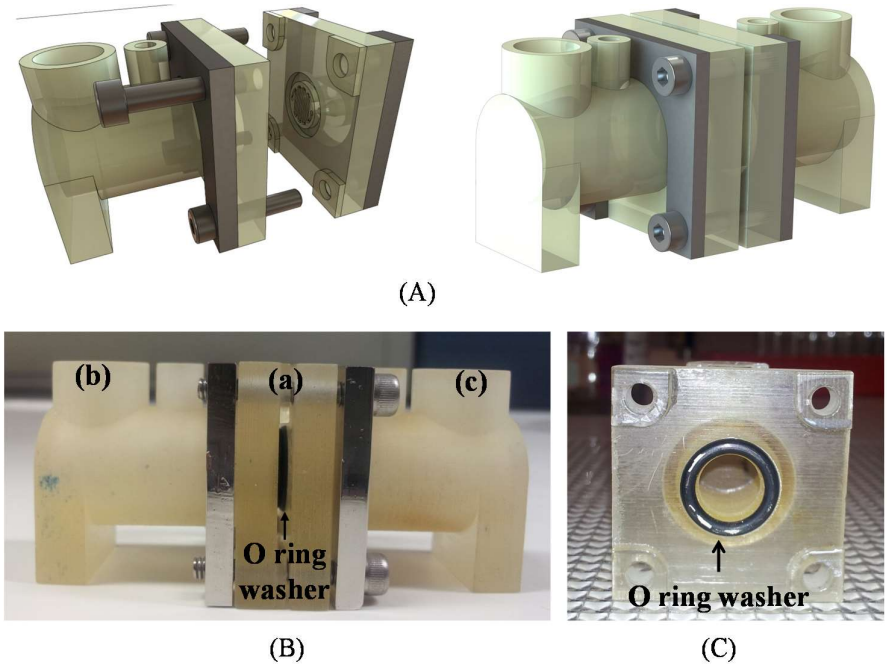

Figure 3.5 (A) schematic of transport cell; (B) photo of transport cell; (a) is a place to put the polypyrrole coated Pt/PVDF membranes, (b) shows anti-epilepsy drug feeding side and (c) demonstrates the receiver side of transported anti-epilepsy drug; (C) cross-section view photo of transport cell.

As Figure 3.5 exhibits a PPy coated Pt/PVDF flat membrane was placed in between of two parts of transport cell with the PPy coating facing the drug/ACSF reservoir side. The two parts of the cell are connected using 4 screws and O-rings to ensure a leak proof seal is formed. Section (b) of the cell shows the feed side of the transport cell which contains the drug/ACSF solution whilst section (c) is the receiving side and only contains ASCF. Samples were taken from the receiving side at set intervals to assess the transport properties of the PPy/PVDF membrane.

3.3.4.2 Stimulated state

The same transport cell set up described above was used for studying the electrochemically controlled transport of lacosamide through the PPy/PVDF membrane. However, in these experiments the cell was connected to the electrochemical equipment described above and shown in Figure 3.6.

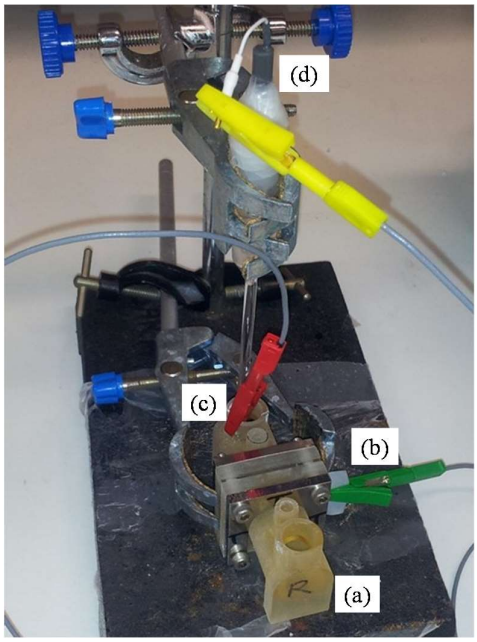

Figure 3.6 Transport cell connection to an e-DAQ system for stimulation studies; (a) transport cell, (b) Pt/PVDF membrane as working electrode; (c) auxiliary electrode, (d) Ag/AgCl reference electrode (section 3.2.4.2).

Controlled potential stimulation was employed to electrochemically control the transport of lacosamide through the PPy coated Pt/PVDF membranes. Three different oxidizing and reducing potentials were applied to the surface of the PPy coated Pt/PVDF flat membranes. The oxidizing and reducing potential were chosen from the cyclic voltammograms of PPy coated membranes. Additional voltages were investigated ±100 mV about each oxidising and reducing voltage. The aim of this procedure was to achieve the fully oxidized and fully reduced states of conducting polymer layer which has been deposited on the surface of the membranes. These

potentials were chosen from the cyclic voltammograms of these conducting polymer coated composite membranes.

3.3.5 Scanning Electron Microscopy

Scanning Electron Microscopy (SEM) images of conducting polymer film surfaces were taken using a field emission SEM (JOEL JSM-7500FA). SEM analysis was conducted using the SEM instrument described in Chapter 2.

3.3.6 Transported anti-epilepsy drug concentration measurement using HPLC system

In this study Agilent HPLC instrument was utilized to measure the concentration of transported lacosamide molecules. In this HPLC instrument a C18 column T3, 5 µm which is supplied by Atlantis columns utilized in conjunction with a UV/Vis detector to detect lacosamide from ACSF solution. Figure 3.7 presents a picture of Agilent HPLC instrument. This instrument includes;

(a) solution pumps;
(b) UV-VIS detector;
(c) Auto sampler and;
(d) Column

This HPLC instrument is connected to a PC which provides Agilent Chemstation Rev.B.04.02 SPI software for the instrument.

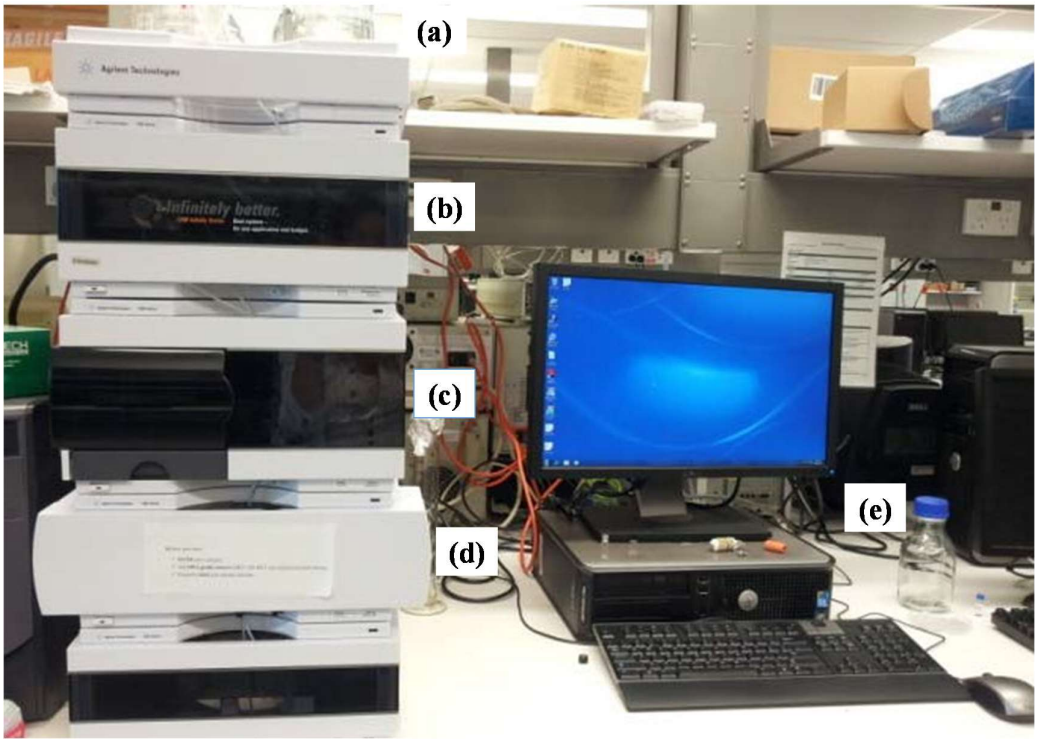

Figure 3.7 HPLC instrument; (a) Pump, (b) UV-VIS detector, (c) auto sampler, (d) column and (e) PC.

3.4 Results and Discussion

3.4.1 Electroactivity

3.4.1.1 Study the electroactivity of lacosamide molecules

Since transport studies will be performed at an applied voltage (stimulated release in section 3.4.3.2 below) it is important to investigate if the drug lacosamide has any electroactivity. This will indicate if the lacosamide molecule is likely to be effected by the stimulating voltage. If the lacosamide molecules are electrically active, it can have significant influence on the concentration of transported dug molecules across the membrane. If lacosamide molecules carry positive or negative charge, applying positive or negative voltages can repulse or absorb these molecules to the surface of membranes. This absorption/repulsion can effect on the amount of transporting drug molecules across the membrane.

Figure 3.8 present the cyclic volammogram of lacosamide/PBS solution. This experiment has been carried out to study the electroactivity of lacosamide. The 5th CV of each concentration is shown Figure 3.8 with no redox peaks observed suggesting that the lacosamide molecule does not possess any electroactivity in the potential window investigated. The large current at voltages lower than -0.2V is due to the reduction of residual dissolved oxygen in the solution.

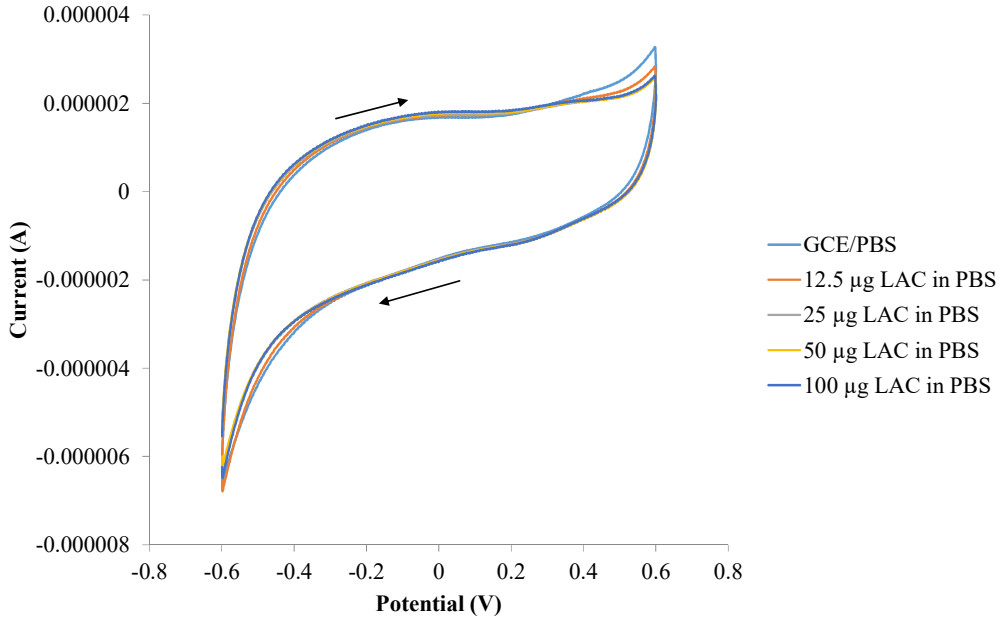

Figure 3.8 Cyclic voltammograms of lacosamide (12.5, 25, 50 and 100 µg/ml) in PBS, scan rate = 50 mV/s. Arrows show the direction of the potential scan.

3.4.2 Conducting polymer film characterization

3.4.2.1 Polypyrrole coated Flat Pt/PVDF membrane

Cyclic voltammetry was used to investigate the redox peaks of the conducting polymers deposited on the surface of flat Pt/PVDF membranes. Figure 3.9 (a) shows the 5th cycle of the CVs of PPy/*p*TS deposited on the Pt/PVDF with different electropolymerisation conditions (Table 3.1). This Figure reveals that longer electropolymerisation time led to a PPy/*p*TS film which has higher electrical capacitance. By increasing the electropolymerization time, the amount of charge passing was higher and leads to more polymer growth. The amount of charged

passed by applying 1 mA/cm^2 for 1, 2, 5 and 10 min is 108, 216, 540 and 1080 mC respectively (surface area of growth region is 1.8 cm^2). The area encompassed by CV curve represents the capacity of the conducting polymer.

Similar to Figure 3.9 (a) the effect of applying longer electropolymerization time has been observed in Figure 3.9 (b). However, the current density is higher in Figure 3.9 (b). Longer electropolymerisation time caused deposition of PPy/*p*TS film with a higher electrical capacity; however no clear redox peaks are seen in Figure 3.9 (b). The charge passed for growth for 1 mA/cm^2 for 10 min is 1080 mC which is exactly the same as the amount of charge passed for 2mA/cm^2 for 5 min. Therefore, the currents generated during the CVs of these PPy/*p*TS films are very similar as is expected.

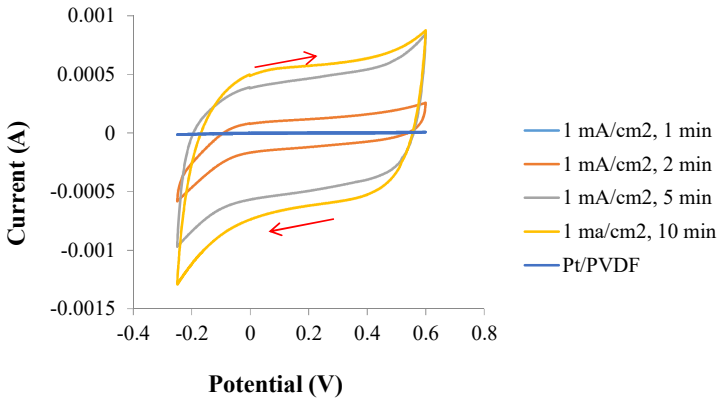

(a)

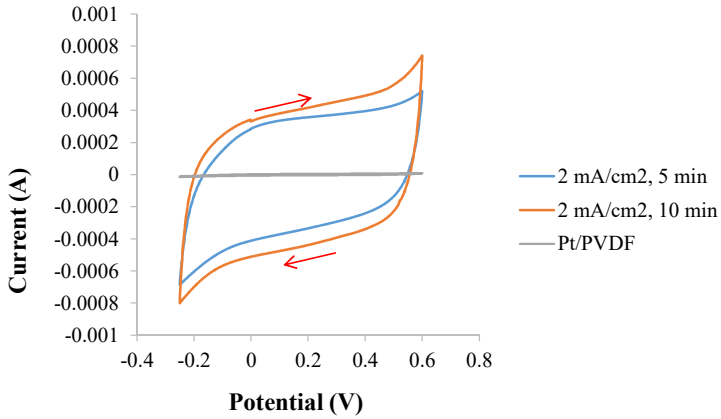

(b)

Figure 3.9 (a) Cyclic voltammograms of PPy/*p*TS which has been deposited on the surface of Pt/PVDF flat membrane with different electropolymerisation condition,

scan rate = 50 mV/s. The CV of PPy/*p*TS which is grown by applying 1 mA/cm^2 for 1 min is overlapped with the CV of Pt/PVDF; (b) Cyclic voltammograms of PPy/*p*TS which has been deposited on the surface of Pt/PVDF flat membrane with different electropolymerisation condition, scan rate = 50 mV/s.

According to Figure 3.10 the highest electrical capacitance is seen for PPy/*p*TS which has been synthesized by applying 1 mA/cm^2 for 10min (total charge passed is 1080mC).

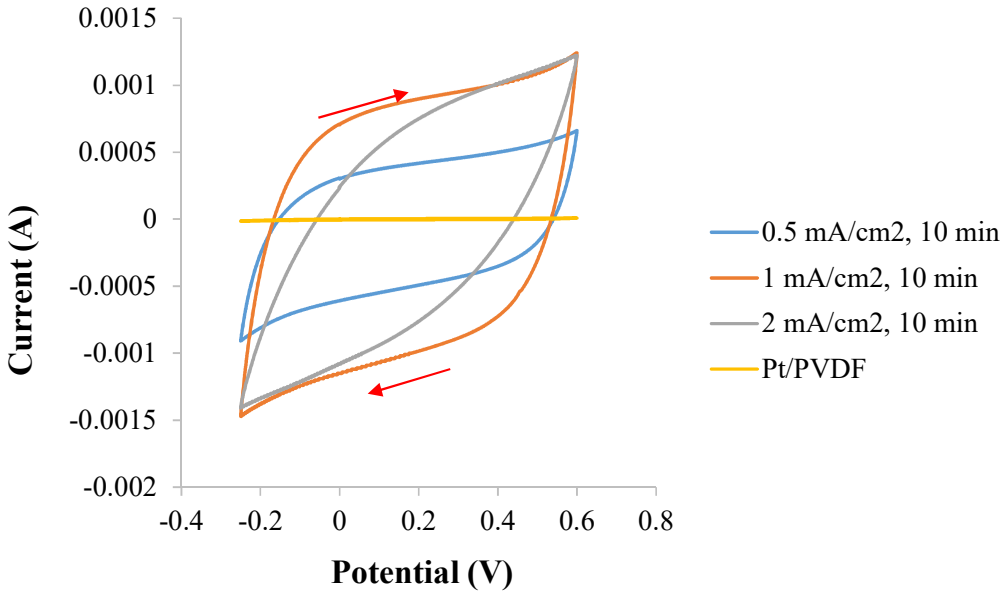

Figure 3.10 Cyclic voltammograms of PPy/*p*TS which has been deposited on the surface of Pt/PVDF flat membrane with different electropolymerisation condition, scan rate = 50 mV/s. The electrolyte was ACSF.

A board range of electropolymerisation conditions were investigated to synthesise PPy/*p*TS/Pt/PVDF as a means of optimizing the best growth cell (Figure 3.3) configuration and connection to the e-DAQ system (Figure 3.4). The grow cell was newly fabricated and PPy/*p*TS was chosen as the first dopant to initiate the preliminary experiments. Figure 3.11 shows the CV of PPy/DBSA/Pt/PVDF flat membrane which has been synthesized by applying 2mA/cm^2 for 90 seconds. The PPy/DBSA polymer appears to be electroactive; however it is difficult to observe redox peaks of this conducting polymer.

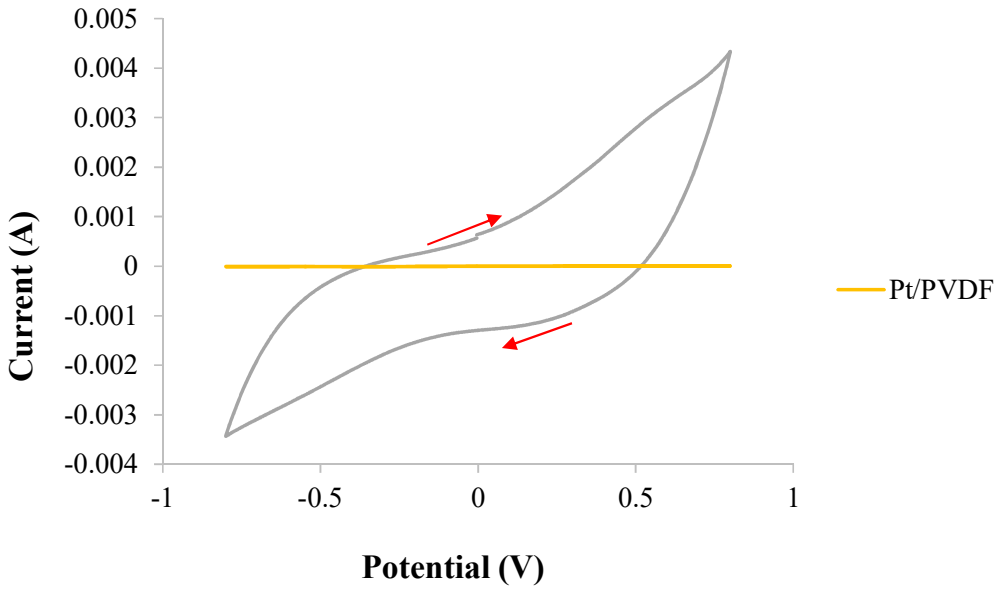

Figure 3.11 Cyclic voltammograms of PPy/DBSA which has been deposited on the surface of Pt/PVDF flat membrane by applying 2mA/cm^2 for 1.5 minute, scan rate is 50mV/s. The electrolyte was ACSF.

CVs of PPy/DS/Pt/PVDF flat membrane which has been synthesized by applying 0.5mA/cm^2 for 15 min. According to the redox switching property of PPy (Figure 3.12) the oxidizing and reducing peak were seen in this CV at approximately +250 mV and 0.0 mV respectively.

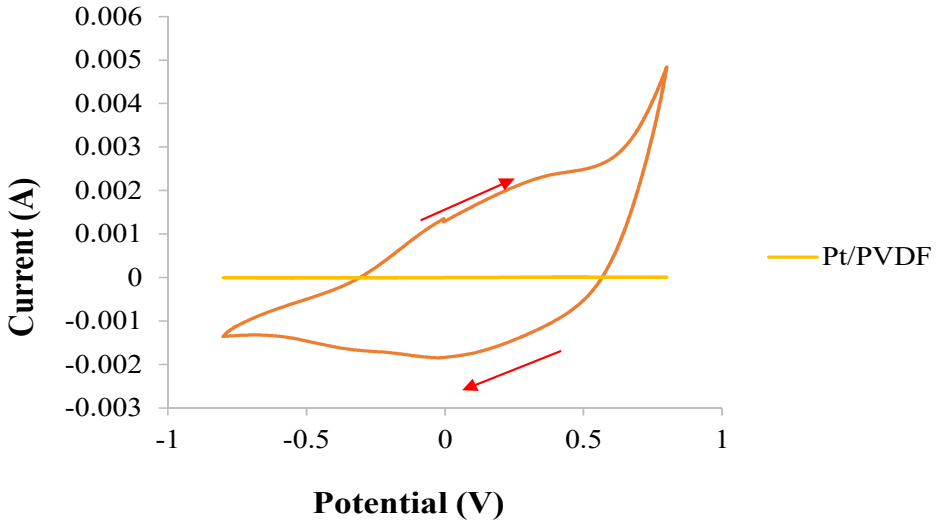

Figure 3.12 Cyclic voltammograms of PPy/DS which has been deposited on the surface of Pt/PVDF flat membrane by applying 0.5mA/cm^2 for 15 min, scan rate is 50mV/s. The electrolyte was ACSF.

Figure 3.13 exhibits the cyclic voltammograms of PPy/HA conducting polymer which has been deposited on the surface of Pt/PVDF membrane by applying 0.25mA/cm^2 for 12 min. An oxidizing peak is seen around +450 mV. For reducing voltage around -500 mV a very small peak can be observed.

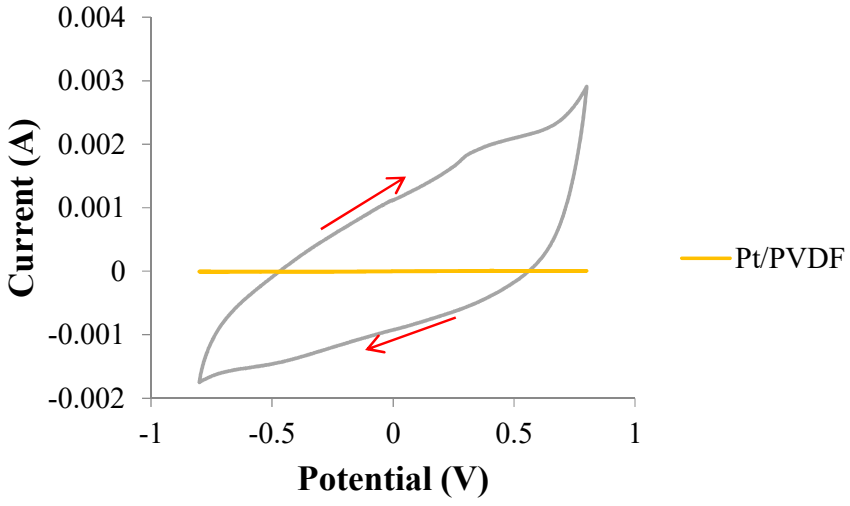

Figure 3.13 Cyclic voltammograms of PPy/HA which has been deposited on the surface of Pt/PVDF flat membrane by applying 0.25mA/cm^2 for 12 min, scan rate is 50mV/s. The electrolyte was ACSF.

Figure 3.14 is the cyclic voltammograms of the PPy/PSS/Pt/PVDF membrane. This conducting polymer was synthesized by applying 1 mA/cm^2 for 6 min. According to Figure 3.14 two clear oxidizing and reducing peak are seen for this conducting polymer.

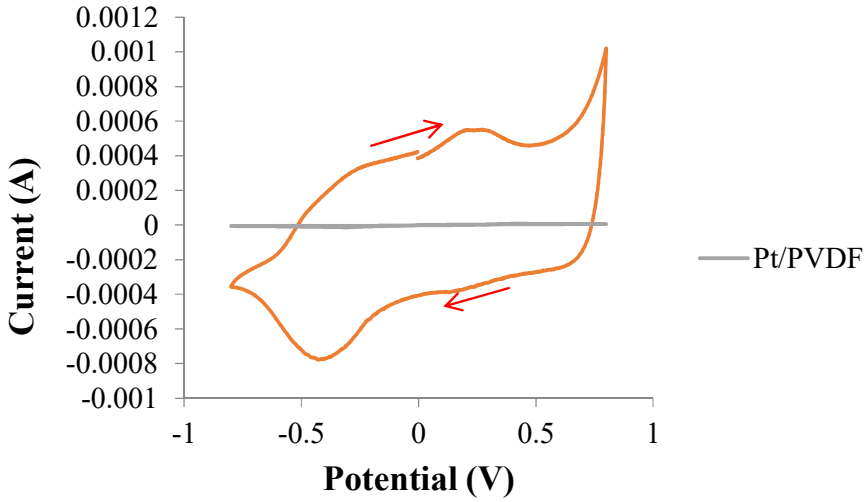

Figure 3.14 Cyclic voltammograms of PPy/PSS which has been deposited on the surface of Pt/PVDF flat membrane by applying 1 mA/cm^2 for 6 min, scan rate is 50mV/s.

The electropolymerisation conditions are different for each dopant. For instance, to fabricate PPy/PSS on the surface of Pt/PVDF membrane longer time than PPy/*p*TS was applied. By applying shorter electropolymerisation time the uniform PPy/PSS did not form on the surface of the membrane. In some cases because of the concentration of pyrrole or dopants or electropolymerisation condition, an additional oxidation wave can be seen in the CV [17]. According to the literature, if the concentration range of pyrrole monomer is 0.01-0.5 M, an additional oxidation wave occurs. By lower concentration of pyrrole, the higher switching potentials are required. Counterion movement to the polymer structure was completed at around +300 mV. In the reverse direction counterions (PSS^-) began to move out from the polymer and this process was saturated at around -500 mV.

Table 3.2 presents the summary of oxidizing and reducing peaks of conducting polymer coated Pt/PVDF membranes.

Table 3.2 Oxidizing/reducing peaks of composite membranes.

Dopants	Oxidizing peak (mV)	Reducing peak (mV)	Electrical capacitance (mF)
DS	+250	0.0	3.24
HA	+450	-500	0.34
PSS	+300	-500	0.81
*p*TS	+300	-400	0.23
CS	+400	-300	0.06

3.4.2.2 Morphology

3.4.2.2.1 Optimization of the sputter coated platinum layer on the surface of flat PVDF membrane

SEM studies revealed that sputter coating of the membrane surfaces did not cover and block all of the pores on the surface even with 200 nm layer of Pt (figure 3.15 (d)). Figure 3.15 exhibits that platinising with the lowest thickness to the highest had a minor effect on the microporous structure of the membrane. Figure 3.15 (a) has higher porous structure than figure 3.15(d). The thickness of Pt layer has been determined by instrumental setting. In order to confirm the visual observation made of the porosity from the SEMs water flux experiments were conducted.

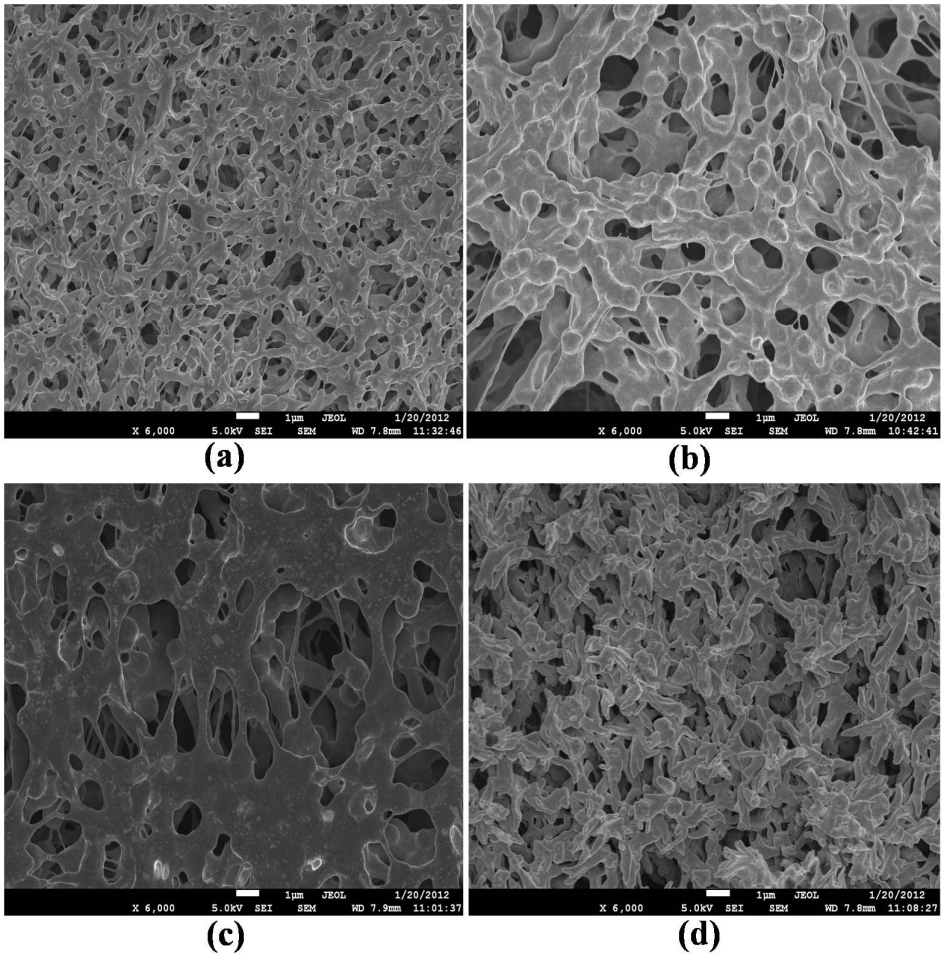

Figure 3.15 SEM images of platinised PVDF flat membrane of nominal 0.22 µm pore size. Thickness of platinum layer is (a) 30 nm, (b) 75 nm, (c) 100 nm (d) 200 nm.

3.4.2.2.2 Study the effect of sputter coated platinum layer on the surface of flat PVDF membrane

The water flux tests carried out on the flat PVDF membranes which have been sputter coated with different thickness of Pt layers. Thickness of platinum layer was 30, 75, 100 and 200 nm. Figure 3.16 exhibits the water flux values for these Pt/PVDF flat membranes.

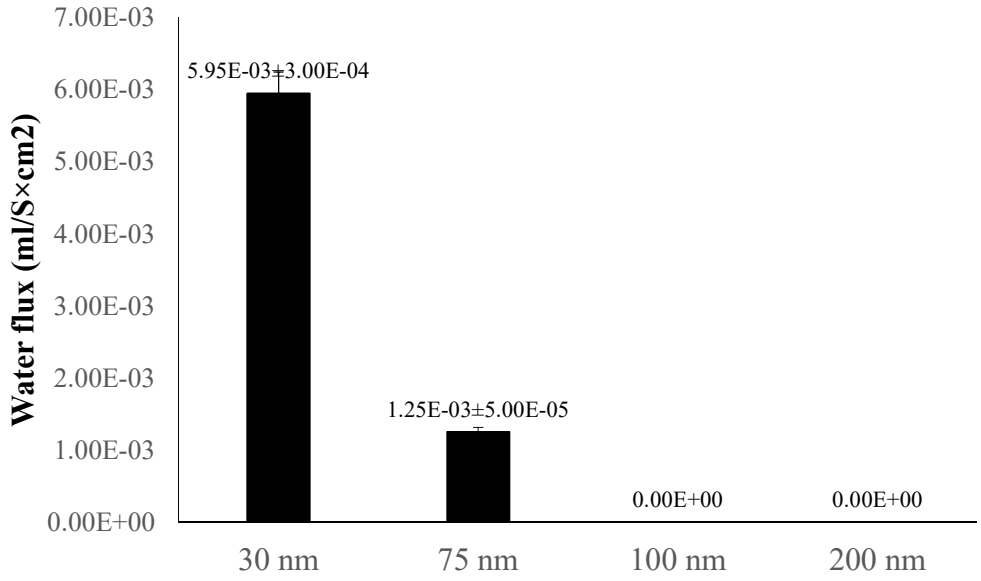

Figure 3.16 Water flux of sputter coated PVDF membranes with 30, 75, 100 and 200 nm of Pt layer. Error bars represent 95% confidence.

The largest water flux belongs to the 30 nm Pt layer coated Pt/PVDF flat membrane and followed by 75 nm Pt coated membrane. Water flux of 75 nm coated Pt/PVDF membrane is approximately 83.3% less than the water flux for 30 nm coated membrane. Therefore, utilizing thicker sputter coated layer of Pt would lead to have much less water flux. By moving from 75 nm coated Pt/PVDF membrane to 100 and 200 nm sputter coated Pt layer on the surface of PVDF membrane, the value of water flux has reached the zero. In the other word, increasing the thickness of sputter coated layer of Pt to more than 75 nm has blocked some of the pores on the surface of flat PVDF membrane. For 100 and 200 nm sputter coated flat Pt/PVDF membrane, the structure of flat membrane is much less porous than the PVDF membrane which has been coated with 30 and 75 nm thickness of Pt. Hence, these membranes are not appropriate candidates to be utilized for drug transport study.

3.4.2.2.3 Polypyrrole coated Flat Pt/PVDF membrane

3.4.2.2.3.1 Thickness of Pt coating layer

Figure 3.17 exhibits cross sectional SEM images of the polymer coated Pt/PVDF membrane with the coated Pt indicated by the shiny region. The other bright line

which exists next to the resin side of the membrane is the gold coated layer. To make the polymer layer more distinguishable, a layer of gold with 18 nm thicknesses was sputter coated on the conducting polymer membrane.

As a part of this study the thickness of Pt coated layer which has been deposited on the surface of PVDF membrane by using sputter coater machine, has been measured. This measurement was done for three different samples in three different areas and the average of these measurements is 79.15±0.62 nm. To confirm the Pt and gold coated layers (for Figures 3.19) the backscattered mode imaging was used which highlights dense regions. In addition, EDS analysis was performed to confirm these two shiny regions are Pt and gold.

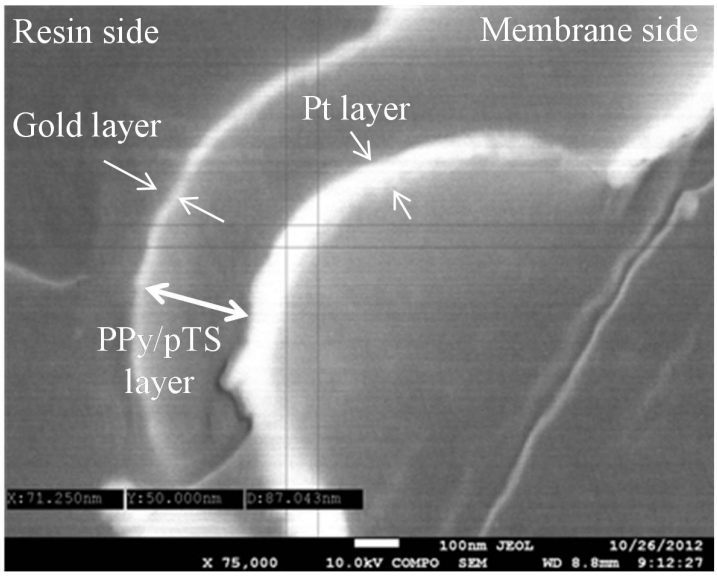

Figure 3.17 Thickness of Pt layer in PPy/*p*TS/Pt/PVDF membrane

3.4.2.2.3.2 Thickness of deposited polypyrrole layer

SEM images of PPy coated Pt/PVDF membrane demonstrates formation of a typical nodular morphology of electropolymerized polypyrrole films [20, 21]. However, the surface of these polymers coated Pt/PVDF membranes still remained porous. SEM images in figure 3.18 shows the effect of increasing electropolymerisation time on the porosity of conducting polymer PPy/*p*TS coated Pt/PVDF membranes.

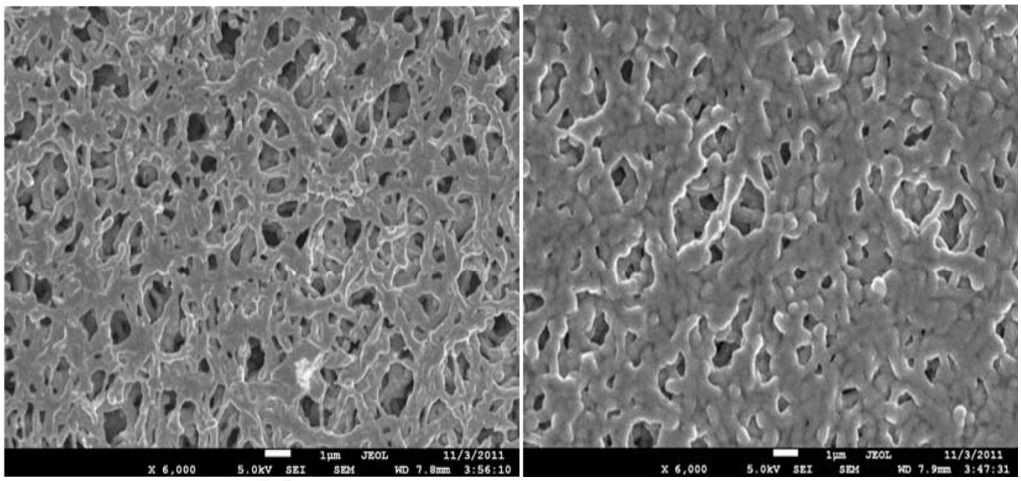

Figure 3.18 SEM images of PPy/*p*TS deposited on PVDF membrane grown at a current density of 1 mA/cm^2 for (a) 5 min and (b) 10.

Electropolymerisation for longer time (figure 3.18 (b)) leads to have a decrease in the porosity of the membrane. Porosity is an important factor as it will have an effect on the transport properties of the drug solution from one side of the composite membranes to the other. To gain a better understanding of the thickness of the deposited PPy layer on the surface of these platinized PVDF membranes, some cross sectional SEM images were obtained.

The PPy was deposited on the surface of Pt/PVDF membranes. In the SEM images which are presented in figure 3.19, this conducting polymer layer is sandwiched between two bright lines. These bright lines are a gold coating layer deposited on the surface of the PPy and Pt from the PVDF coating process. The resin and membrane sides have been indicated in the Figure. The thickness of deposited polymer layer on the surface of Pt/PVDF membranes is quiet uniform for both 10 and 5 min polymer synthesis. The lack of any membrane porosity observed in Figure 3.19 is due to the epoxy (used for sample preparation) filing in those pores.

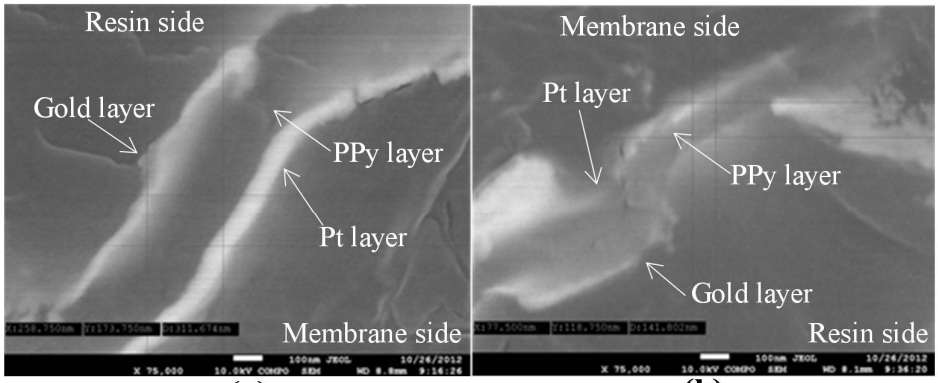

Figure 3.19 SEM images of the cross section of PPy/*p*TS (grown at 1 mA/cm^2) coated Pt/PVDF membranes; (a) for 10 min and (b) after 5 min; the resin and membrane sides have been indicated in the SEM images.

The thickness of PPy/*p*TS deposited layer on the surface of Pt/PVDF membrane was measured using a similar procedure for measurement of Pt layer thickness. Thickness measurements have been done in five different points of a sample. The measured values and average value are presented in Table 3.2.

Table3.2 Measuring the thickness of polymer layer

Electropolymerisation condition of PPy/*p*TS	Point 1 (nm)	Point 2 (nm)	Point 3 (nm)	Point 4 (nm)	Point 5 (nm)	Average (nm)
10 min at 1 mA/cm^2	278.7	276.2	292.3	300.9	285.0	286.7
5 min at 1 mA/cm^2	141.8	198.7	141.2	145.0	183.7	162.1

Results from the conducting polymer layer thickness measurements have revealed that the average PPy/*p*TS layer thickness increases with longer electropolymerisation time. The thickness of PPy/*p*TS layer which has been deposited for 10 min is roughly 1.8 times thicker than the PPy/*p*TS layer that has been electropolymerized for 5 min. This result is not surprising since the thicker polymer had twice the amount of charge applied during growth.

3.4.2.2.3.3 Water flux of flat Pt/PVDF polypyrrole coated membrane

The effect of PPy deposition and also the electropolymerisation condition on the amount of water flux of PPy/*p*TS/Pt/PVDF flat membrane was investigated. Figure 3.20 shows the differences between water flux of plain PVDF, Pt/PVDF (75 nm), PPy/*p*TS coated (grown at 1 mA/cm^2) Pt/PVDF by applying for 5 min and 10 min.

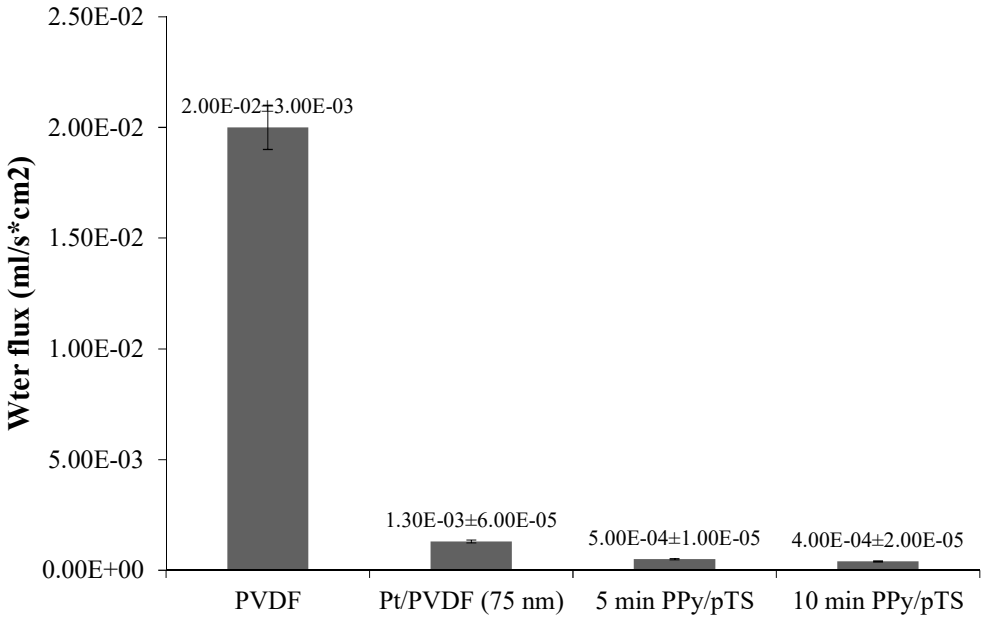

Figure 3.20 Water flux of PVDF, Pt/PVDF, PPy/*p*TS/Pt/PVDF (5 min and 10 min at 1mA/cm2); Error bars represents 95% accuracy confidence.

Sputter coating of 75 nm Pt layer on the surface of PVDF membrane has decreased approximately 93.5% of the water flux of the plain flat PVDF membrane with 0.22 µm pore size. Afterwards, the water flux of PPy/*p*TS/Pt/PVDF which have been electro synthesised for 5 min and 10 min by applying 1 mA/cm^2 current density, was measured. According to Figure 3.20 deposition of PPy/*p*TS layer on the surface of Pt/PVDF membrane decreased the water flux to 61.5% (5 min growth) and 69.2% (10 min growth). Therefore, deposition of PPy/*p*TS layer significantly decreases the water flux values. Water flux of 10 min grown PPy/*p*TS grown membrane is 20% less than the water flux of 5 min grown membrane.

3.4.2.2.4 Porosity of conducting polymer coated flat Pt/PVDF membranes

The effect of applying different current density on the porosity of membranes was investigated. Three different composite membranes have been fabricated with the same electropolymerisation time but different applied current densities. Figure 3.21 exhibits the SEM images of these conducting polymer coated Pt/PVDF membranes. These three composite membranes have been fabricated by growing the PPy/*p*TS for 10 min at 0.5 (a), 1 (b) and 2(c) mA/cm^2 current density.

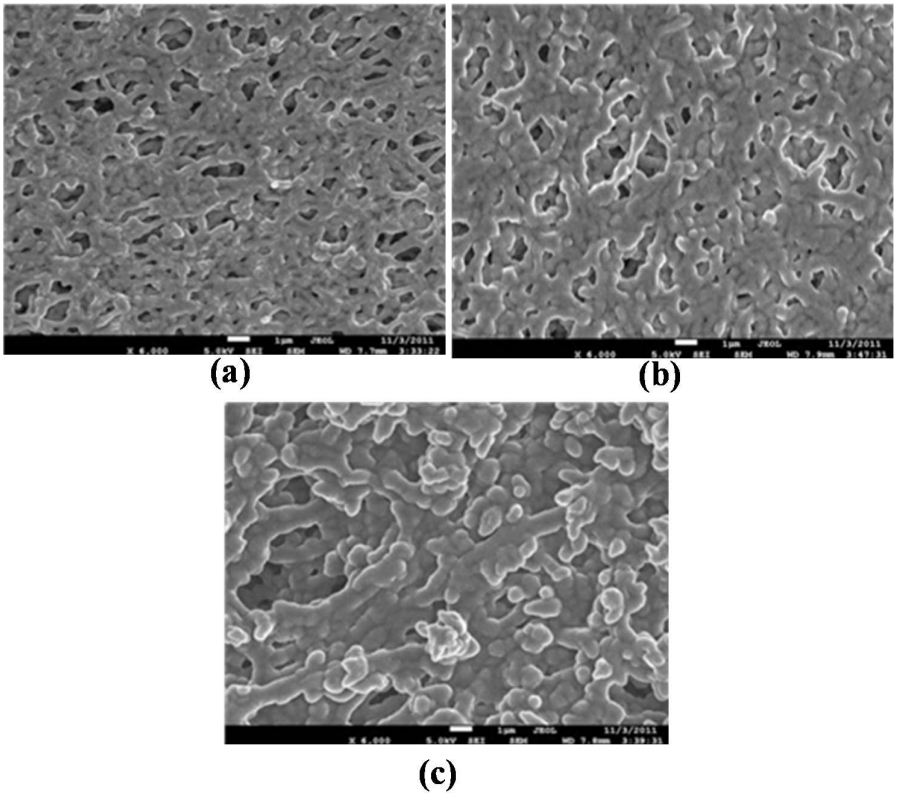

Figure 3.21 SEM images of PPy/*p*TS grown on PVDF membrane for 10 min at (a) 0.5mA/cm^2, (b) 1 mA/cm^2, and (c) 2mA/cm^2.

According to SEM images (Figure 3.21) the porosity of these composite membranes has decreased by moving from image (a) to (c). This indicates that by applying higher current density (i.e. 2mA/cm^2) more PPy/*p*TS was deposition on the surface of Pt/PVDF membrane. As has been mentioned before, the degree of porosity will have an affective on the amount of drug that can be transported through these composite conducting polymer coated platinized PVDF membranes.

3.4.2.2.4.1 Effect of polypyrrole dopant on the porosity of flat membranes

The SEMs presented in Figure 3.22 exhibit the effect of using different counterions during electropolymerisation of PPy on the surface morphology. Similar to the other SEM images which have been presented in Figures 3.18 and 3.21, formation of a typical nodular morphology is observed [20, 21]. According to Figure 3.22 (a) and 3.15(b), after sputter coating of a 75 nm Pt layer on the surface of PVDF membrane, the surface has become less porous. The PVDF membrane which is the base of composite membrane has a porous structure and when it coated with Pt and conducting polymer the porous structure remains evident. The porosity is reduced as a result of Pt coating and also CP deposition which is discussed in the following section.

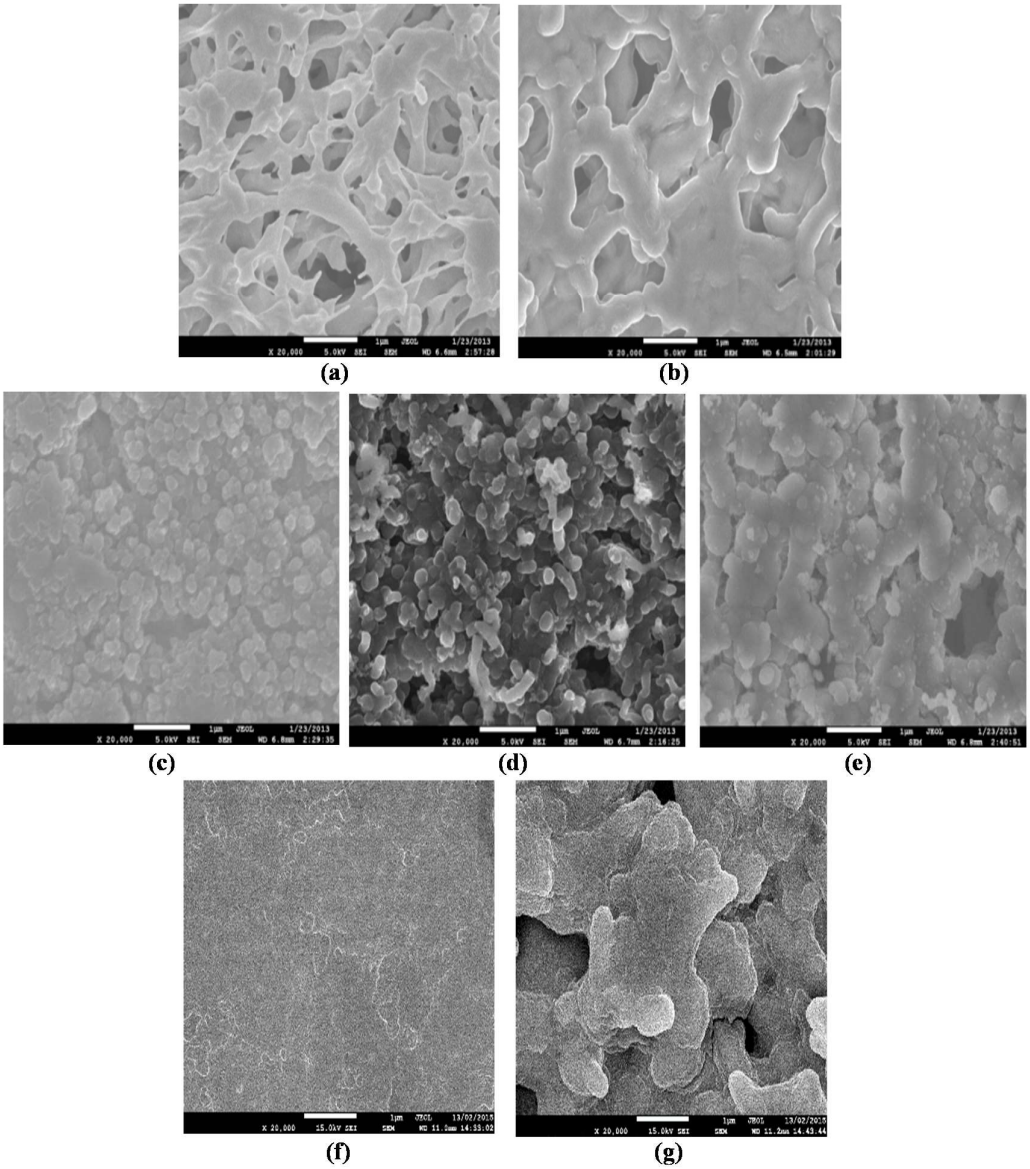

Figure 3.22 SEM images of the surface of PPy coated PVDF membranes; (a) is plain PVDF, (b) is PPy/*p*TS coated Pt/PVDF with 1 mA/cm^2 for 1.5 min, (c) is PPy/DBSA coated Pt/PVDF with 2 mA/cm^2 for 1.5 min, (d) is PPy/DS coated Pt/PVDF with 0.5 mA/cm^2 for 15 min, (e) is PPy/HA coated Pt/PVDF with 0.25 mA/cm^2 for 12 min, (f) is PPy/PSS coated Pt/PVDF with 1 mA/cm^2 for 1.5 min and (g) is PPy/CS coated Pt/PVDF with 0.25 mA/cm^2 for 1.5 min.

Upon visual inspection of the SEMs it appears that the porosity of PPy coated membranes varied from one counterion to the other. The electropolymerization condition for each membrane was different based on using deferent dopant to fabricate each of them.

The highest porosity belongs to PPy/*p*TS (figure 3.22 (c)) followed by PPy/CS (figure 3.22 (i)), PPy/DS (figure 3.22 (e)) and PPy/HA (figure 3.22 (f)). The porosity of PPy/DBSA (figure 3.22 (d)) and PPy/PSS (figure 3.22 (h)) is very much less than the other PPy coated membranes. Therefore, among all of these PPy coated Pt/PVDF membranes PPy/*p*TS, CS and DS seem to be the better choice to study drug molecules transport through a polymer coated membranes. These membranes still possess sufficient porosity after PPy deposition which may allow drug molecules to transport from one side of these membranes to the other side.

To confirm the results from SEM images, water flux experiments (Figure 3.23) were conducted for all of conducting polymer coated Pt/PVDF membranes shown in Figure 3.22.

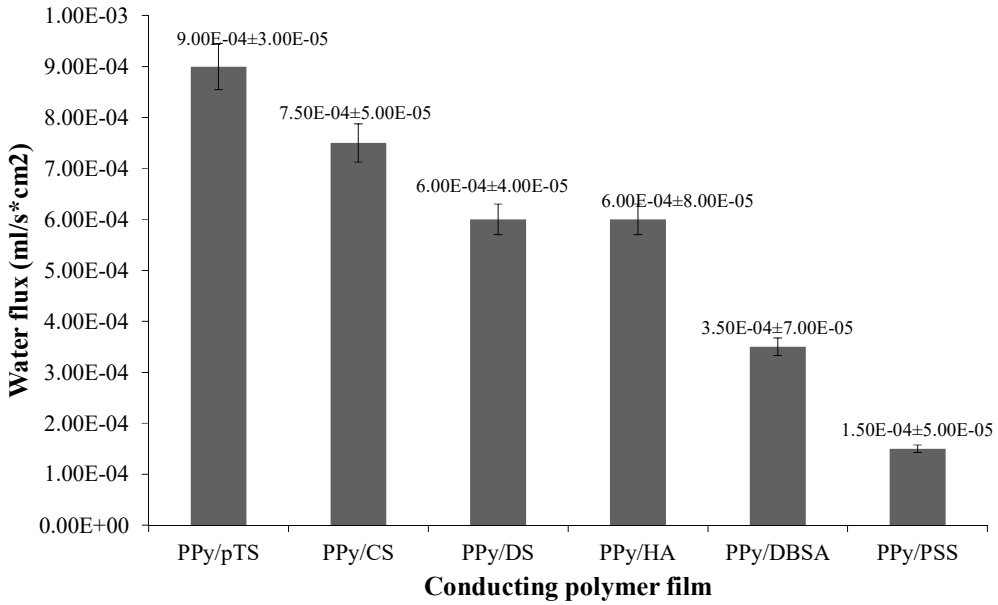

Figure 3.23 Water flux of PPy/*p*TS, PPy/CS, PPy/DS, PPy/HA, PPy/DBSA and PPy/PSS conducting polymer films grown at same condition which has been presented in Figure 3.22. Error bars represents 95% accuracy confidence.

PPy/*p*TS coating shows the highest water flux (9×10^{-4}) followed by PPy/CS (7.5×10^{-4}) with PPy/DS and), PPy/HA having similar values (6×10^{-4}). PPy/DBSA (3.5×10^{-4}) and PPy/PSS (1.5×10^{-4}) show the lowest water fluxes. These conducting polymers

have had less porous structure according to the SEM images (Figure 3.22). For better understanding of the characteristics of deposited PPy layer on the surface of Pt/PVDF membranes, SEM images from the cross-section of these membranes have been taken which are presented in figure 3.24.

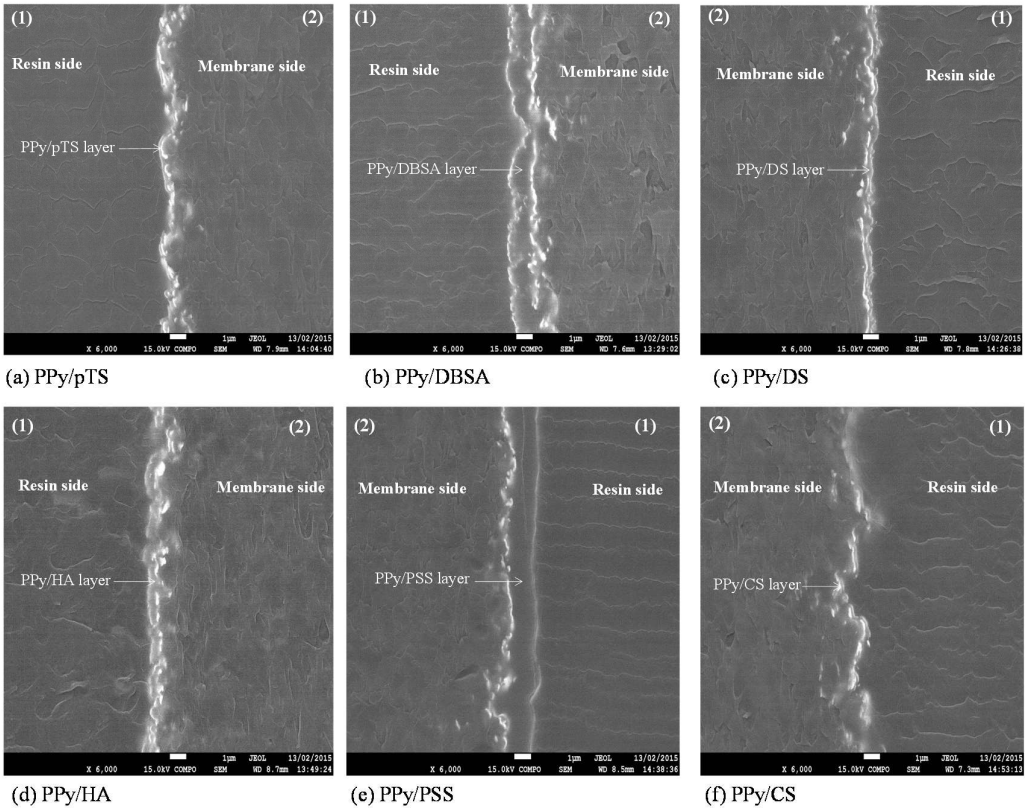

Figure 3.24 SEM images of the cross section of; (a) PPy/*p*TS coated Pt/PVDF, (b) PPy/DBSA coated PVDF, (c) PPy/DS coated Pt/PVDF, (d) PPy/HA coated Pt/PVDF, (e) PPy/PSS coated Pt/PVDF and (f) PPy/CS coated Pt/PVDF membranes. The side which is indicated by number (1) is the resin side and number (2) side is the membrane side.

The PPy layer is the area which has been encapsulated in between two shiny bright lines (as indicated by the arrows in Figure 3.24). The line which is in the resin side represents the gold coated layer and the other line which is in the membrane side is the Pt layer. For all PPy coated membranes, the polymer layer covered the surface uniformly. However, the thickness of this layer varied due to the different dopants used to form PPy. PPy/PSS exhibited the largest thickness at 1.7±0.37 µm followed by PPy/DBSA (1.38±0.2 µm), PPy/HA (0.46±0.11 µm), PPy/DS (0.24±0.05 µm),

PPy/CS (0.12±0.03 μm) and finally the thinnest layer was PPy/*p*TS (0.09±0.04 μm). This layer has been deposited on the surface of Pt/PVDF membrane by applying 1 mA/cm^2 for 90 seconds. The PPy/*p*TS layer possesses the thinnest layer and also exhibited the highest porosity (Figure 3.22) in addition the PPy/*p*TS coating demonstrated the highest water flux value (Figure 3.23).

3.4.3 Lacosamide transport study through flat PPy coated Pt/PVDF membrane

In this work an aqueous solution of lacosamide (0.1 mg/ml) prepared in ACSF is placed in the feed side of the transport cell (Figure 3.1), whilst on the other side (receiving side) there is ACSF only. The composite membrane is placed between the both sides. The transport of the lacosamide through the composite membrane, from the feed side to the receiving side, is monitored over a 10 min period with samples taken from the receiving side at 1 min intervals. A transport time of 10 min was chosen due to the final application of these composite membranes. The in vivo application of these membranes to deliver therapeutic level of anti-epilepsy drug to the brain was the clue of choosing drug transport studies time intervals. In his study the rapid release of drug after detection of pre seizure brain activity is important. Therefore, we limited the stimulated and non-stimulated transport studies only on the first min and continue that just only for10 min. The longer time than 10 min was not the concern and main goal of this project.

Analysis of lacosamide in the samples taken from the receiving side was performed using HPLC and the UV-vis detector. It is not possible to just use UV-vis as a detection system for lacosamide due to interferences at the wavelength of lacosamide detection coming from the transport media (ACSF). The HPLC separate the lacosamide from the interfering species in the ACSF. The HPLC procedure for detection of lacosamide involves the use of a mobile phase consisting of Milli-Q water, acetonitrile and methanol (65: 26.2: 8.8, v/v/v) that was filtered and degassed. Separation was carried out isocratically at ambient temperature using a flow rate of 0.8 ml/min. Detection was achieved with UV-vis detection set to the wavelength of lacosamide adsorption of 205 nm. Figure 3.25 exhibits the calibration curve constructed for the lacosamide.

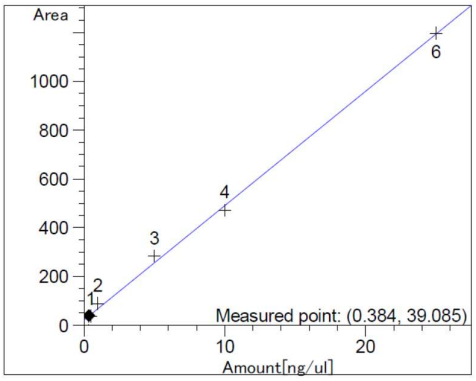


```
std1 at exp. RT: 7.415
VWD1 A, Wavelength=205 nm
Correlation:           0.99901
Residual Std. Dev.:   22.50033
Formula: y = mx + b
      m:     46.97766
      b:     21.05587
      x: Amount
      y: Area
```

Figure 3.25 Lacosamide calibration curve

3.4.3.1 Non-stimulated state

In the non-stimulated state no external voltage is applied to the membrane with the transport properties determined purling on the characteristics of the PPy coated composite membrane. According to the fabrication and characterisation of composite membrane, PPy/*p*TS, PPy/PSS and PPy/CS were chosen to be utilized for drug transport studies. These four conducting polymers exhibited more suitable electrical activity and redox properties on the base of their cyclic voltammograms. Figure 3.26 presents the concentration of transported lacosamide molecules through composite membranes at non-stimulated state. PPy/CS shows the maximum concentration of transported drug after 10 min (22.7 µg/ml) followed by PPy/*p*TS (3.9 µg/ml). PPy/PSS does not shows any drug transport at non-stimulated state which confirms the porosity of PPy/PSS composite membrane completely impedes the transport. According to the water flus result (Figure 3.23) the minimum amount of water transported through PPy/PSS coated Pt/PVDF membrane.

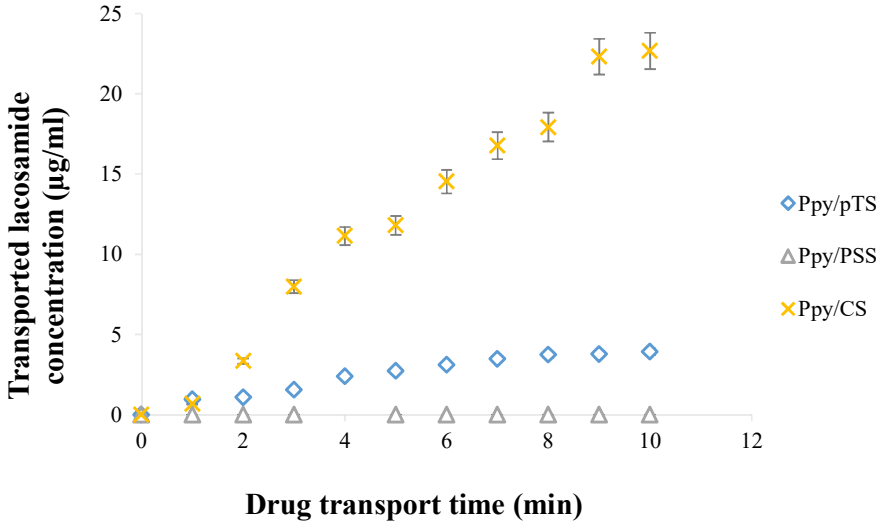

Figure 3.26 Concentration of lacosamide transported through PPy/*p*TS (1 mA/cm^2, 1.5 min), PPy/PSS (1 mA/cm^2, 1.5 min) and PPy/CS (0.25mA/cm^2, 1.5 min) coated flat membrane under non stimulated state for 10 min.

3.4.3.2 Stimulated state

In the stimulated state a voltage is applied to the membrane which causes charge to flow through the conducting polymer coated membrane. Hence, an electric filed begins to establish within the membrane pores[22]. Electromechanical materials such as conducting polymers are capable of changing their dimensions physically when an external electrical signal is applying through them. Upon the application of a sweeping voltage to the PPy ions move into and out of the polymer main structure during redox[23]. Because of this phenomenon, the volume of conducting polymer can change by more than 10% and also an approximate 30% change in length and thickness have been reported recently[24-26]. Changing in the dimension of deposited conducting polymer on the surface of Pt/PVDF membrane as a result of redox switching caused a dimension changing of this porous structure. In the other word, applying and external voltage causes redox switching which can lead to change in the dimension of pores on the surface of conducting polymer coated Pt/PVDF membranes. Applying an external voltage can influence the surface pore to change dimension which is the one of the basis for drug transport studies at the stimulated states in this system. All of stimulated drug release figures (Figures 3.27-

3.34) includes a passive (non-stimulated) release curve of lacosamide to compare the release profile between stimulated and non-stimulated states easier.

3.4.3.2.1 Oxidized state

To study the transport of lacosamide molecules across PPy coated Pt/PVDF membrane at oxidized states, an oxidizing potential of each PPy film was chosen based on the redox peaks in their respective cyclic voltammograms. To study drug transport through conducting polymer coated Pt/PVDF membrane for each PPy film, three oxidizing potential were applied to the surface of deposited PPy. One of these three oxidizing potentials was chosen based on oxidation potential observed from the CV whilst the other two represent ±100mV about the oxidation voltage.

Figure 3.27 shows the concentration of transported lacosamide through PPy/*p*TS membrane while applying three different oxidizing potentials. +300 mV is the oxidising potential which was chosen from the cyclic voltammograms of PPy/*p*TS (1 mA/cm^2, 90 sec) film (Figure 3.10). The oxidized state of PPy/*p*TS is accompanied by *p*TS movement and absorption from the solution to the polymer structure [27-30]. Therefore, the structure of conducting polymer expands and swells. The surface pores of PPy/*p*TS membrane are more closed at this state. However, the diffusion mechanism across the PPy/*p*TS membrane caused transport of some lacosamide molecules. Figure 3.27 also demonstrates the effects of applying potentials 100 mV either side of the oxidation potential. The transport values vary depending on the voltage applied. Therefore, under different electrical stimulation the transport properties vary. This variation can be the result of several things combined such as porosity, electrostatic attraction/repulsion. The minimum transported concentration belongs to +200 mV. Therefore, the porosity of PPy/*p*TS membrane was at the minimum state while applying +200 mV. Drug transported concentration for +300 mV and +400 mV is roughly the same. At +300mV the PPy/*p*TS is oxidized and at +400mV it is still fully oxidized, so it would not expect to see a significant difference between 300 and 400. However, at 200mV the PPy/*p*TS is not fully oxidized.

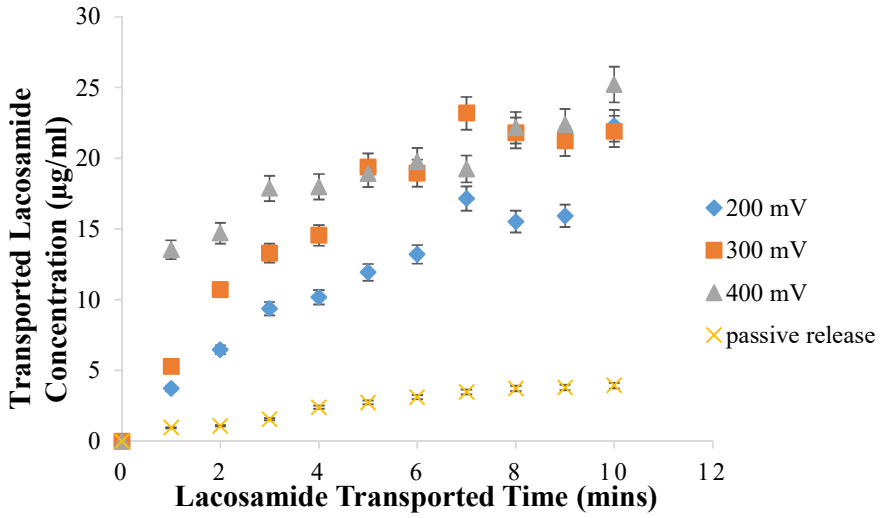

Figure 3.27 Concentration of transported lacosamide through PPy/*p*TS (90 sec, 1 mA/cm^2) coated flat membrane while applying three oxidized potential for 10 min.

Figure 3.28 presents the concentration of transported lacosamide through PPy/CS/Pt/PVDF flat membrane after 10 min. Samples were collected every minute. +300 mV was picked up from PPy/CS film CV as an oxidizing potential. Figure 3.28 shows that the minimum transport concentration belongs to +400 mV potential which means the PPy/CS/Pt/PVDF flat membrane structure is less porous at this state. The concentration of transported lacosamide for +300 mV and +200 mV is approximately the same. Therefore, for PPy/CS film applying the highest oxidizing potential leaded to have more effect on the movement of CS counterions from the solution to the main structure of pyrrole.

Drug transport study at oxidized state was carried out for PPy/PSS/Pt/PVDF flat membrane as well as the other conducting polymer coated flat membranes. -350 mV was the oxidising potential of the PPy/PSS film according to its CVs. -250, -350 and -450 mV were applied to the surface of PPy/PSS/Pt/PVDF film to study transport of lacosamide across this conducting polymer coated flat membrane. For all of these oxidizing potentials the concentration of transported lacosamide through the membrane was zero. In the other word, the structure of PPy/PSS/Pt/PVDF membrane while applying all of the oxidizing potentials was non-porous.

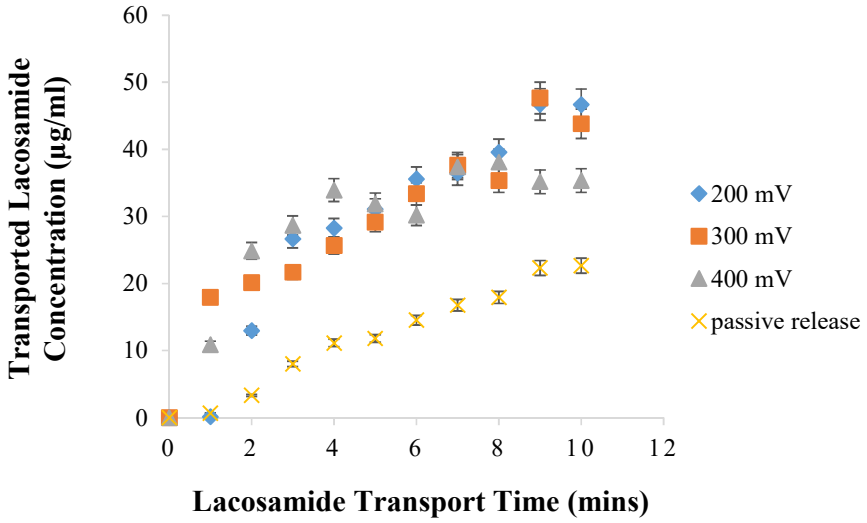

Figure 3.28 Concentration of transported lacosamide through PPy/CS/Pt/PVDF coated flat membrane while applying three oxidized potential for 10 min.

3.4.3.2.2 Reduced state

Similar to the oxidized state, the concentration of transported lacosamide through conducting polymer coated Pt/PVDF flat membrane was investigated at reduced state. Three different reducing voltages were applied to the surface of PPy coated Pt/PVDF membranes. One of these reducing potentials was chosen according to the cyclic voltammograms of conducting polymer films and two other potentials were that chosen potentials which has been pulsed and subtracted by 100 mV. At reducing state, counterion leaves the polymer structure and move to the solution [27-30]. Hence, the structure of conducting polymer and also the membrane become more contracted. The contraction of PPy coated Pt/PVDF membrane makes the surface pores of the membrane more open. In the other word, porosity of membranes at reducing state is higher than oxidizing and also passive states. Therefore, the concentration of transported drug at this state supposed to be higher.

Figure 3.29 exhibits the concentration of transported lacosamide through PPy/*p*TS/Pt/PVDF membrane after 10 min while applying three reducing potentials. -400 mV was the voltage that reduction peak has happened in the PPy/*p*TS cyclic voltammograms. However, the maximum transport concentration was observed by

applying -300 mV which means at this state the porosity of PPy/*p*TS/Pt/PVDF flat membrane is the highest.

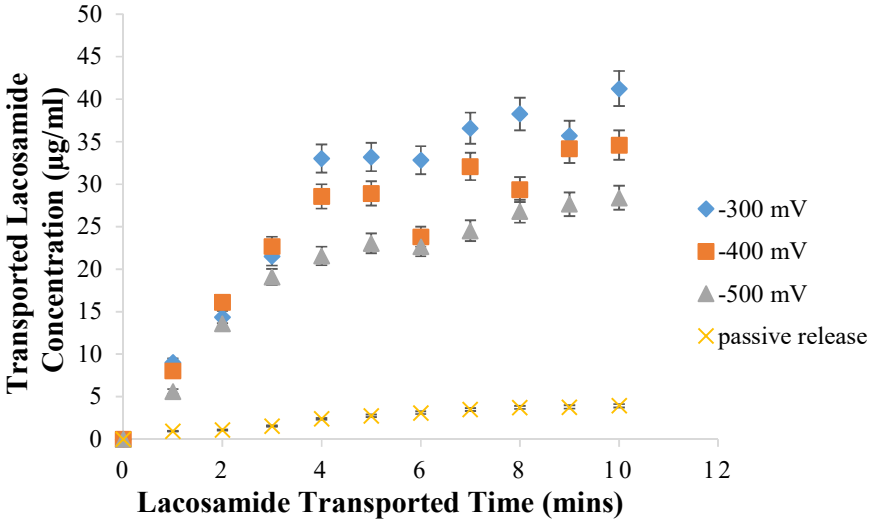

Figure 3.29 Concentration of transported lacosamide through PPy/*p*TS/Pt/PVDF (90 sec, 1 mA/cm^2) coated flat membrane while applying three reducing potential for 10 min.

Figure 3.30 shows the concentration of transported lacosamide through PPy/PSS/Pt/PVDF membrane by applying -400, -500 and -600 mV. -500 mV was peaked up according to the cyclic voltammograms of PPy/PSS film and the maximum transport of lacosamide is seen by applying this potential. Applying -400 mV shows any detectable transport of lacosamide molecules and the concentration of transported drug by applying -600 mV is lower than drug concentration at -500 mV. Hence, the porosity of PPy/PSS/Pt/PVDF membrane by applying -500 mV is at the highest state.

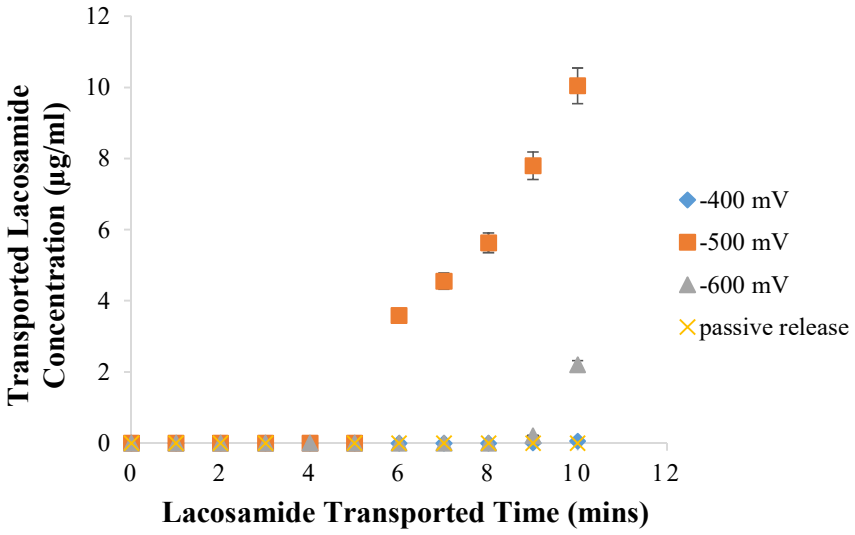

Figure 3.30 Concentration of transported lacosamide through PPy/PSS/Pt/PVDF (90 sec, 1 mA/cm^2) coated flat membrane while applying three reducing potential for 10 min.

Concentration of transported lacosamide through PPy/CS/Pt/PVDF membrane is presented in figure 3.32. -200, -300 and -400 mV was applied to the surface of the membrane. -300 mV was chosen as a reducing potential according to the cyclic voltammograms of PPy/CS film. However, the highest transport concentration of lacosamide molecules was observed by applying -400 mV and then followed by -300 mV and -200 mV. Therefore, the porosity of PPy/CS/Pt/PVDF membrane, while applying -400 mV is much higher than the porosity of this composite membrane at the other reducing states.

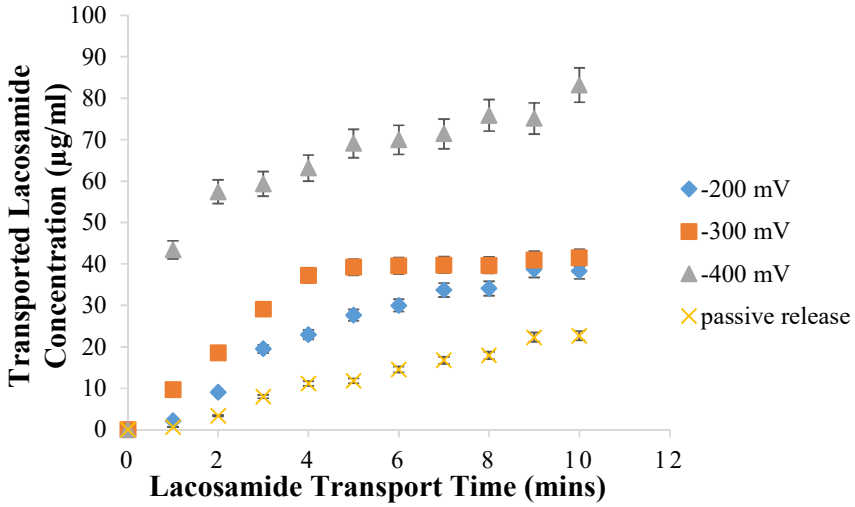

Figure 3.31 Concentration of transported lacosamide through PPy/CS/Pt/PVDF (90 sec, 1 mA/cm^2) coated flat membrane while applying three reducing potential for 10 min.

Figure 3.32 shows the comparison between concentrations of transported lacosamide across PPy/*p*TS/Pt/PVDF membrane at fully reduced and fully oxidized states. As it has been explained before, the porosity of conducting polymer coated Pt/PVDF membrane is at the higher state while applying oxidizing potential. In comparison, the porosity of the composite membrane is at the lowest state by applying educing potential to the surface of composite membrane. Hence, the concentration of transported lacosamide across this composite membrane is higher at the fully oxidized state and lower at the reduced state.

For PPy/*p*TS/Pt/PVDF membrane concentration of transported lacosamide molecules across the composite membrane at fully reduced state by applying -300 mV is 41.25±0.35 µg/ml. the concentration of transported drug at fully oxidized state is 22.30±0.12 µg/ml. Results reveals that the amount of transported drug molecules at fully reduced state is roughly 1.85 times higher than fully oxidized state. The surface pores of PPy/*p*TS/Pt/PVDF flat membrane at reduced state are 2 times more open than these pores at oxidized state. Hence, PPy/*p*TS responds sufficiently to an external stimulation and applying an external voltage to the surface of this

conducting polymer leaded to significant dimensional changes in the porous structure of flat composite membrane.

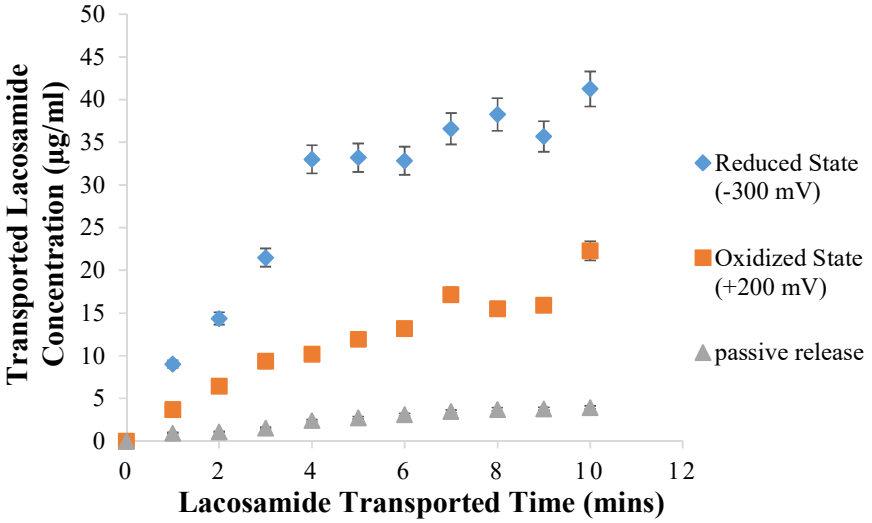

Figure 3.32 Comparison between concentrations of transported lacosamide through PPy/*p*TS/Pt/PVDF (90 sec, 1 mA/cm^2) flat membrane at fully reduced and fully oxidized states.

Figure 3.33 exhibits the results of the comparison between concentrations of transported lacosamide molecules at fully reduced and fully oxidized states for PPy/PSS/Pt/PVDF flat membrane. For this conducting polymer coated membrane, at fully oxidized state (i.e. -350 mV) any drug molecules transported from the feed side to the receiver side. This means at this state, this composite membrane does not have any porous structure. At reduced state by applying -500 mV the surface pores has become open gradually during 10 min time. At the end of the experiment concentration of transported drug molecules to the receiver side was 10.05±0.65 µg/ml. The difference between the concentration of transported drug for this conducting polymer at fully reduced and fully oxidized states is very obvious. By changing between fully oxidized states to the fully reduced state, the non-porous structure of PPy/PSS/Pt/PVDF turned to a porous structure.

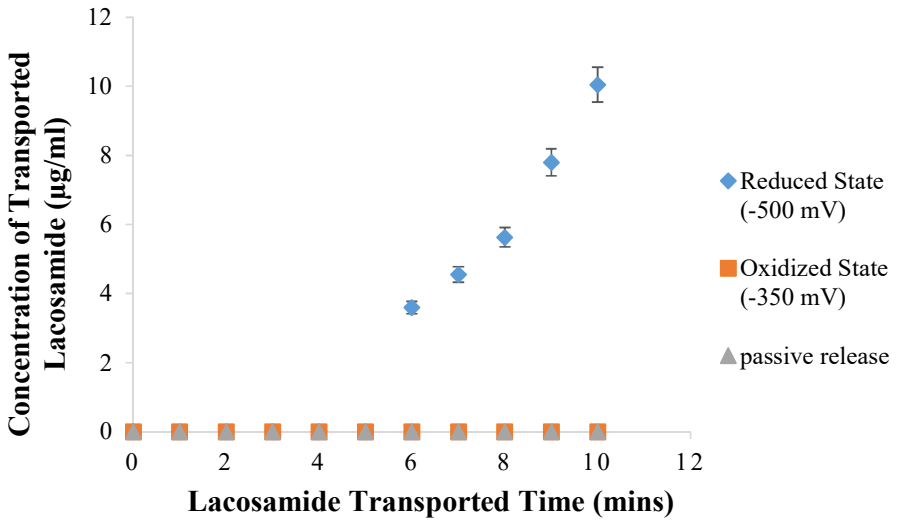

Figure 3.33 Comparison between concentrations of transported lacosamide through PPy/PSS/Pt/PVDF (90 sec, 1 mA/cm^2) flat membrane at fully reduced and fully oxidized states.

Figure 3.34 presents the difference between concentrations of transported lacosamide at full reduced and fully oxidized states across PPy/CS/Pt/PVDF flat membranes. Applying -400 mV to the fully reduce PPy/CS conducting polymer leaded to transport of 83.16±0.85 µg/ml. At oxidized state by applying +400 mV 35.35±54 µg/ml drug transported from the feed side to the receiver side. Final concentration of transported lacosamide at fully reduced state is roughly 2.34 times higher than the concentration of transported drug at fully oxidized state. Concentration differences between fully oxidized and fully reduced state for PPy/CS/Pt/PVDF membrane is highest one among all of the conducting polymer coated Pt/PVDF membranes.

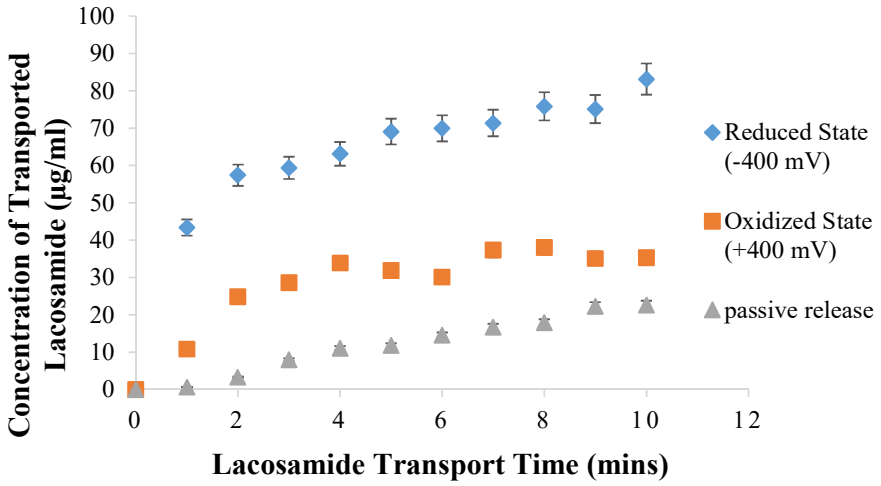

Figure 3.34 Comparison between concentrations of transported lacosamide through PPy/CS/Pt/PVDF (90 sec, 1 mA/cm2) flat membrane at fully reduced and fully oxidized states.

Considering all of the drug rlease figures, the maximum level of lacosamide release is 83.16±5.4 µg/ml which occured when the PPy/CS/Pt/PVDF membrane was stimulating under the reducing voltage (-400 mV). Also for both fully oxidized (-350 mV) and passive state of PPy/PSS/Pt/PVDF membrane no release was observed. According to the literature [34,35], the recommended effective dosage of lacosamide is 200-400 mg/day with this dosage being able to reduce 38-41% seizure frequency in adluts. The comparison of highest release concentration through composite membranes and the approved effective dosage shows a huge difference. However, the point is the release concentration from composite memebrane occured in just 10 mintues of stimulation, and more importantly this amount of drug will be introduced directly into the brain tissue. However, the effective dosage which is suggested in literature is the concentration of drug in blood stream and there is no study no show how much of drug molecues in the blod stream can pass the blood rain barrier and affect the brain tissue. Therefore, making an accurate comparison about the effectiveness of the concentration of released drug from composite flat memebranes is very difficult.

3.5 Conclusion

In this chapter the fabrication of conducting polymer coated Pt/PVDF flat membrane has been presented. These membranes played the role of a gating system to study transport of an anti-epilepsy drug from reservoir side to the receiver side.

Different characterization methods were utilized to find the optimize condition to fabricate these membranes. As a result of characterization experiments PPy/*p*TS, PPy/CS and PPy/PSS were chosen to be used for drug transport studies. The electrical activity of lacosamide molecules was examined and revealed that this drug molecule does not have electrical activity.

Non-stimulated drug transport study showed that PPy/CS coated membrane has the maximum and PPy/PSS coated membrane has the minimum amount of passive transport.

By applying constant oxidizing or reducing voltages for all of the composite membranes, it has revealed that transport of lacosamide molecules at reduced state is higher than oxidized state. Among all of the conducting polymers PPy/CS showed the maximum amount of transport drug at stimulated state and then followed by PPy/*p*TS and PPy/PSS.

3.6 References

1. J.M Davy, C.O Too, S.F Ralph, G.G Wallace, Synt Met, 1999. **99**: p. 191-199.
2. H Zhao, W.E Price, G.G Wallace, J. Membr. Sci, 1998. **148**: p. 161-172.
3. B.W Liechty, D.R Kryscio, B.V Slaughter, N.A Peppas, Annu. Rev. Chem. Biomol. Eng, 2010. **1**: p. 149-11.
4. D Esrafilzadeh, S.E Moulton, E.M Stewart, G.G Wallace, JCR, 2013. **169**: p. 313-320.
5. G.A Hughes, Nanomed, 2005. **1**: p. 22-30.
6. R Langer, MRS Bulletin, 2006. **31**: p. 477-485.
7. R Ravichandran, Sh Mukherjee, S Ramakrishna, J. R. Soc. Inteface, 2010. **7**: p. 559-59.

8. Zh Yue, S.E Moulton, M.J Cook, S Oleary, G.G Wallace, Adv. Drug Deliv. Rev, 2013. **65** : P. 559-569.
9. E Jager, N Masurkar, N.F Nworah, B Gaihre, G Alici, G.M Spinks, Sens. Actuator B-Chem. 2013. **183**: p. 283-289.
10. H Xu, C Wang, J Zoval, M Madou, Biosens Bioelectron, 2006. **21**: p. 2094-2099.
11. A.S Lee, S.F Peteu, J.V Ly, A.G Requicha, M.E Thompson, Ch Zhou, Nanotechnol, 2008. **19**: p. 165501-165509.
12. F Garnier, G Tourillon, M Gazard, J.C Dubois, J. Elactroanal. Chem, 1983. **148**: p. 299-303.
13. C.H Masterangelo, P.F Man, J.R Webster, 2000. p. 184.
14. K.D Kreuer, J. Membr. Sci, 2001. **185**: p. 29-39.
15. J.M Ribo, M.C Anglada, A Dicko, Butll. Soc. Cat. Cien, 1992. **XIII**(1): p. 335-351.
16. J Pellegrino, Ann. N.Y. Acad. Sci, 2003. **984**: p. 289–305.
17. M Zhou, J Heinze, J. Phys. Chem. B, 1999. **44**: p. 1733-1748.
18. S Mawa, K Yoshidac, P Sommer-Larsend, R.B Stein, Sens. Actuator A, 2001. **89**: p. 175-184.
19. F Fusalba, D Blanger, J. Phys. Chem. B, 1999. **103**: p. 9044-9054.
20. P Lemon, J Haigh, Mater. Res. Bull, 1999. **34**(5): p. 665-672.
21. A Kaynak, Mater. Res. Bull, 1997. **32**(3): p. 271-285.
22. A.J Brad, L.R Faulkner, *Electrochemical methods, Fundamentals and Applications*. 1980: John Wiley & Sons, New York.
23. S Pouzet, N.L Bolay, A Richard, Synt Met, 1993. **55**: p. 1495-1500.
24. H Ge, G.G Wallace, Anal Chem, 1989. **61**(21): p. 2391-2394.
25. Li S, H.S White, Electrochem. Soc., 1993. **140**(9): p. 2473-2476.
26. S.N Bhadani, M Kumari, S.K Sen Gupta, G.C Sahu, Appl. Polym. Sci, 1997. **64**(6): p. 1073.
27. L.L Miller, B Zinger, Q.X Zhou, J.Am. Chem. Soc, 1987. **109**(8): p. 2267-2272.
28. T Matencio, M.A De Paoli, R.C.D Peres, R.M Torresi, S.I Torresi, Synt Met, 1995. **72**(1): p. 59-64.

29. C Zhong, K Doblhofer, Elechtrochemica Acta, 1990. **35**(11-12): p. 1971-1976.
30. P.G Pickup, Electroanal. Chem, 1987. **225**(1-2): p. 273-280.
31. T Lindfors, A Lewenstam, A Ivask, Electrochimica Acta, 1998. **43**(23): p. 3503-3509.
32. M.A Ghanem, P.N Bartlett, P Groot, A Zhukov, Electrochem Commun, 2004. **6**: p. 447–453.
33. R.A Flores-Estrella, M.J Aguilar Vega, M.A Smit, Int. J. Electrochem. Sci, 2008. **3**: p. 1065 - 1080.
34. C Fattore, E Perruca, Drugs, 2011. **71** (16) : 2151-2178.
35. L.J Stephen, M.J Brodie, CNS Drugs, 2011. **25** (2) : 89-107.

4 DRUG TRANSPORT STUDIES THROUGH CONDUCTING POLYMER COATED PLATINIZED TUBE MEMBRANES

4.1 Chapter aims

Release of lacosamide from the inside of a PVDF tube membrane has been investigated in this chapter. The outer surface of these tube membranes were coated with a Pt layer followed by polymerisation of a layer of polypyrrole using a range of dopants. These tube membranes act as a drug reservoir and a gating system simultaneously. Different characteristics of these tube membranes were investigated

as well as their transport properties under non-stimulated, stimulated (constant and pulsed potential) states.

4.2 Introduction

Utilizing nanofibers for drug delivery applications is based on their unique functionality such as using both biodegradable and non-degradable material, possibility to deliver a wide range of therapeutic agents and applying different technique for drug loading. These drug loading techniques include coating, embedding, and also encapsulating of drug or the other therapeutic agents. A more controllable drug release kinetics can be achieved by these techniques[1] with hollow nanofiber structures providing a promising opportunity to encapsulate target drug molecules[2]. Figure 4.1 show transmission electron microscopy (TEM) images from the surface and cross section of PCL nanofibers. These hollow/nano tube membranes were prepared by coaxial electrospinning technique. The inset SEM images clearly show the hollow structure of this tube membrane. This tube membrane was utilized to release BSA protein[2].

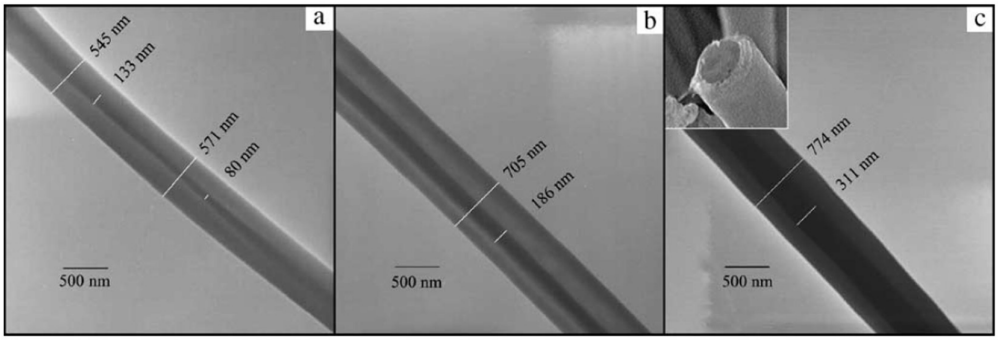

Figure 4.1 TEM images of hollow tube membrane structure composed of PCL. The core is BSA-loaded PEG. The inset in picture c shows the cross section of this tube membrane. Scale bars represent 500 nm[2].

Therefore, high drug loading concentration and also loading of insoluble and intractable drugs are possible. Some therapeutic agents such as antibiotics[3], anti-cancer drugs[4], polysaccharides[5], proteins[6], and growth factors[7] have been

incorporated into nanofiber tube membranes, produced by electrospinning process. These nanofibers have the potential to be used in different biological applications including scaffolds for tissue engineering [8-11]. In addition, the adhesiveness property of these tube membranes to the biological surfaces is an ideal feature for using these tube membranes as topical drug delivery devices[12]. Figure 4.2 demonstrates three different protocols for drug loading of an electrospun nanofiber tube membrane.

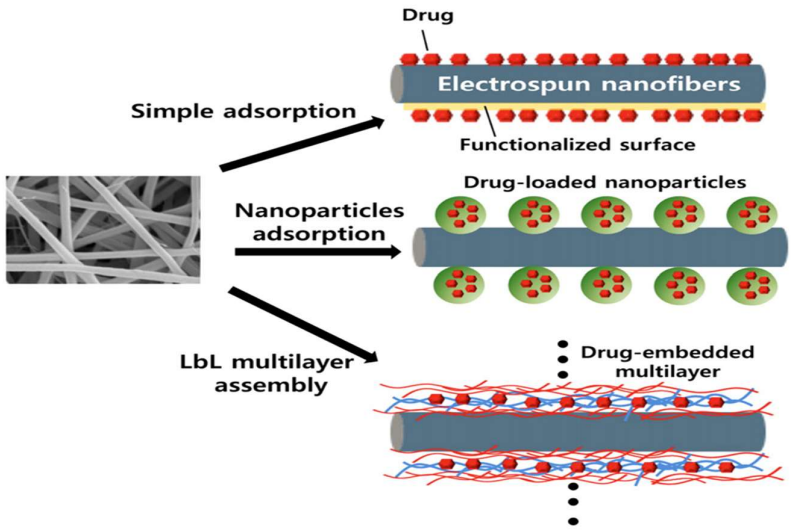

Figure 4.2 Three physical techniques of drug loading on the surface of an electrospun tube membrane[12].

Carbon nanotube membranes (CNTs) are the other tube membrane shape materials which recently have been utilized in biological applications [13-16]. Some therapeutic agents such as peptides [17-19], nucleic acid[20-22] and drugs[23-25] have been investigated to be delivered by using CNTs. It has been shown that CNTs are able to penetrate into the cell which offers the potential of using this material as a carrier of small drug molecules[26, 27].

The development of novel and efficient drug delivery systems is very important to improve the pharmacological profiles of some therapeutic molecules. There are so many different drug delivery systems currently available which have been presented in chapter 1[13]. Using flat composite PVDF membranes has been explained in the

previous chapter. In this chapter the PVDF membranes in a tube membrane format have been utilized as drug delivery system.

4.3 Experimental

4.3.1 Materials

Pyrrole was purchased from Merck, purified by distillation, and stored at -18 ^{o} C. Parra toluene sulfonic acid sodium salt (*p*TS) was purchased from BOH Chem. Chondroitin 4-sulphate sodium salt form bovine trachea (CS) was purchased from Fluka. Poly (4-styrene sulfonic acid) sodium salt (PSS), dodecylbenzenesulfonic acid sodium salt (DBSA), dextran sulphate sodium salt (DS) and hyaluronic acid (HA) had been supplied by Aldrich chemistry. Lacosamide (LCM) with the generic name of Vimpat was provided from St. Vincent Hospital in Melbourne. Figure 3.2 in chapter 3 shows the chemical structure of *p*TS, CS, PSS, DBSA, DS and HA dopants and also LCM molecules.

Artificial cerebrospinal fluid (ACSF) was prepared to be used as electrochemistry solution and also drug transport study experiment. The preparation protocol of ACSF was explained in chapter 3 section 3.3.1.

The PVDF membrane tube membrane was supplied by Ecofine Water Treatment Equipment Co (China). The tube membrane diameters are; outer diameter is 1000 μm with an inner diameter of 630 μm. Similar to the flat membranes (section 3.3.1 in Chapter 3) work, these tube membranes were coated on the outer surface by a 75 nm layer of platinum (Pt) (as optimized in Chapter 3) using an Edwards Auto 306 magnetron sputter coater.

The outer surface of these substrate PVDF membranes was coated with a layer of platinum (Pt) using Edwards sputter coater 302 Auto instrument with four different thickness of Pt layer. Sputter coating was carried out under 2.5×10^{-3} Pa vacuum. The desired thickness of the Pt layer was achieved through instrumental set up with a sputtering power for Pt of 40 W. Homogeneity was tested by SEM cross section imaging and tube membranes were put horizontally in the sputter coater.

4.3.2 Electrochemical Polymerization of Polymer Films

Polypyrrole coated platinised tube membrane PVDF membranes (PPy/Pt/PVDF) were electrochemically synthesized. The electrochemical polymerisation of polypyrrole composite tube membranes process was carried out using a three electrode set up which is shown in Figure 4.3.

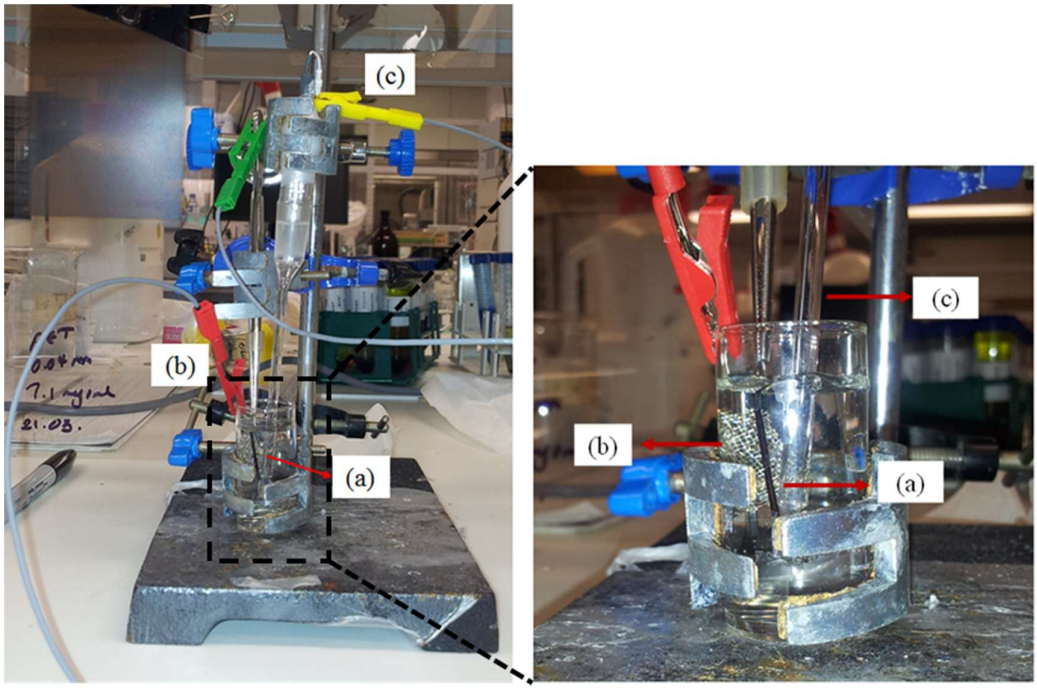

Figure 4.3 Three electrode set up for electropolymerisation onto platinized hollow tube membrane PVDF membrane; (a) platinised tube membrane as working electrode, (b) platinum mesh as auxiliary electrode and (c) Ag/Ag/Cl reference electrode. All of these electrodes are connected to the potentiostat using connection leads.

The electropolymerisation of conducting polymers on the outer surface of Pt/PVDF tube membranes was achieved by applying a current density of 1 mA/cm^2 for 60 sec. A platinum mesh was used as an auxiliary electrode. Reference electrode was Ag/Ag/Cl and the platinized surface of the PVDF tube membrane worked as working electrode. In Figure 4.3 the outer surface of the tube membrane is black which due to deposition of PPy. After electropolymerisation the PPy coated tube membrane PVDF membranes were remove from the electropolymerisation set up, rinsed with sufficient amount of Milli-Q water and dried at room temperature.

4.3.3 Polypyrrole coated PVDF membrane characterization

4.3.3.1 Electroactivity

4.3.3.1.1 Cyclic voltammetry

In order to investigate the electrochemical properties of the conducting polymer films grown on the surface of Pt/PVDF tube membranes, the PPy/Pt/tube membrane was placed in a three electrode electrochemical set up as the working electrode combined with a platinum mesh counter electrode and an Ag/AgCl reference electrode. ACSF was utilized as the electrolyte and five cyclic voltammograms (CVs) were measured using an eDAQ e-recorder (v5.5.11) potentiostat. The potential range was ±800 mV with the voltage scanned at a rate of 50mV/s.

4.3.3.1.2 Scanning Electron Microscopy

Scanning Electron Microscopy (SEM) images of conducting polymer coated tube membrane surfaces and cross sections were taken using a field emission SEM (JOEL JSM-7500FA). This technique has been described in Chapter 2.

4.3.4 Anti-epilepsy drug transport through the PPy coated Pt/PVDF tube membrane

4.3.4.1 Non-stimulated state

Investigation of lacosamide transport from inside of polypyrrole coated Pt/PVDF tube membranes was carried out at non-stimulated state. Once the tube membranes were coated with PPy they were filled with drug using a 5ml syringe (BD PrecisionGlide^{TM} needle 25G 1 - 0.5mm × 25mm). Both ends of the tube membrane were sealed with wax to prevent the drug from leaching out. The drug filled tube membrane was placed in a petri dish which contains 15 ml ACSF solution with

samples taken every 60 sec for 10 min. Drug transport studies through flat PVDF membranes was carried out for 10 min. Therefore, drug release studies by using these conducting polymers coated Pt/PVDF tube membrane was conducted for 10 min.

4.3.4.2 Stimulated state

To perform the stimulated release of lacosamide from inside of tube membrane polypyrrole coated membranes a three electrode set up was employed. The drug filled PPy/PVDF tube membrane was placed vertically in a beaker containing 15 ml ACSF (Figure 4.4). The PPy/PVDF tube membrane was the working electrode with the Ag/AgCl and Pt mesh acting as the reference and auxiliary electrodes respectively (Figure 4.4). As Figure 4.4 shows, the Pt/PVDF tube membrane was hold by a tweezer and the other end of this tweezer was connected to the potentiostat by a connection lid. The applied voltages to the conducting polymer coated tube membrane were chosen according to the redox peaks of these polymers in their cyclic voltammograms.

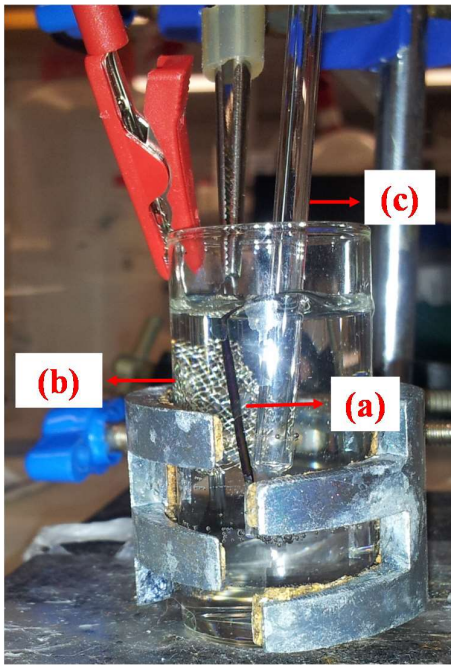

Figure 4.4 Stimulated drug release study from inside of polypyrrole coated tube membrane. (a) Polypyrrole coated outer surface of tube membrane, (b) platinum mesh as an auxiliary electrode, and (c) Ag/AgCl reference electrode.

4.3.5 Released anti-epilepsy drug concentration measurement using HPLC system

Agilent HPLC instrument was used to analyse the concentration of released lacosamide from inside of conducting polymer coated tube membranes. HPLC system has been explained in detail in chapter 2.

4.3.6 Water flux measurements

To investigate water flux for polypyrrole coated platinised tube membranes, Milli-Q water was injected into the polymer coated tube membranes and both ends of these tube membranes were sealed by melted wax (Figure 4.4). The water filled tube membranes were placed horizontally in a petri dish and amount of transported Milli-Q water from inside of these polymer coated tube membranes to the outside were measured every 60 sec for 10 min overall. This experiment was repeated 3 times for each sample.

4.4 Results and Discussion

4.4.1 Conducting polymer film growth and characterization

4.4.1.1 Electroactivity

4.4.1.1.1 Study the electroactivity of lacosamide molecules

Investigating the electroactivity of lacosamide molecules is important because if the lacosamide molecule is electroactive, it may have significant influence on the released properties of the drug molecules in the drug transport experiments, release of lacosamide from inside of conducting polymer coated tube membrane were carried out at stimulated and pulsed potential states. The electroactivity of lacosamide has been investigated at section 3.4.1.1.1 in Chapter 3.

4.4.1.1.2 Pt/PVDF polypyrrole coated tube membrane

Immediately after application of the current density (i.e. 1 mA/cm^2) the generated oxidation potential for PPy/*p*TS and PPy/CS during electropolymerisation was +0.7 V and +0.65 V for PPy/DBSA and PPy/PSS. The electropolymerization conditions were chosen based on the optimized growth conditions which have been presented in chapter 3. The potential generated during polymer deposition has an influence on the formation and structure of the electro polymerized polypyrrole with films exhibiting this oxidation potential leading to a highly conjugated and electroactive polymer [28]. Previous work has reported on variations in electrochemistry and physical properties of PPy when different size dopants are used during growth [29, 30]. In addition all of these dopants have been shown to be compatible with a range of biological cells [31, 32] making them ideal candidates for materials to be used in drug delivery and biological applications.

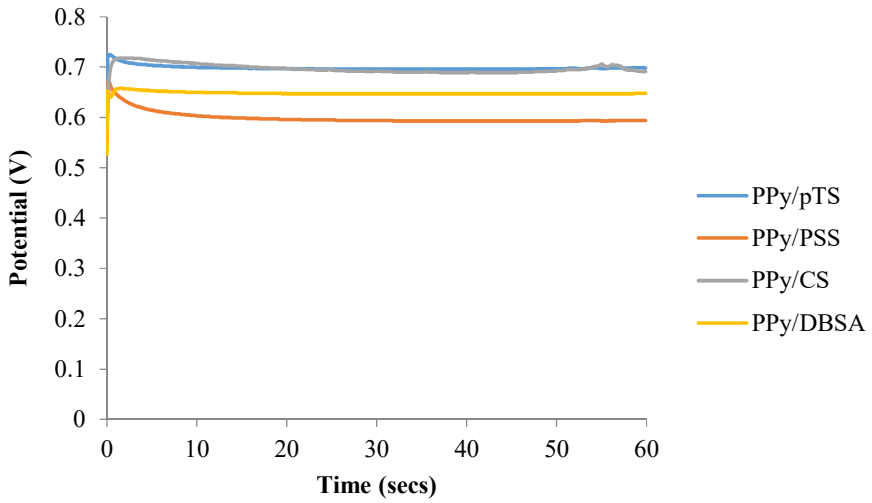

Figure 4.5 Comparison between oxidation voltage generation during galvanostatic electropolymerisation of polypyrrole with *p*TS, PSS, CS and DBSA counterions with a three electrode set up; Ag/AgCl as a reference and an auxiliary Pt mesh as counterion electrode. The electropolymerization condition was applying 1mA/cm^2 for 60 sec for all of the conducting polymers.

Cyclic voltammograms of the PPy coated tube membranes were measured (Figure 4.6). The CVs shows variation between PPy/*p*TS, PPy/DBSA, PPy/CS and PPy/PSS coated Pt/PVDF tube membranes. According to this figure, PPy/PSS demonstrates the highest capacity and clear redox peaks, followed by PPy/CS. The CV of PPy/DBSA was unusual and PPy/*p*TS does not show electrical activity. According to

Figures 3.13 and 3.12 in Chapter 3 PPy/DBSA and PPy/*p*TS exhibited redox peaks. However, using a hollow tube membrane as working electrode leads to having a conducting polymer film with unusual electroactivity. The cylinder shape of working electrode in comparison with the flat working electrode in the previous chapter can be one of the reasons of having unusual electrical activity of grown conducting polymer films. In addition, the growth cell which was utilized in Chapter 3 (Figure 3.3) provided much better configuration to synthesized polypyrrole on the surface of flat membranes. In the growth cell, the platinum mesh electrode covers the whole surface of working electrode. However, in three electrode set up to synthesize polypyrrole on the outer surface of PVDF tube membranes (Figure 4.4), the platinum mesh did not surrounded the whole surface of PVDF tube membrane which is based on the electropolymerization cell set up shown in Figure 4.4

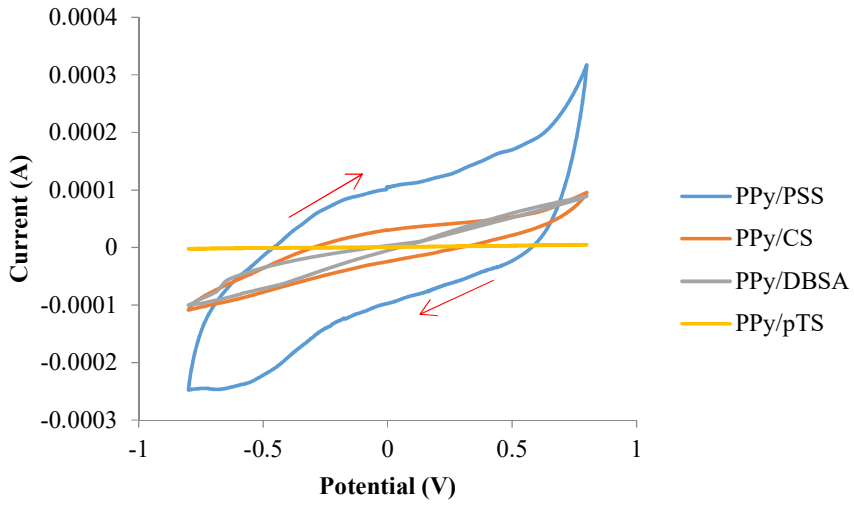

Figure 4.6 Comparison of cyclic voltammograms of PPy/*p*TS, PPy/DBSA, PPy/CS and PPy/PSS which has been deposited on the outer surface of Pt/PVDF tube membrane; Scan rate is 50mV/s.

The cyclic voltammograms of PPy/PSS coated Pt/PVDF tube membrane a broad oxidization peak is seen around 0.0 mV and a small reduction peak is observed

around -500 mV. PPy/CS showed a very broad oxidizing peak around +100 mV and a reducing potential around -300mV. According to the cyclic voltammograms of PPy/PSS and PPy/CS, these conducting polymers are more appropriate candidates to study drug release at stimulation state in comparison with PPy/*p*TS and PPy/DBSA. As previously mentioned and according to the CVs in Figure 4.6, the redox peaks for these two composite tube membranes are clearer. Therefore, PPy/PSS and PPy/CS possess sufficient electrical activity to be stimulated by an external electrical field to act as drug release gate.

4.4.1.2 Morphology of tube membrane Pt/PVDF polypyrrole coated membrane

The surface and cross-section SEM morphology studies were carried out for the PPy/Pt/tube membranes. Figure 4.7 show the surface of the PPy coated Pt/PVDF tube membranes to be typical for polypyrrole films [33-36]. All of these PPy coated tube membranes exhibit porosity indicating the polymer growth conditions maintained a porous structure which is critical to ensure drug transport. The differences between using different counterions for electropolymerisation of polypyrrole on the surface morphology of tube membranes is not as obvious in comparison with flat composite membranes (Figure 3.27 in Chapter 3). This could be due to different geometry of the tube membranes.

For each composite tube several SEM images were taken from different areas of the tube. According to these images which all of them have not presented in this thesis because of the similarity, there was no distinguishable difference in morphology, porosity or topography of different areas of a conducting polymer coated tube.

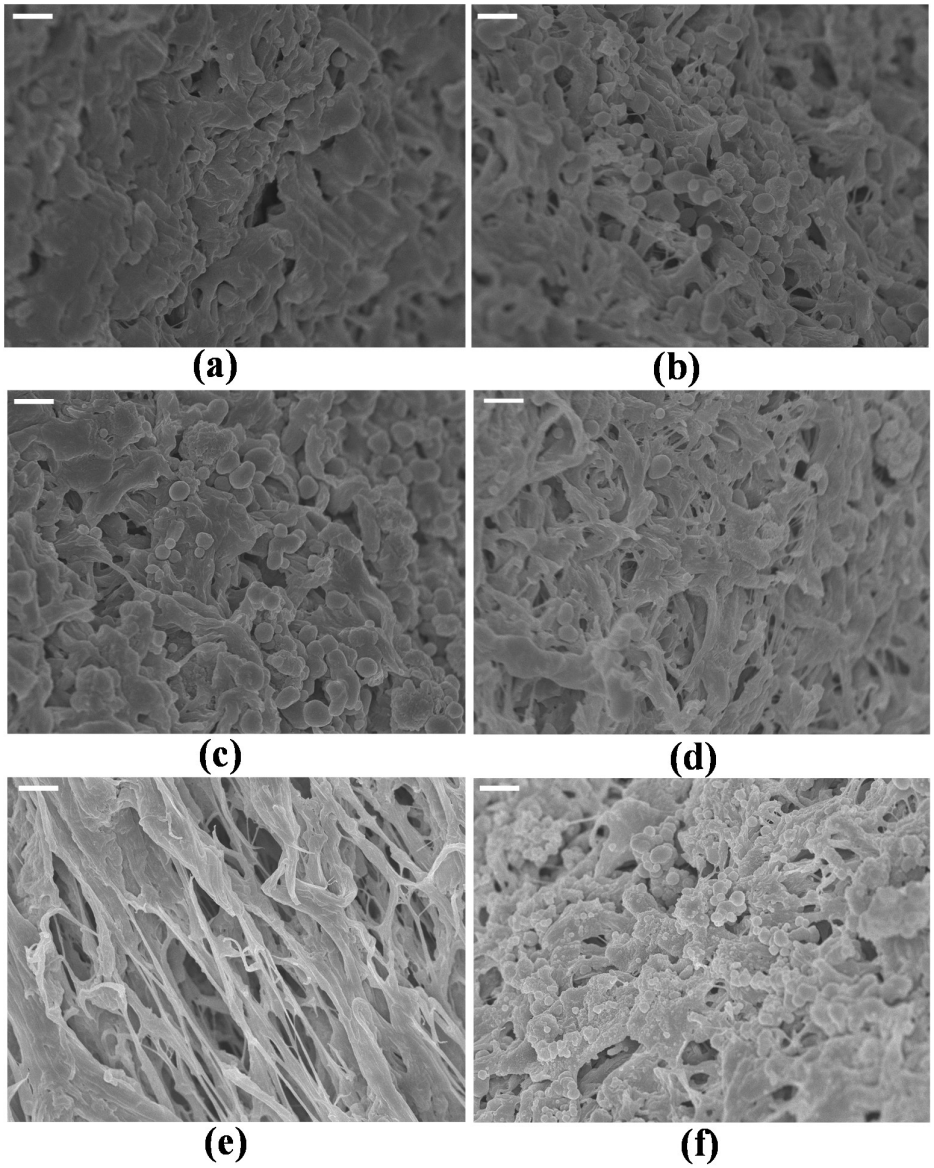

Figure 4.7 SEM images of (a) PVDF, (b) Pt/PVDF, (c) PPy/*p*TS/Pt/PVDF, (d) PPy/CS/Pt/PVDF, (e) PPy/DBSA/Pt/PVDF and (f) PPy/PSS/Pt/PVDF tube membrane surfaces. The scale bar indicates 1 μm.

Figure 4.8 presents the cross section SEM images of PVDF, Pt/PVDF, PPy/*p*TS/Pt/PVDF, PPy/CS/Pt/PVDF, PPy/DBSA/Pt/PVDF and PPy/PSS/Pt/PVDF tube membranes.

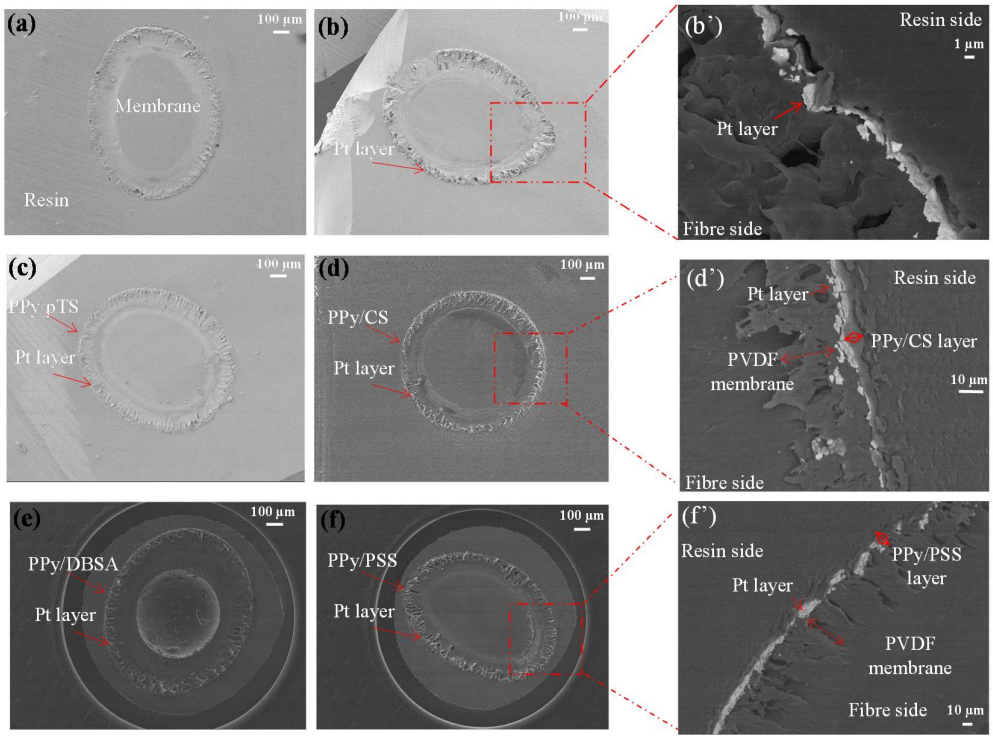

Figure 4.8 SEM images from the cross section of (a) PVDF, (b) Pt/PVDF, (c) PPy/*p*TS/Pt/PVDF, (d) PPy/CS/Pt/PVDF, (e) PPy/DBSA/Pt/PVDF and (f) PPy/PSS/Pt/PVDF composite tube membranes; (b'), (d') and (f') are higher magnification images of Pt/PVDF, PPy/CS/Pt/PVDF and PPy/PSS/Pt/PVDF respectively.

There is no obvious difference between images (a) and (b) in Figure 4.8 despite the outer surface of the PVDF tube membrane being coated by 75 nm Pt layer. Using high magnification SEM images it was possible to measure the PPy thickness deposited on the Pt/tube membrane PPy/*p*TS coated tube membrane; there is 10.01±0.35 µm polymer layer which has been deposited on the outer surface of the tube membrane. For PPy/CS and PPy/DBSA coated tube membranes (Figure 4.8 (d) and (e)) there does not appear to be any significant changes in the diameter of the tube membrane. Figure 4.8 (f) belongs to the PPy/PSS coated PVDF tube membrane. The greatest changes in the diameter of tube membrane occurred for this sample (Figure 4.8 (f) and (f')). Thickness of PPy/PSS deposited layer on the surface of tube membrane is 20.12±0.62 µm. Therefore, similar to the PPy coated flat PVDF membrane studies (Chapter 3, section 3.4.1.2.2.1), PPy/PSS deposited film possesses the highest thickness.

4.4.2 PPy/Pt/tube membrane drug release study

4.4.2.1 Non-stimulated state

Prior to conducting the non-stimulated release experiments water flux of these PPy coated tube membranes was measured. However, due to the small scale of the PPy/Pt/tube membrane it was not possible to measure the very small quantity of Milli-Q water passing through the membrane. Therefore no data was obtained from the water flux experiments on the Pt/tube membrane prior to coating with PPy (as was performed in Chapter 3). Visually it possible to observe Milli-Q water passing through the membrane indicating that the Pt coating did not block the pores of the membrane.

Before starting drug release studies in this session, it has to be menitioned that molecular interactions are extensively dependent on the condition under which theexperiment is being carried out. For instance, sample material, surface chemical modification, and more importantly the surrounding medium, are the experimental conditions which can have an important impact on the interactions between molecules. The condensation of water vapor in the experimental medium caused the capillary forces. However, if the experiment is being conducted in fluids or aquoes solutions, the capillary force vanishes [37, 38]. All drug release experiments of this chapter has been performed in aquos solution, therefore, the callipary force practically dose not have an influence on the result.

The release properties of the PPy/Pt/tube membrane were investigated under a non-stimulated state. The outer surface of these PVDF tube membranes was coated by PPy which had been doped with *p*TS, CS, DBSA or PSS counterions. As Figure 4.9 exhibits, concentration of released lacosamide from inside of these composite tube membranes is very low in comparison with the concentration of drug transport results in Chapter 3. The lower concentration of release with PPy coated tube membranes in comparison with flat membranes may be due to much smaller volume of drug solution. The amount of LCM/ACSF solution inside of tube membranes is much less than the amount of drug solution in the feed side of transport cell that was utilized or drug transport through flat membranes.

The maximum release was measured from the PPy/*p*TS coated Pt/PVDF tube membrane (2.0 ± 0.1µg/ml) followed by PPy/PSS (1.8 ± 0.4 µg/ml) then PPy/CS

(1.4 ± 0.5 µg/ml). The minimum drug release concentration was observed from PPy/DBSA (0.5 ± 0.0 µg/ml) according to the SEM images of these conducting polymer coated Pt/PVDF tube membranes the thickness of PPy/PSS is the highest. Therefore, this sample exhibited the minimum drug transport at the passive state. Diffusion mechanism is the main driving force facilitating drug release in the non-stimulated state.

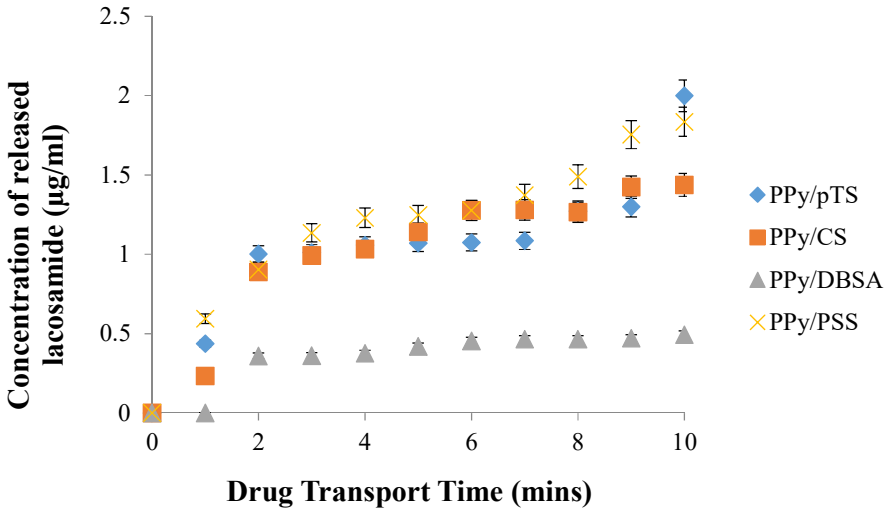

Figure 4.9 Concentration of released lacosamide from inside of PPy/*p*TS, PPy/CS, PPy/DBSA and PPy/PSS coated platinized tube membranes at passive state for 10 min.

4.4.2.2 Stimulated state

4.4.2.2.1 Oxidized state

Similar to section 3.4.3.2.1 in Chapter 3 three oxidizing potentials were applied to the outer surface of conducting polymer coated tube membranes. One of these oxidizing voltages was chosen from the cyclic voltammograms of these conducting polymer films and two other voltages was that oxidizing potential which has been added and subtracted by +100 mV. Drug release study at stimulated state was performed only for the PPy/CS/Pt/PVDF and PPy/PSS/Pt/PVDF tube membranes. These PPys were chosen as they exhibited the best electroactivity (Figure 4.6).

Having sufficient electrical activity is very important and an effective factor in terms of investigating drug release at stimulated states. The conducting polymer which possesses better electrical activity is able to respond to the electrical stimulation more effectively. At oxidized, reduced and also pulsed potential states, release of drug from polymer coated tube membranes occurs due to the response of the deposited conducting polymer layer to the applied voltages.

Figure 4.10 shows the concentration of released lacosamide from inside of the PPy/CS coated Pt/PVDF tube membrane. +250 mV was the oxidizing potential according to the cyclic voltammograms of this conducting polymer. However, the lowest released concentration has been observed by applying +350 mV and then followed by +150 mV and +250 mV. This release result may be due to the less porous structure of PPy/CS/Pt/PVDF tube membrane by applying +350 mV than the other voltages. According to the literature [39] at the oxidized state, the structure of conducting polymer swells. Because of deposition of PPy/CS on the surface of Pt/PVDF tube membrane, the conducting polymer has a porous structure (Figure 4.7). Swelling of PPy/CS at oxidized state could lead to covering some of the surface pores and ban drug release. At fully oxidized state, the structure of conducting polymer becomes more hydrophilic [40] and swollen, which could cause minimum drug release.

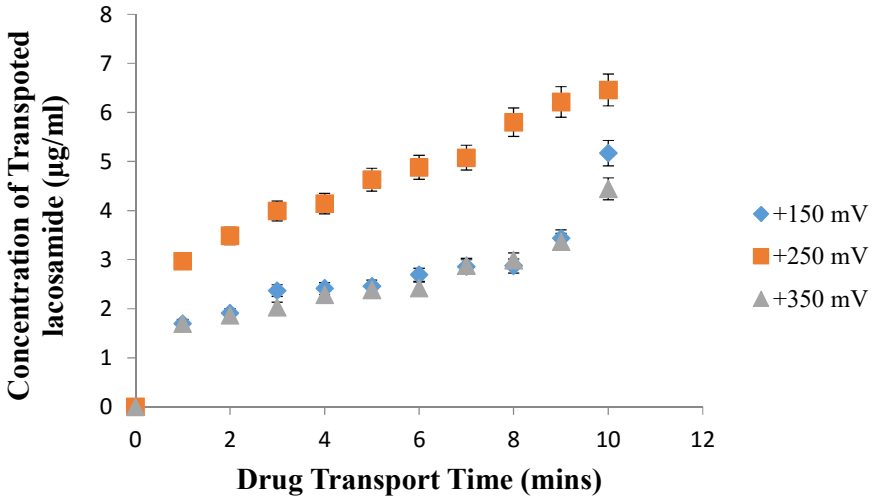

Figure 4.10 concentration of released lacosamide from inside of PPy/CS coated Pt/PVDF tube membrane at oxidized state.

Concentration of released lacosamide from inside of the PPy/PSS coated Pt/PVDF tube membrane is presented in Figure 4.11. The stimulating voltage of +100 mV was chosen from the cyclic voltammograms of this conducting polymer as the oxidation peak voltage (Figure 4.6). As for the PPy/CS work presented above stimulation was examined ±100 mV of this potential Stimulation of the outer surface of this conducting polymer by +200 mV leaded to having minimum drug release concentration and then followed by 0.0 and 100 mV.

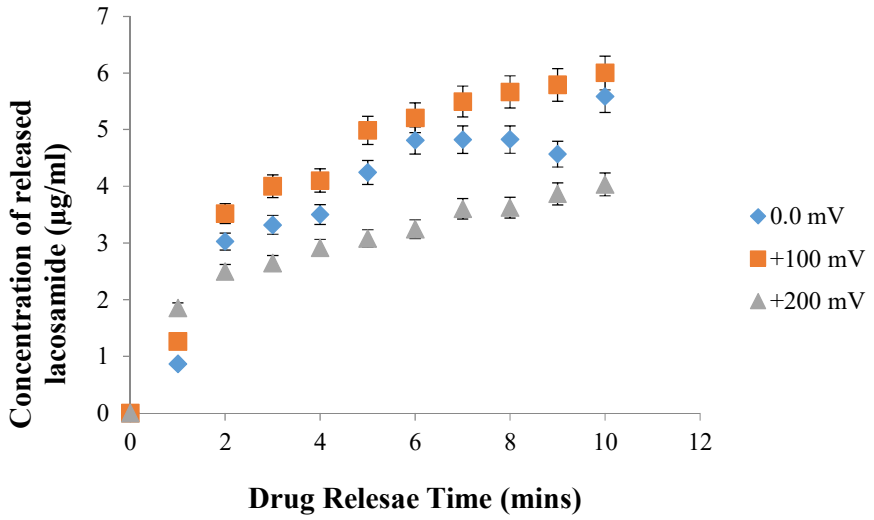

Figure 4.11 Concentration of released lacosamide from inside of PPy/PSS coated Pt/PVDF tube membrane at oxidized state (+100mV) and at potentials ±100mV of the oxidation potential.

According to Figures 4.10 and 4.11, the oxidation potentials which have been picked from the cyclic voltammograms of these polymers (Figure 4.6) exhibited the maximum concentration of drug release for both PPy/CS and PPy/PSS coated Pt/PVDF tube membranes. While, applying the oxidation potentials which were +100 mV higher than the potential in their CVs (Figure 4.6) leads to have minimum drug transport release. Maximum drug release concentration from PPy/CS coated Pt/PVDF tube membrane is 7.1% higher than maximum drug concertation for PPy/PSS coated tube membrane. In addition, the minimum drug release concertation for PPy/CS film is 9.2% higher than the minimum release concentration for PPy/PSS.

For PPy/CS coated Pt/PVDF tube membrane, by applying +150 mV which is 100 mV less than the oxidation potential indicated by CV (Figure 4.6) leaded to 25.0% decrease in the concentration of drug release. Also, applying +350 mV which is 100 mV higher than the oxidation potential indicated by CV (Figure 4.6) caused 31.3% decrease in drug release concentration.

7.53% decrease was observed for PPy/PSS film by applying 0.00 mV. This potential is 100 mV less than the oxidation potential which was indicated by CV (Figure 4.6). In addition, applying 200 mV leaded to have 32.83% decreases in the concentration of drug release in comparison with drug concentration by applying +100 mV. A potential of+100 mV was chosen as the oxidation potential from the cyclic voltammograms of PPy/PSS film (Figure 4.6).

4.4.2.2.2 Reduced state

To study the effect of applying reducing voltage to the surface of conducting polymer coated Pt/PVDF tube membranes three reducing voltages were applied. One of them was chosen according to the cyclic voltammograms of conducting polymer films. The other applied potentials were ±100 mV to that chosen voltage to stimulate conducting polymer layer until its fully reduced state by applying one of these reducing voltages.

Figure 4.12 exhibits the concentration of released lacosamide from inside of PPy/CS coated Pt/PVDF tube membrane. The voltage of -220 mV was chosen from the CV of this conducting polymer (Figure 4.6) as the reducing voltage, although the highest concentration of released lacosamide was observed at -120 mV. Concentration of released lacosamide by applying -220 mV is less than the concentration of release drug molecules by applying -120 mV. Finally, by stimulating the PPy/CS by -320 mV the minimum amount of drug molecules released from inside of the tube membrane.

According to the literature [39, 40], at reduced state in comparison with oxidized state, the structure of conducting polymer is contracted. Because of deposition of PPy/CS on a porous structure which is Pt/PVDF tube membrane (Figure 4.7), applying reduction potential caused shrinkage in the structure of polymer coated tube membranes. Therefore, surface pores become more open and facilitate the release of drug molecules to the outside.

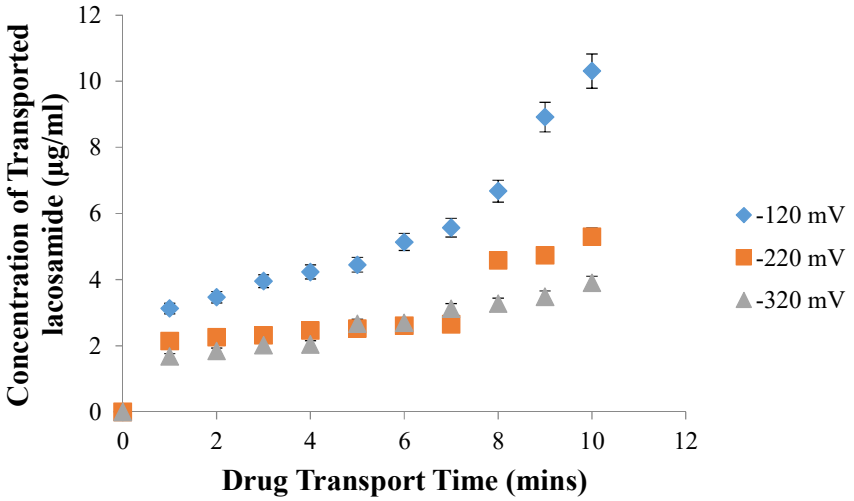

Figure 4.12 Concentration of released lacosamide from inside of PPy/CS coated Pt/PVDF tube membrane at reduced state (-220 mV) and at potentials ±100mV of the reduction potential.

Figure 4.13 shows the concentration of released lacosamide from PPy/PSS coated Pt/PVDF tube membrane at reduced state. From the recorded CVs (Figure 4.6) the reduction peak is observed at -550 mV. Maximum released concentration observed by applying -650 mV. Released concentration for -450 mV and -550 mV is approximately the same.

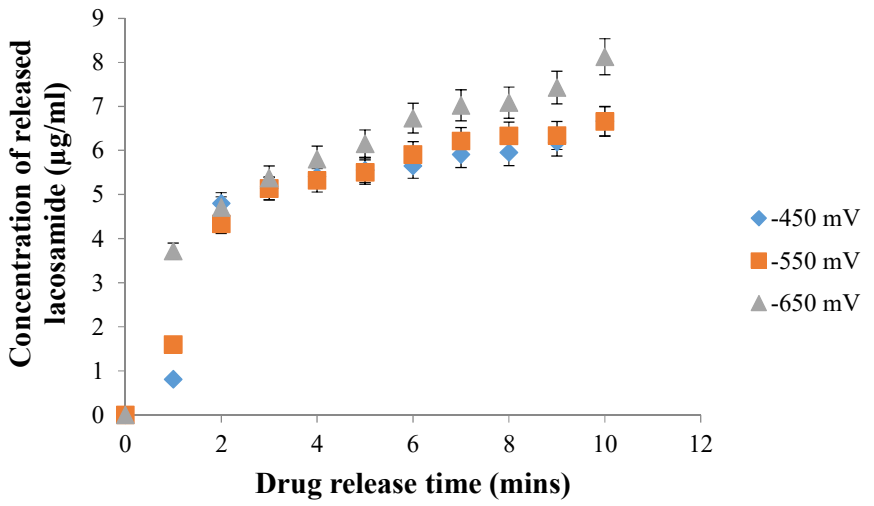

Figure 4.13 Concentration of released lacosamide from inside of PPy/PSS coated Pt/PVDF tube membrane at reduced state.

For PPy/CS (Figure 4.12) maximum concentration of released drug occurred by applying -120 mV which is 100 mV lower than the redox reduction potential (Figure 4.6). For PPy/PSS (Figure 4.13) this maximum release was observed by applying -650 mV which is 100 mV higher than the redox reducing potential (Figure 4.6). Maximum release concentration for PPy/CS is 21.14% higher than the maximum concentration for PPy/PSS.

Figure 4.14 presents the comparison between concentrations of released lacosamide at fully oxidized (+350 mV) and fully reduced (-120 mV) states for the PPy/CS polymer. To achieve fully oxidized state +350 mV applied to the surface of PPy/CS coated Pt/PVDF tube membrane. After 10 min in the fully oxidised state 4.4 ± 0.2 µg/ml of lacosamide was released compared to 10.3 ± 0.2 µg/ml from the fully reduced state indicating approximately 2.3 times higher release under an oxidized state. In Figure 4.14 after 10 min of applying -120 mV which is the fully reduced potential the PPy/CS film exhibited a burst release of lacosamide.

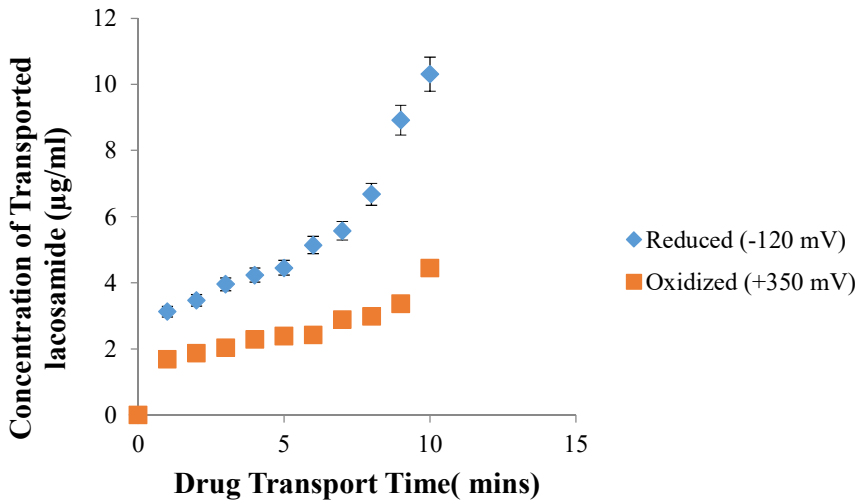

Figure 4.14 Comparison of released lacosamide from PPy/CS/Pt/PVDF tube membrane at fully oxidized (+350 mV) and fully reduced (-120 mV) states.

Comparison between concentrations of released lacosamide from inside of PPy/PSS coated Pt/PVDF tube membrane at fully oxidized (+200 mV) and fully reduced state (-650 mV) is presented in Figure 4.15. The concentration of released lacosamide after 10 min at fully oxidized state is 4.0 ± 0.3 µg/ml, whilst in the reduced state the concentration of released lacosamide was 8.1 ± 0.4 µg/ml. The concentration of released lacosamide at fully reduced state is approximately 2 times greater than when in the fully oxidized state.

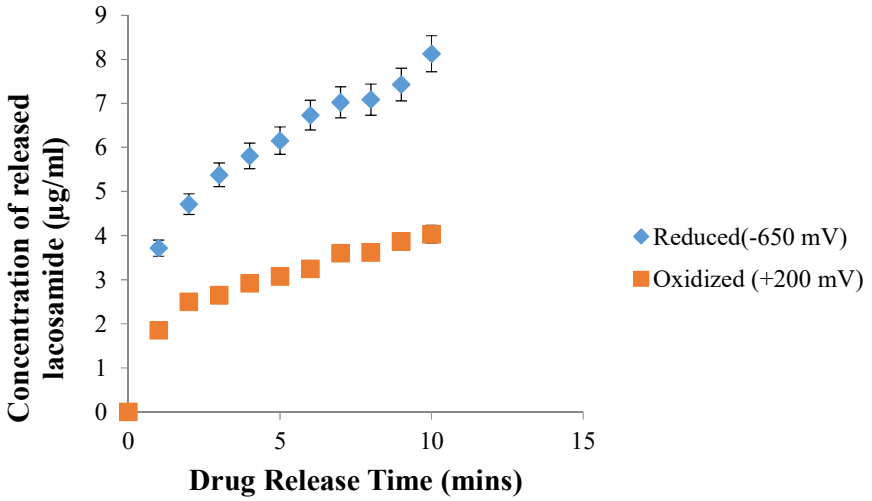

Figure 4.15 Comparison between concentrations of released lacosamide from inside of PPy/PSS/Pt/PVDF tube membrane at fully oxidized and fully reduced states.

At fully reduced state the total concentration of release LCM from PPy/CS coated Pt/PVDF tube membrane is 27.2% higher than the concentration of LCM release from PPy/PSS coated membrane. However, the concentration of released LCM at fully oxidized state is approximately similar for bot conducting polymers.

One noticeable difference between release profile of PPy/PSS and PPy/CS is the rate of release concentration after 5 min applying of reducing potential. For PPy/CS the concentration of release LCM at time = 10 min is 57.3% higher than the concentration of LCM at time = 5 min. For PPy/PSS this increase percentage is 23.5%. Therefore, drug molecules could release from PPy/CS coated Pt/PVDF tube membrane approximately 2.4 times faster than PPy/PSS coated Pt/PVDF tube membrane.

According to drug release figures, the maximum level of lacosamide release is 10.31±6.3 µg/ml which was observed by applying -120 mV (reducing potential) to PPy/CS/Pt/PVDF tube membrane. In addition, the minimum concentration of release is 4.03±0.1 µg/ml and has happened for PPy/PSS/Pt/PVDF tube membrane by applying +200 mV as an oxidizing voltage. Based on studies have been done on the efficient level of lacosamide molecules in human body [41, 42], the recommended level of lacosamide is 200-400 or 200-600 mg/day which is approved as an effective dosage. Obviously, there is a huge difference between the recommended level of lacosamide and the higest level of drug release from conducting polymer coated tube

membrnes. Similar to the flat membrane studies, the recomnded concentration represents the level of drug on blood stream which is much higher than the actual amount of drug concentration needed on the brain tissue. As it has been mentioned in chapter 3, it is practically not possible to make a valid comparison about the sizures supressing efficiency of the concentration of release lacosamide from neither flat nor tube membranes.

It should be mentioned that before switching the potential to oxixdized or rduced states, there might be some drug molecules in the recievrr side which is the ouside of the tube mmembrane. Therefore, a ΔC concentration difference of drug molecules exsits between inside and ouside of the membrane. However, the difference in ΔC can be an issue when a very concentrated or saturated solution is being used. In these cases the peresence of drug molecules ouside of the tube membrane can block the release pathway of inside drug molecules. In the expereminets of this chapter, the concentration of drug molecules in both inside and outside of the tube is very low; therefore, the effect of changing ΔC is negligible. Sicne, the drug molecules which already exsit outside of the membrane can not shut the release pores of the tube membrane.

4.4.2.2.3 Pulsed potential state

One of the most important goals of this project is fabricating a drug release device which is capable of releasing an anti-epilepsy drug to provide an on/off release profile. Therefore, release of lacosamide from PPy coated Pt/PVDF tube membranes were investigated at pulsed potential.

Figure 4.16 presents the results of lacosamide release from PPy/CS/tube membrane. The initial potential is the reducing voltage (i.e. -120 mV) which is applied for 2 min followed by switching the potential to the oxidizing voltage (i.e. +350 mV) for a further 2 min. The pulse width is 4 min and two pulses were applied. The first 2 min of applying a reducing potential resulted in a release of lacosamide and upon switching to an oxidising potential the release was effectively stopped. When the potential was switched back to the reducing voltage release was again recorded over the 2 min, which stopped when an oxidising voltage was applied.

The concentration of released drug while applying oxidizing potentials in Figure 4.16 is approximately 4.2 less than the concentration of transported drug at single oxidizing state. In addition, the concentration of released lacosamide by switching to reducing potentials is 1.75 times higher than the concentration of released drug under applying single reducing potential.

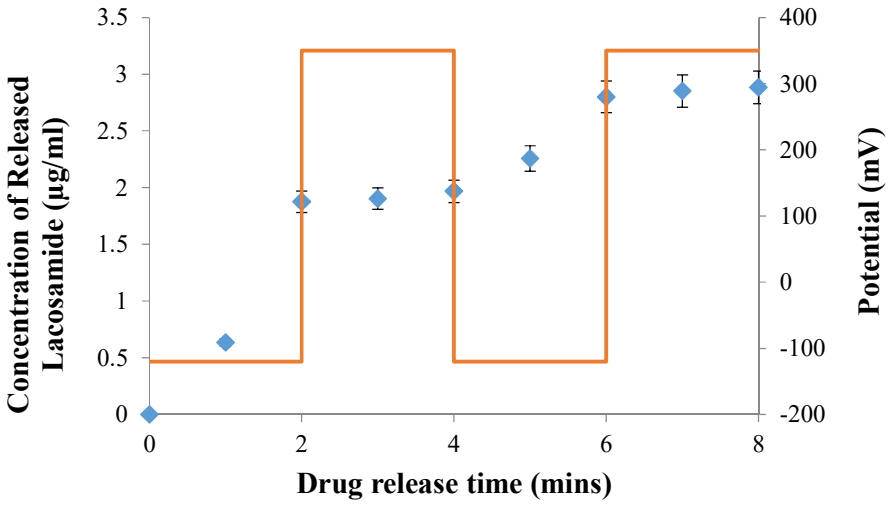

Figure 4.16 Concentration of released lacosamide from inside of PPy/CS/Pt/PVDF tube membrane at pulsed potential state; Right hand side y-axis indicates potential (mV) and left hand side y-axis exhibits the concentration of released lacosamide (µg/ml).

Figure 4.17 exhibits the release of lacosamide from PPy/PSS/tube membrane at pulsed potential state. The initial potential is reducing voltage (i.e. -650 mV) which is applied for 1 min. The voltage is then switched to the oxidizing voltage (+200 mV) 1 min. One pulse cycle last for 2 min and four cycles are applied. By applying the reducing potential for the first min initiated drug release from PPy/PSS/Pt/PVDF tube membrane. However, switching from the reducing state to the oxidizing state did not stop drug release. Continuing to pulse potential state for this conducting polymer coated Pt/PVDF tube membrane did not show the on/off release profile.

Switching from reducing to oxidizing state did not stop drug release because not all of the conducting polymer can response to the external electrical stimulation very fast. Switching from reduced to oxidized or from oxidized to reduced state does not

happen as soon as the electrical stimulation is applied. Since reducing and oxidizing happens because of ion transfer between conducting polymer and the electrolyte, and this process takes time. The size of the counterion plays very important role on the speed of reduction or oxidization of conducting polymer. This may be the main reason of seeing difference between release profile of PPy/PSS and PPy/CS. The PSS counterion has larger molecules than the CS. Therefore, the movement of PSS between polymer structure and electrolyte takes longer time.

PSS molecules are larger than CS molecules so it takes longer for PPy/PSS than PPy/CS to react to the electrical stimulation which leads to drug release profile that is not as sufficient as PPy/CS release profile.

According to Figure 4.17 the concentration of released lacosamide while application of reducing voltage is approximately 1.6 times higher than the concentration of released drug by applying constant reducing voltage. Furthermore, the concentration of released lacosamide at single oxidizing state is 1.4 times less than the concentration of transported lacosamide at pulsed oxidizing state.

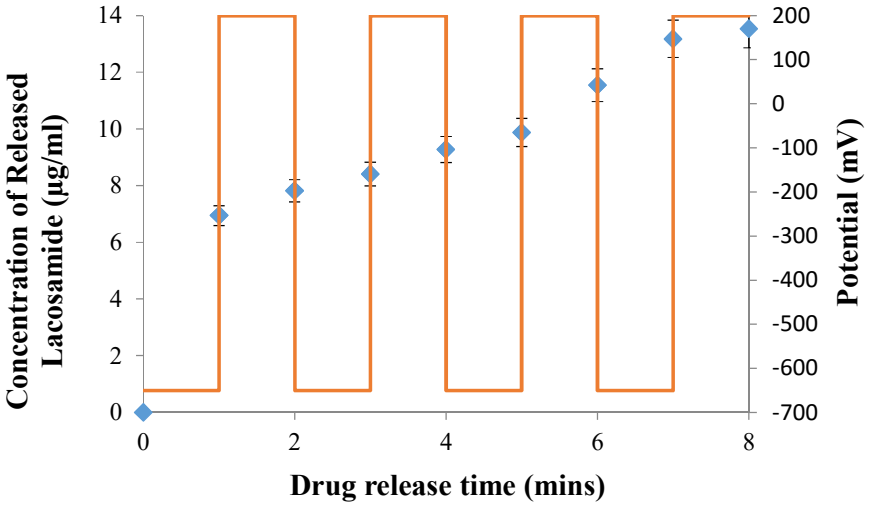

Figure 4.17 Concentration of released lacosamide from inside of PPy/PSS/Pt/PVDF tube membrane at pulsed potential state; Right hand side y-axis indicates potential (mV) and left hand side y-axis exhibits the concentration of released lacosamide (µg/ml).

For both conducting polymer coated Pt/PVDF tube membranes, the overall concentration of release lacosamide at pulsed potential state is less than drug released concentration at single reduced states. According to the previous results (Figures 4.10 and 4.11) application of oxidizing potential decreases the release of drug molecules. At pulsed potential state, when a reducing potential is applying drug release happens and otherwise application of oxidizing potentials declines the release of drug. Therefore, the overall drug release at pulsed potential is less than drug release at application of single reducing potential.

The concentration of drug release for PPy/CS coated Pt/PVDF tube membrane at the end of two pulses is almost the same as concentration of released drug at single oxidized state after 8 min. However, the concentration of released drug at single reduced state after 8 min is 56.82% higher than the overall concentration at the end of pulsed potential studies. These results reveal that by utilizing the pulsed potential state, the total concentration of release drug is less, but the release profile is much more controllable. Continuing the pulsed potential states can increase the concentration of released drug.

Results for PPy/PSS coated Pt/PVDF tube membrane are different from PPy/CS tube membrane. After applying two pulses to the surface of PPy/PSS coated Pt/PVDF tube membrane, the total concentration of released lacosamide is just 3.33% higher than the concentration of released lacosamide after 8 min of applying single reducing potential and 56.95% higher than the concentration of release lacosamide after 8 min of applying single oxidizing voltage. Therefore, it seems that for PPy/PSS applying pulsed potential state leaded to release more lacosamide molecules. However, unlike to the PPy/CS coated Pt/PVDF tube membrane the PPy/PSS did not show the controllable release profile as sufficient as PPy/CS. For PPy/PSS applying more pulses may be leaded to have more suitable release profile. The concentration of released lacosamide for PPy/PSS is 65.75% higher than concentration of drug release for PPy/CS after two pulses and 78.71% after applying 4 pulses.

4.5 Conclusion

Conducting polymer coated Pt/PVDF tube membranes have been fabricated and been utilized as gating and reservoir system simultaneously to study release of an anti-epilepsy drug. The *p*TS, DBSA, CS and PSS were used to synthesize polypyrrole on the outer surface of Pt/PVDF tube membranes. This surface had been coated with 75 nm layer of Pt before conducting the electropolymerization experiments. For all of these dopants, 1 mA/cm^2 current density for 60 sec was applied.

Later on, the characterization of these conducting polymer coated tube membranes was investigated. According to their cyclic voltammograms PPy/CS and PPy/PSS coated tube membranes exhibited more sufficient electrical activity and redox properties. Therefore, these two conducting polymer coated tube membranes were chosen to be utilized for drug release studies. Similar to the flat composite PVDF membrane, the concentration of released drug at reduced state was higher than oxidized and also non-stimulated states. The total concentration of released lacosamide from PPy/CS coated Pt/PVDF tube membrane at stimulated states was higher than PPy/PSS.

By applying the pulsed potential state, composite tube membranes exhibited the on/off release profiles. The on/off release profile of PPy/CS is more sufficient than PPy/PSS. PPy/CS coated tube membrane showed better respond regards switching between reduced and oxidized states in comparison with PPy/PSS coated tube membrane. However, the overall concentration of release lacosamide from PPy/CS at pulsed state was less than the total release concentration at single reduction state. For PPy/PSS the total concentration after applying four pulses was higher than the release concentration by applying single reducing voltage.

4.6 References

1. T.J Sill, V.R.H.A., Biomat, 2008. **29**: p. 1989-2006.
2. H.l Jiang, P.C Zhao, K.J Zhu, W.A Chen W.A, JCR, 2005. **108**(237-243).
3. K Kim, C Chang, D.F Fang, B.S Hsiao, B Chu, M Hadjiargyrou, JCR, 2004. **98**: p. 47-56.
4. J Xie, Pharm.Res, 2006. **23**: p. 1817-1826.
5. E Loung-Van, K.N Chua, K.W Leong , V Nurcombe, S.M Cool, Biomat, 2006. **27**: p. 2042-2050.
6. J Zeng, F Czubayko, T Kissel, J.H Wendorff, A Greiner, Biomacromol, 2005. **6**: p. 1484–1488.
7. C.L Casper, K.L Kiick, J.F Rabolt, Biomacromol, 2005. **6**: p. 1998–2007.
8. S Agarwewal, A Greiner, Polymer, 2008. **49**: p. 5603-5621.
9. K.N Chua, P.C Zhang, H.F Lu, J Wen, S Ramakrishna, K.W Leong, H.Q Mao, Biomat, 2005. **26**: p. 2537-2547.
10. J.V Araujo, I.B Leonor, E.D Pinho, R.L Reis, N.M Neves, J. Biomater. Sci., Polym.Ed., 2008. **19**: p. 1261-1278.
11. S Janjanin, M.T Morgan, R.A Shanti, R.S Tuan, J. Surg. Res, 2008. **149**: p. 47-56.
12. H.S Yoo, T.G Park, Adv. Drug Delive. Rev, 2009. **61**: p. 1033–1042.
13. A Bianco, M Prato, Chem. Bio, 2005. **9**: p. 674–679.
14. C.R Martin, Nat Rev Drug Discov, 2003. **2**: p. 29-37.
15. A Bianco A, Adv Mat, 2003. **15**: p. 1765-1768.
16. N.W Shi Kam, J Am. Chem. Soc, 2005. **127**: p. 6021-6026.
17. D Pantarotto, R Graff, J Hoebeke, J.P Briand, M Prat, A Bianco, J Am. Chem. Soc, 2003. **125**: p. 6160-6164.

18. D Pantarotto, J Hoebeke, F Brown, E Kramer, J.P Briand, S Muller, M Prato, A Bianco, Chem Biol, 2003. **10**: p. 961-966.
19. C Salvador-Morales, E Sim, J Sloan, M.L.H Green, R.B Sim, Mol Immunol, 2005.
20. D Luo, Trends Biotechnol, 2004. **22**(101-103).
21. G.D Schmidt-Wolf, Trends Mol Med, 2003. **9**: p. 67-72.
22. D Liu, Curr Med Chem, 2003. **10**: p. 1185-1315.
23. T.M Allen, Sci, 2004. **303**: p. 1818-1822.
24. K Kostarelos, Adv Colloid Interface Sci, 2003. **106**: p. 147-168.
25. G Zheng, F Patolsky, Y Cui1, W.U Wang, Ch.M Lieber, Nat Rev Cancer, 2005. **5**: p. 161-171.
26. D Pantarotto, M Prato, A Bianco, Chem Commun (Camb), 2004: p. 16-17.
27. N.W Shi Kam, P.A Wender, H Dai, J. Am. Chem. Soc, 2004. **126**: p. 6850-6851.
28. S.K Marx, I Barness, Z Liron, Biosens. Bioelectron, 2001. **16**: p. 239-244.
29. T Okuhara, Anal. Chim. Acta, 1982. **142**: p. 281-284.
30. H Zhang Peng, Q Nie, L.S Yao, Analyst, 2001. **126**: p. 189-194.
31. A.H Kuptsov, G.N Zhizhin, *Polymer Data Handbook*. 1998: Oxford University Press.
32. S.M Jones Reddy, T.J Vadgama, Anal. Chim. Acta, 1998. **363**: p. 203-213.
33. J.B Sanchez, F Berger, J.Y Rauch, P Fievet, Mat. Res. Bulletin, 1997. **32**(3): p. 271-285.
34. P Lemon, J Haigh, Mat. Res. Bulletin, 1999. **34**(5): p. 665-672.
35. S.N Bhadani, G Sahu, Appl. Polym. Sci, 1997. **64**: p. 1073.
36. L. L Miller,J. Am. Chem. Soc, 1987. **109**: p. 2267-2272.
37. H.M Grandin, M Textor, *Intelligent Surfaces in Biotechnology : Scientific and Engineering concept*. 2012: Wiley Press, USA.
38. A Nokhpdchi, G.P Martin, Pulmonary Drug Delivery. 2015: Wiley Press, USA.
37. M.B Samani, G.M Spinks, Ch Cook, SSM, 2006. **6168**: p. 1-10.
38. G.G Wallace, G.M Spinks, L.A.P Kane-Maguire, P.R Teasdale, *Conductive Electroactive Polymers*, ed. T. Edition. 2009: CRC Press.
41. C Fattore, E Perruca, Drugs, 2011. **71** (16) : 2151-2178.

42. L.J Stephen, M.J Brodie, CNS Drugs, 2011. **25** (2) : 89-107

5 INVESTIGATING DRUG INTERACTIONS WITH CP SURFACES USING QCM TECHNIQUE

5.1 Chapter aims

Transport of lacosamide drug molecules through flat and tube Pt/PVDF membranes coated with polypyrrole has been investigated in Chapter 3 and 4. However, one of the important factors in the case of drug delivery study which is the affinity of drug molecules to the surface of CPs has not been studies. Therefore, the main focus of this chapter is investigation of the interaction of the anti-epilepsy drug lacosamide with the surface of CPs by using QCM technique.

5.2 Quartz Crystal Microbalance

Researchers have been interested quantify the absorption of molecules such as protein and drug molecules to the surface of conducting polymers. A number of techniques which have been utilized are QCM[1], surface plasma resonance (SPR)[2], ellipsometry[3], FTIR[4] and atomic force microscopy (AFM)[5]. Among all of these techniques, QCM has been utilized to carry out a number of studies to investigate the existence of drugs with different concentrations. Much research has been developed on the base of QCM for drug discovery studies in the pharmaceutical industry, and, a number of drugs have been detected using QCM technique at nM to mM concentrations[6-13]. Moreover, other media such as serum or urine have been used to study drug detection with a range of nm to μM[14-16].

The recent improvement of the QCM technique is the capability to measure the interaction of even tiny molecules such as ions or solute transport[17] at the liquid-solid interface. In addition, with this advanced technique, energy dissipation characterization or viscoelastic behavior study of the deposited mass upon the material coated quartz crystal sensor is possible.

The most explicit factor of changing f is adsorption or desorption of mass. Hence, many researchers design their experiments with maximized detectable mass binding with the metal coated quartz crystal surface. For example studying the immobilized enzyme biosensors on the QCM sensors[18, 19].

Despite of an explosive growth which has been made in the development of QCM application to investigate a wide variety of molecular systems at the solution-surface interface, a lack of study in terms of drug-drug carrier surface interaction has been observed. In this chapter the interaction of an anti-epilepsy drug with the surface of PPy polymerized using a range of different dopants was investigated.

5.3 Experimental

5.3.1 Materials

Pyrrole was purchased from Merck, purified by distillation, and stored at -18 ^{o} C. Parratoluene sulfonic acid sodium salt (*p*TS) was purchased from BOH Chem. Chondroitin 4-sulphate sodium salt from bovine trachea (CS) was purchased from Fluka. Poly (4-styrene sulfonic acid) sodium salt (PSS) and dodecylbenzenesulfonic acid sodium salt (DBSA) had been supplied by Aldrich chemistry. Lacosamide (LCM) with the generic name of Vimpat was provided form St. Vincent Hospital Melbourne (Professor Mark Cook). Figure 5.1 shows the chemical structure of *p*TS, CS, PSS and DBSA dopants and also LCM molecules.

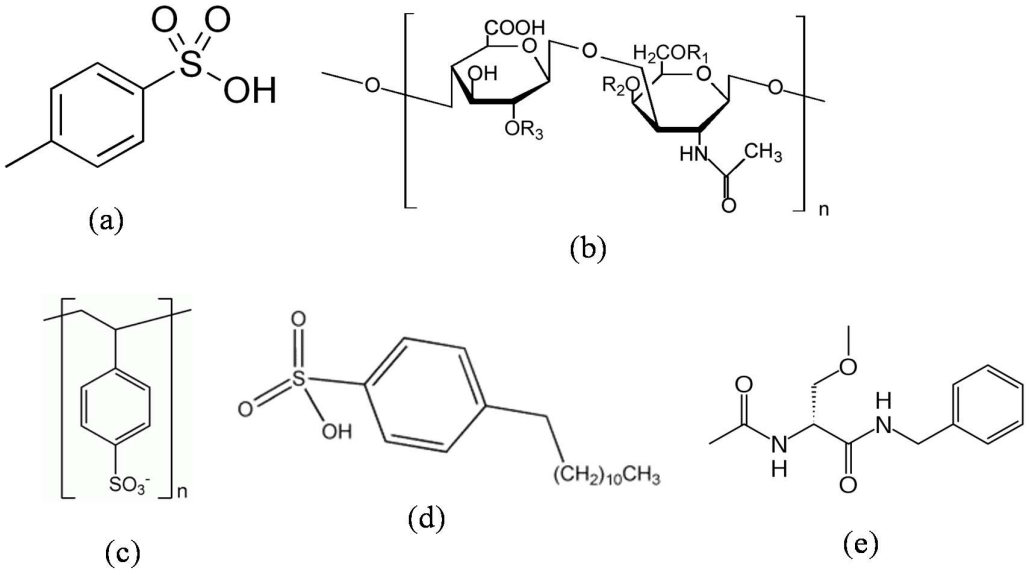

Figure 5.1 chemical structure of; (a) Parratoluene sulfonic acid sodium salt (*p*TS), (b) Chondroitin 4-sulphate sodium salt form bovine trachea (CS), (c) Poly (4-styrene sulfonic acid) sodium salt (PSS), (d) Dodecylbenzenesulfonic acid sodium salt (DBSA) and (e) lacosamide (LCM) molecules.

Artificial cerebrospinal fluid of the brain (ACSF) was prepared from two solutions with the proportion of 50:50 v/v; solution A was made from NaCl (8.66 g), KCl (0.224 g), $CaCl_2.2H_2O$ (0.206 g), $MgCl_2.6H_2O$ (0.163 g) which has been dissolved in 500 ml pyrogen-free water. Solution B was made of $Na_2HPO_4.7H_2O$ (0.214 g), $NaH_2PO_4.H_2O$ (0.027 g) which was dissolve in 500 ml pyrogen-free water. ACSF was stored at 4^{o} C prior to use. All of the chemicals used to prepare ACSF were purchased from BASF.

5.3.2 Electrochemical Polymerization of Polymer Films

Electrochemical polymerization of the Polypyrrole (PPy) conducting polymer film was carried out using a Q-sense electrochemistry module (QEM 401) axial flow cell with a Q- Sense E4 quartz crystal microbalance system (Q-Sense AB, Västra, Frölunda, Sweden, Figure 5.2). During the electropolymerization process the deposited film QCM-D parameters were recording. The QCM sensor was an AT cut quartz crystal with a 10 mm diameter gold electrode (QSX301) with a fundamental resonance frequency of 5 MHz. The gold sensor surface of the quartz crustal was cleaned prior to electropolymerization. Cleaning process was performed using piranha solution (70% sulphuric acid and 30% hydrogen peroxide) for 3 min, and then gold sensor surface was rinsed thoroughly with deionized water and dried with nitrogen gas. The electropolymerization aqueous monomer solution composition is presented in Table 5.1.

Table5.1 Electropolymerisation aqueous monomer solution composition

Conducting polymer Film	**Pyrrole concentration (M)**	**Counterion concentration**
PPy/*p*TS	0.2	0.05 M
PPy/CS	0.2	2 mg/ml
PPy/PSS	0.1	0.1 M
PPy/DBSA	0.1	0.1 M

Each monomer solution was deoxygenated with nitrogen gas bubbling for 10 min prior to use to remove dissolved oxygen. The Q-sense electrochemistry cell consisted of a platinum counter and a gold working electrode with a World Precision Instruments® Dri-RefTM reference electrode (Figure 5.2). Conducting polymer films were grown galvanostatically (current density of 1 mA/cm^2 for 1 min for all films) on the surface of gold-coated Q-Sense quartz sensors using an eDAQ e-corder 410 recorders and EA163 potentiostat which is connected to the Q-Sense instrument (Figure 5.2). Electropolymerization was performed in a three electrode system utilizing the gold QCM crystal as the working electrode, a Ag/AgCl (3 M NaCl) reference electrode and a platinum auxiliary electrode) with the resulting voltage generated during polymerization being recorded. The monomer solution was flowed through the Q-Sense electrochemistry axial flow cell at 60µl/min. Electropolymerization process was executed with applying constant current. The temperature within the Q-Sense chamber was maintained at 22 ± 0.02^{o}C using the instrument software. Subsequently, the conducting polymer coated quartz sensors were removed from the E-cell and rinsed in distilled water and dried with nitrogen gas bubbling (Figure 2.4 in Chapter 2).

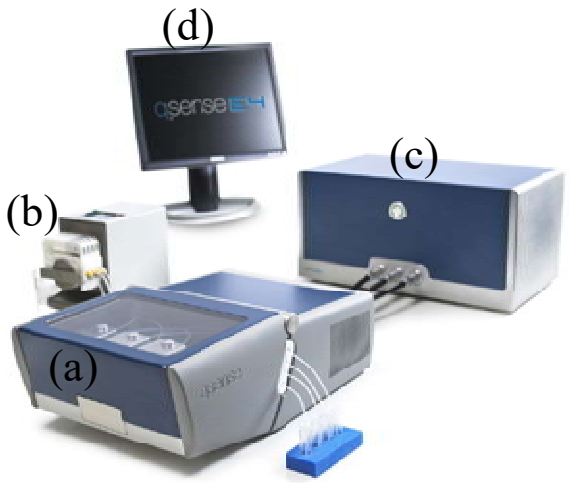

Figure 5.2 Quartz crystal microbalance (QCM) instruments; (a) Q-sense sensors, (b) pump, (c) QCM main body, (d) PC accompanied with QCM instrument which provide appropriate software.

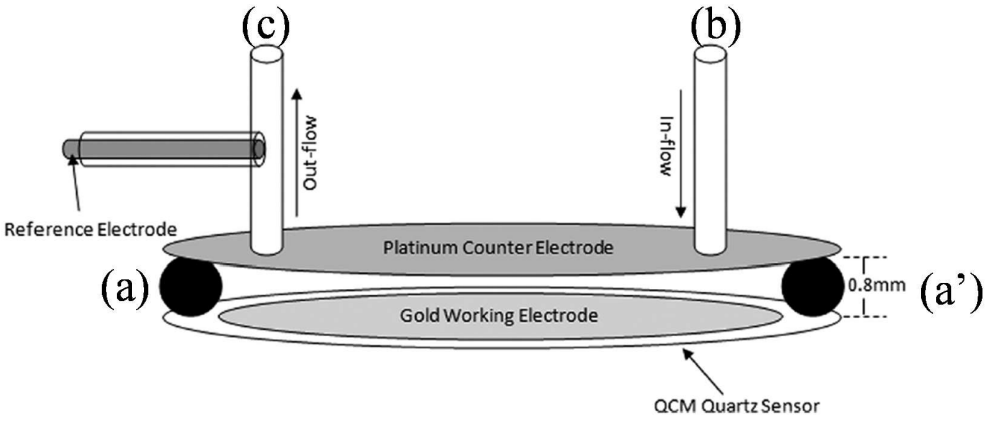

Figure 5.3 Q-sense electrochemistry axial flow cell chamber schematic; (a) and (a') present the O-ring washer, (b) is the inlet of QCM cell; and (c) is the outlet. Reference, counter and working electrodes are labelled in the figure.

5.3.3 Film Characterization

5.3.3.1 Electroactivity

5.3.3.1.1 Cyclic voltammetry

In order to investigate the electrochemical properties of the PPy films they were grown on the surface of a gold Mylar sheet in place of the QCM crystals with the electropolymerization conditions being exactly the same. The OCP films grown on the surface of gold Mylar were then placed in a three electrode electrochemical cell containing a platinum mesh counter electrode, Ag/AgCl (3M NaCl) reference electrode, and the conducting polymer films on the surface of the gold Mylar as the working electrode. ACSF was utilized as the electrolyte and 5 cyclic voltammograms (CVs) were measured using an eDAQ e-recorder (v5.5.11) and potentiostat (Figure 4.4). The potential ranges were ± 600 and ±800 mV with scan rates of 25 and 50mV/s used.

5.3.3.2 Profilometry Topography

The surface roughness of the polymer films were examined by using a Veeko Wyko NT9100 optical profilometer (Figure 2.12 in Chapter 2). For each sample at least three measurements were carried out. To measure surface roughness of conducting

polymer films Q-sense sensors were used since optical profilometer does not damage the quartz crystal.

5.3.3.3 Goniometry Measurement

A Dataphysics optical contact angle goniometer was used to measure the mean static contact angle of the conducting polymer films. For each sample at least three measurements were carried out using deionized water droplets of 1 µl for each reported value. Figure 2.8 in Chapter 2 shows the Dataphysics optical contact angle goniometer used in this study. Applying oxidizing and reducing potential to the surface of OCPs changes the wettability of the surface which is distinguishable by measuring the contact angles. In addition electropolymerisation of polypyrrole with different counterions leads to have different surface properties. Measuring the contact angles reveals any differences in wettability of the surface of OCPs.

5.3.3.4 Scanning Electron Microscopy

Scanning Electron Microscopy (SEM) images of conducting polymer film surfaces were taken using a field emission SEM (JOEL JSM-7500FA). Figure 2.3 in Chapter 2 presents an image of this instrument. Conducting polymer samples for SEM analysis were produced on gold Mylar sheet. Electropolymerisation solution composition has been displayed in Table 5.1. SEM was conducted in order to perform surface morphology analysis.

5.3.4 Quartz Crystal Microbalance with Dissipation Monitoring (QCM-D)

In this study according to the frequency and associated dissipation shift the absorbed layer to the polymer surface is a rigid, non-viscoelastic layer. Therefore, the Sauerbrey model is applicable to extricate measurements from the resulting data set. The Q-tools software package v.3.0.10.286 (Biolin Sci, AB) was utilized to apply Sauerbrey model to determine layer thickness of the conducting polymer and also absorbed mass layer. Layer density (1500 kg m^{-3})[20] and 5^{th} overtone were employed for all modelling to achieve the best data fit. The QCM technique has been described in section 2.5 Chapter 2.

5.4 Results and discussion

5.4.1 Study the cyclic voltammetry

The potentials generated during electropolymerisation of the polypyrrole films on the surface of Q-sense sensors at a constant current of 1 mA/cm^2 with four different counterions, namely *p*TS, CS, DBSA and PSS is shown in Figure 5.4. These four counterions were chosen as they possess a negative charge (Figure 5.1) however *p*TS has the smallest molecular weight. Among these counterions *p*TS and PSS molecules are synthetic in nature whilst CS and DBSA are large organic molecules derived from nature. Previous work[21, 22] has reported on variations in electrochemistry and physical properties of PPy when different size dopants are used during growth. In addition, all of these dopants have been shown to be compatible with a range of biological cells[23, 24], making them ideal candidates for materials to be used in drug delivery and biological applications. It has to be mentioned that Q-tools which is the software combined with QCM-D instrument normalizes the amount of absorbtaion by the surface. Although, a rougher surface area has a higher total surface area; however, it does not necessarily have an increased active surface area. Not all areas of the surface are available and accessible to interact with drug molecules. Therefore, calculation of actual amount of active surface area is not possible practically.

Even though the effect of active surface area has not been applied in this chapter, the main point of this chapter was studying the effect of doping polypyrrole with 4 different dopants on the affinity of LCM molecules to the CP surfaces.

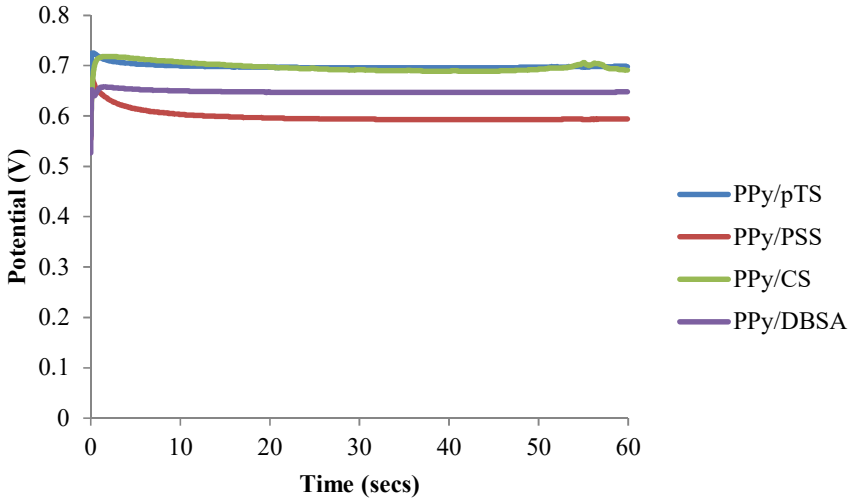

Figure 5.4 Potential (V) generated during electrochemical polymerization of PPy doped with varying dopants; *p*TS, PSS, CS and DBSA at a current density of 1 mA/cm^2 in the monomer growing solution.

Immediately after application of the constant current (employing a current density of 1mA/cm^2) the generated potential for PPy/*p*TS and PPy/CS during electropolymerisation was +0.7 V. For PPy/DBSA this potential is +0.65 V and +0.6 V for PPy/PSS. The potential generated during polymer deposition has an influence on the formation and structure of the electropolymerized polypyrrole with films grown and lower potential leading to a higher conjugated and electroactive polymer. Cyclic voltammetry (section 5.3.3.1) was utilized to investigate the electrochemistry of the conducting polymer films (Figures 5.12). The polymer was cycled between the upper and lower potential limits which were ±800 mV. Figure 5.5(a) present the cyclic voltammograms of PPy/PSS coated Pt/PVDF membrane. The oxidation occurs at +150 mV and reduction peaks was seen at -500 mV. When PPy/*p*TS coated Pt/PVDF membrane was scanned between ±800 mV (Figure 5.5(b)), reduction of this membrane started at about -400 mV, accompanied by the anions movement out of the polymer structure. The cations started to move into the polymer at a more positive potential and this process continued until the potential reached +300 mV. This point is the point that cations stopped moving in and ready to move out on its reverse scan. In Figure 5.5(c) when PPy/CS coated Pt/PVDF membrane scanned from -800 mV to +800 mV, the cation starts to move out of the polymer structure until reaching oxidizing peak which was happened around +200 mV. Continuing

potential application resulted in anions in solution began to move into the polymer and this anion movement continued until reducing peak which was happened at -300 mV. Finally for PPy/DBSA coated Pt/PVDF membrane anion and cation movement between the conducting polymer structure and solution which was ACSF leads to having redox peak. As Figure 5.5(d) presents the oxidizing peak was observed at -350 mV and reducing peak was seen around -500 mV.

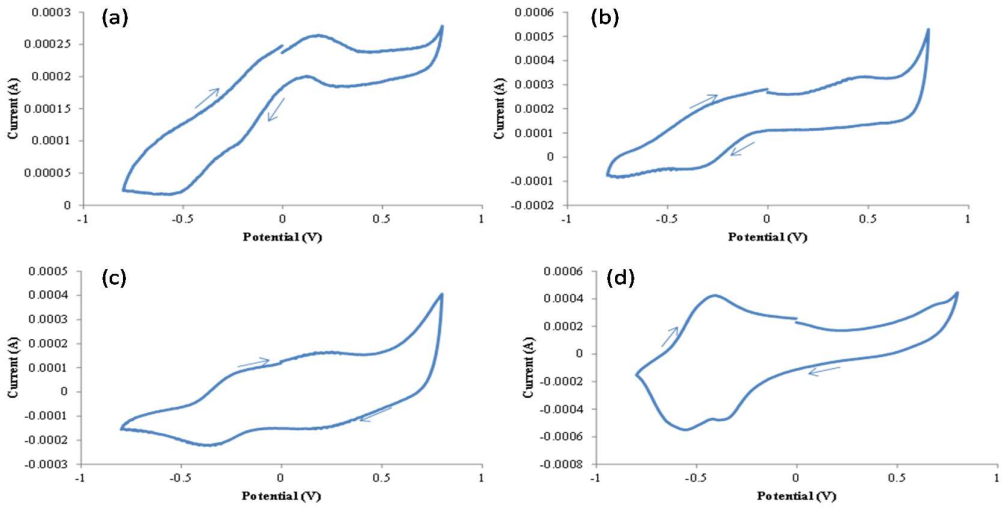

Figure 5.5 Cyclic voltammograms of PPy/PSS (a), PPy/*p*TS (b), PPy/CS (c) and PPy/DBSA (d) coated gold Mylar cycled at 25 mV/s scan rate in ACSF solution at room temperature from -800 mV to +800 mV. Arrows show the direction of the potential scan.

5.4.2 Thickness of Conducting Polymer Films

In-situ electrochemical polymerization of polypyrrole using the QCM-D provided fundamental characterization analyses of the deposited polymer layer. Figure 5.6 presents the Sauerbrey modelled results of OCP thicknesses from each PPy/*p*TS, CS, PSS and DBSA films. To calculate the thickness of the conducting polymer layer the Sauerbrey model has been used. The thickness calculation equation requires the density of the adlayer at the interface which in this case is polypyrrole. According to the literature [11] the density of polypyrrole is 1.47 g cm^{-3}. As it has been described in section 5.3.4, the Sauerbrey model is utilized to analyze rigid and non-viscoelastic adlayers such a deposited conducting polymer layer.

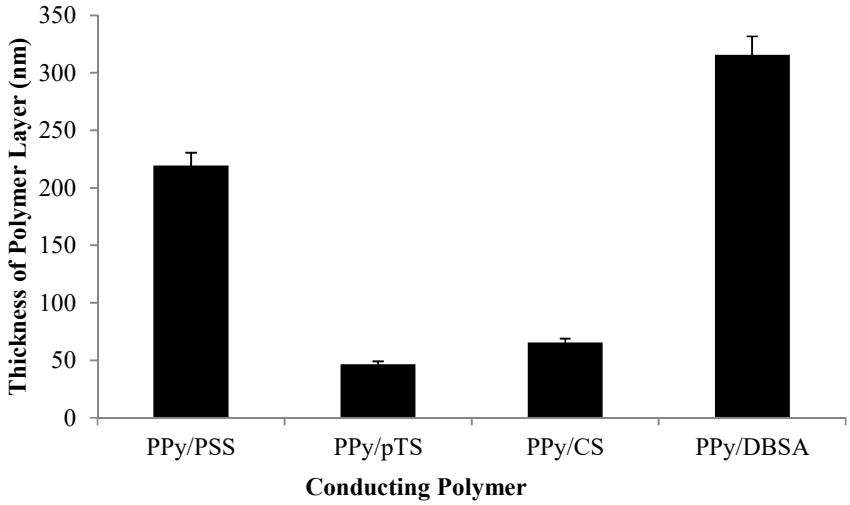

Figure 5.6 Conducting polymer layer thickness values for PPy/*p*TS, PPy/CS, PPy/DBSA and PPy/PSS modelled from QCM-D data using the Sauerbrey Model. Data is the average value (n = 3) with the error bars representing 95% confidence intervals around the mean.

Thickness of the CP film deposited during electrochemical polymerization for PPy/DBSA is the highest followed by PPy/PSS, PPy/CS and PPy/*p*TS. Thickness of PPy/DBSA layer on the surface of quartz crystal is 315.8 ± 6.7 nm which is 6.8 times greater than PPy/*p*TS layer thickness (i.e. 46.8 ± 5.3 nm).

5.4.3 Polymer Morphology, Surface Roughness and Contact Angle

SEM images of the conducting polymer surfaces show the formation of a non-porous layer (Figure 5.7) and reveal a typical nodular morphology of electropolymerized polypyrrole films[25, 26]. However, the surface characteristics of the OCPs grown with different counterions exhibited varying surface roughness value (Figure 5.8). Surface roughness (R_{rms}) is one important property that imparts significant interfacial properties in terms of the attraction of molecules to the interface [27-29]. Surface roughness data was obtained by using a described method in section 5.3.3.2. The values presented in Figure 5.8 show that PPy/PSS has the highest R_{rms} value (i.e. 29.5±0.4 nm) followed by PPy/*p*TS, PPy/CS and PPy/DBSA. These results are in a good agreement with the other researchers results[30, 31]. According to the SEM images (Figure 5.7) possessing larger nodules on the surface for PPy/PSS film leaded to having larger surface roughness[32]. Surface roughness for PPy/*p*TS film is higher

than PPy/CS and PPy/DBSA. Despite that the surface roughness values for all of OCP films presented here are approximately the same to the other studies which have been performed under the same experimental condition[30].

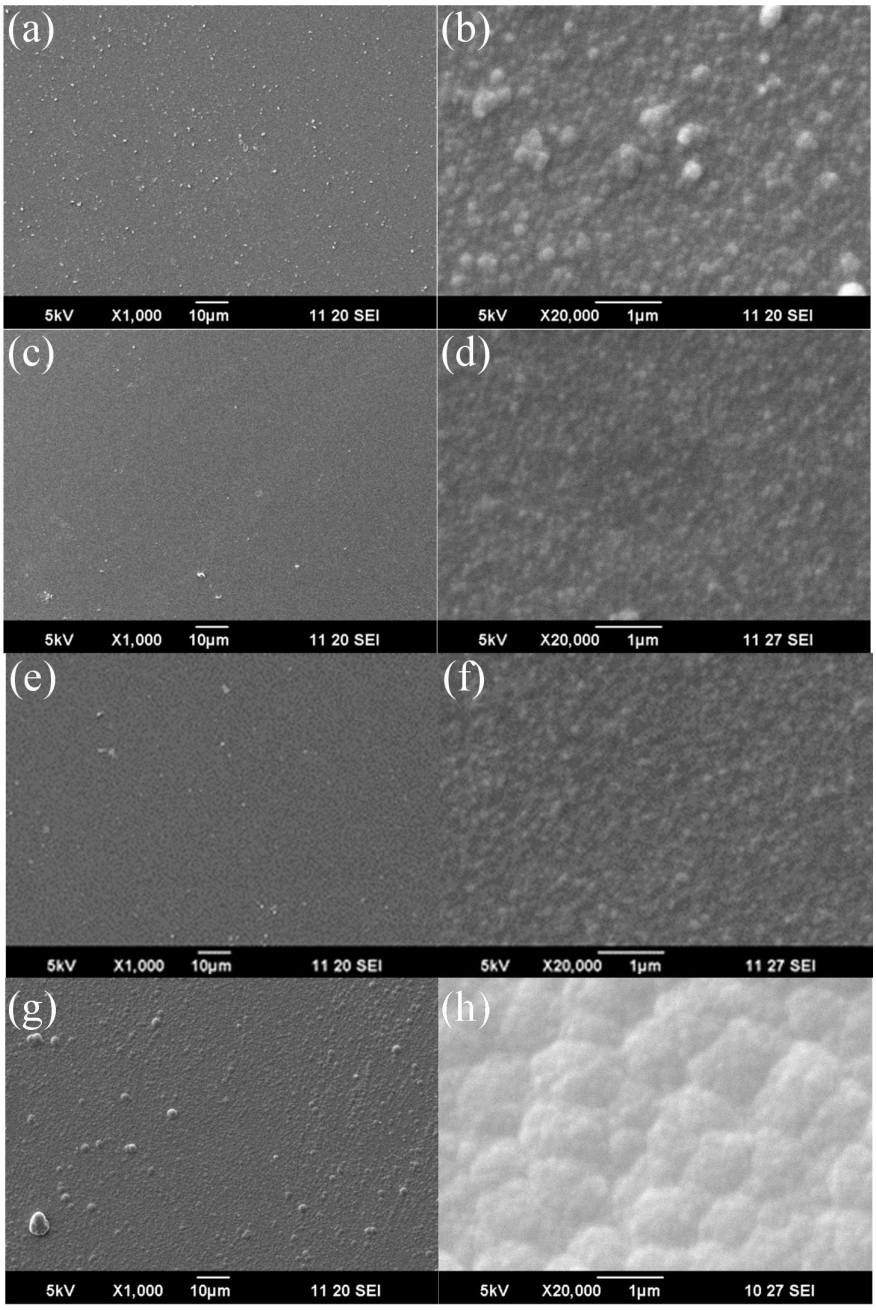

Figure 5.7 Low magnification SEM images (a, c, e and g) and high magnification SEM images (b, d, f and h) of PPy/*p*TS (a and b), PPy/CS (c and d), PPy/PSS (e and f) and PPy/DBSA (g and h) films.

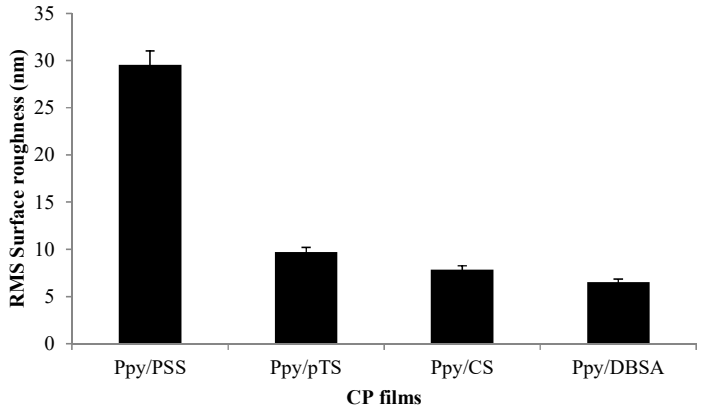

Figure 5.8 Random Mean Square Roughness (R_{rms}) (nm) for PPy/*p*TS, PPy/CS. PPy/PSS and PPy/DBSA films calculated by optical profilometry. Error bars represent 95% confidence intervals surrounding the mean (n=3). The p-value for these data is less than 0.05 (p* = 0.015).

The effect of different counterions on the wettability property of the OCPs was investigated using static water contact angle measurements (Figure 5.9). PPy/*p*TS produced the highest water contact angle (i.e. 60.8±9.6°).The PSS, CS and DBSA molecules contain a number of hydrophilic residual groups respectively (Figure 5.1) which possibly leads to the OCP films grown using these molecules as dopants possessing high hydrophilicity and thus low contact angles[33].

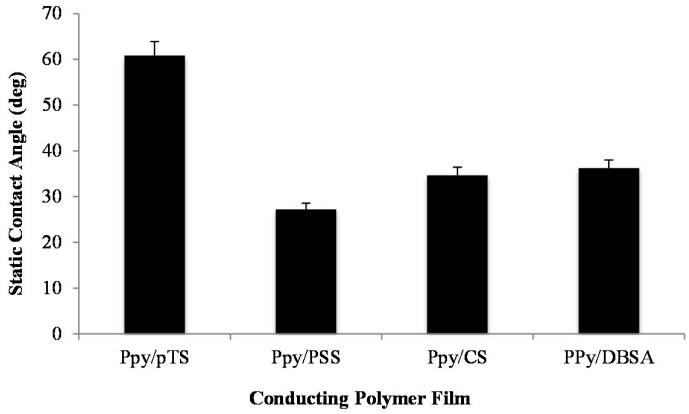

Figure 5.9 Average (n = 3) static contact angle (deg) for PPy/*p*TS, PPy/CS, PPy/PSS and PPy/DBSA films. Error bars represent 95% confidence intervals surrounding the mean.

5.4.4 Electrochemical polymerization and Electroactivity

As it has been indicated in section 5.3.2 a QCM-D instrument was utilized to prepare conducting polymer coated quartz crystals. A solution of pyrrole monomer and counterion (Table 5.1) were introduced to the QCM-D chamber and constant current applied (current density used was 1 mA/cm^2) to the chamber using an eDAQ system (section 5.3.2). Figure 5.10(a) exhibits the frequency (f) responses which occurred as a result of growing conducting polymer on the surface of the quartz crystal. At time = 0 the constant current was applied to the surface of gold quartz crystal to initiate conducting polymer growth. For all of the conducting polymers with different dopants a negative frequency shift was observed indicating an increase in mass at the surface of the crystal. This increase in mass is attributed to the formation of a conducting polymer film. The maximum f shift occurred for PPy/BDSA followed by PPy/PSS, PPy/*p*TS and PPy/CS. Furthermore, a decrease in the gradient of frequency decrease (mass increase) for PPy/DBSA is higher than PPy/PSS, PPy/*p*TS and PPy/CS respectively indicating that the rate of PPy/DBSA deposition is faster. Energy dissipation (D) shifts shown in Figure 5.10(b) are associated with f shifts (5^{th} overtone) and provide an understanding of viscoelastic characteristics of deposited conducting polymer film by measuring the energy dissipative properties of this absorbed layer at the interface[34]. From Figure 5.10(a) and b it is observed that a negative f shift results in a positive D shift. The positive D shifts are highest for PPy/DBSA followed by PPy/PSS, PPy/CS and PPy/*p*TS. However, in general all of the D shifts changes are less than 2.5 units and are therefore considered to be negligible. Hence, D shifts show that a non-viscoelastic and rigid layer has been formed on the surface of quartz crystal[17].

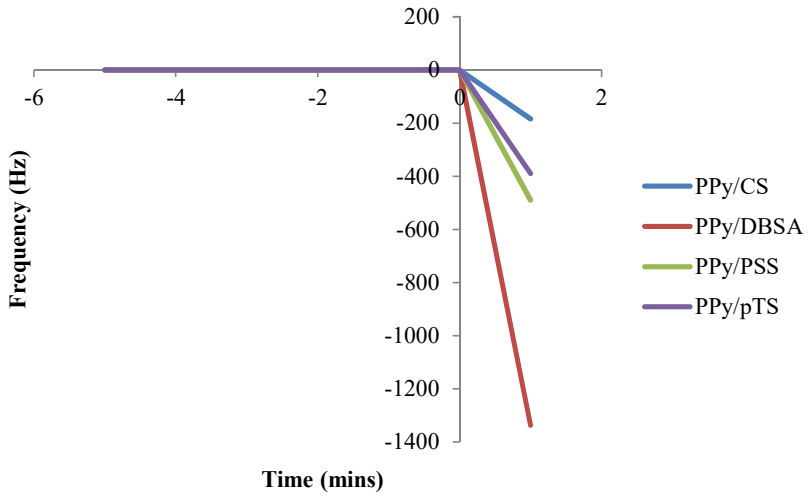

(a)

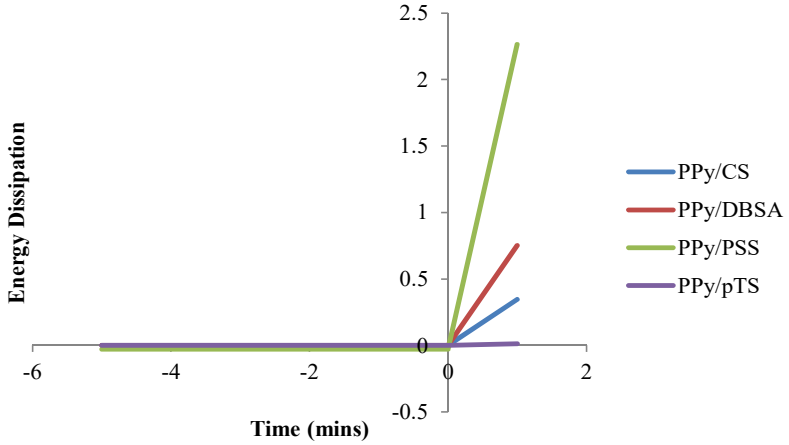

(b)

Figure 5.10 (a): Frequency (*f*) responses to the electropolymerization of pyrrole with the dopants *p*TS, CS, PSS and DBSA; (b): Energy dissipation (D) responses to electropolymerization of pyrrole with; *p*TS, CS, DBSA and PSS counterions.

5.4.5 Study the interaction of ACSF

In order to study the interaction of the drug to the OCP films it is first necessary to study any interaction effects arising from the ACSF used to prepare the drug solutions as the drug solutions are prepared in ACSF.

5.4.5.1 QCM crystal in the Passive state

To study the interaction of ACSF anions and cations a separate solution of each ion were prepared. ACSF includes six different ions which have been mentioned in section 5.3.1. Each solution introduced to the QCM chamber (Figure 5.3) separately with the OCP coated gold QCM crystal being held in the passive state (i.e., no electrical stimulation applied). As Figure 5.11 presents $CaCl_2$ shows the maximum affinity to the surface of the gold coated quartz crystal and after 20 minutes 34.4 ng/cm^2 of mass has absorbed to the surface followed by KCl (34.0±0.2 ng/cm^2), $MgCl_2$ (30.0±0.5 ng/cm^2), Na_2HPO_4 (27.1±0.7 ng/cm^2), NaH_2PO_4 (20.0±0.3 ng/cm^2) and NaCl (18.0±0.4 ng/cm^2). Although NaCl possess the highest concentration among all of these ions, total absorbed mass from this solution after 20 minutes is the lowest one.

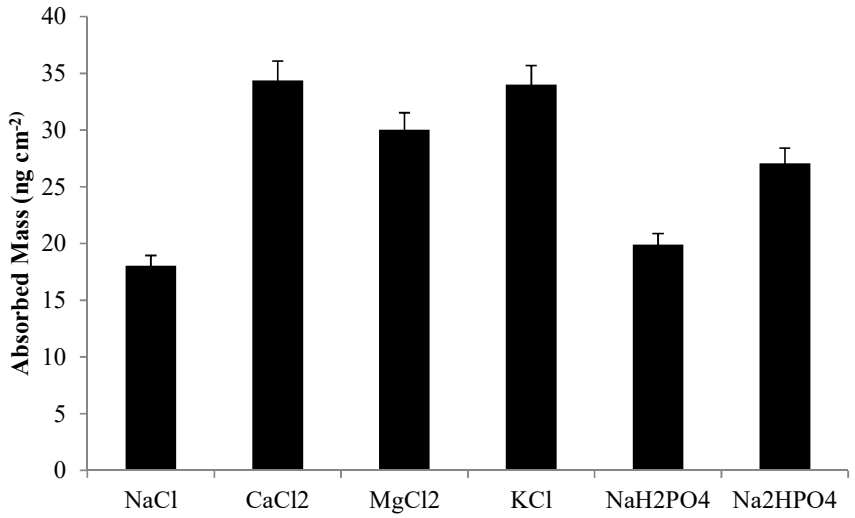

Figure 5.11 Sauerbrey modelled calculated mass due to interaction of ACSF anions and cations.

5.4.5.2 QCM in a stimulated state

Interaction of ACSF solutions with the OCP coated QCM crystal was performed with the OCP under an electrically stimulated state. ACSF were introduced to the QCM chamber. After a period of time an equilibrium state was achieved where by changes in the QCM crystal frequency reached a constant value. At time ≥ 10 min which was after equilibrium state, a negative voltage of -400 mV was applied to the

surface of OCP coated QCM crystal while the solution was flowing through the QCM cell and across the surface of the OCP. When drug molecules interaction at stimulated states was studied for PPy/*p*TS film, a very large negative frequency shift was observed by applying -400 mV. This large *f* changes was not seen at the oxidized state. This part of experiments was designed to clarify that large *f* changes is a result of ASCF absorption to the surface and also hydration of the quartz crystal surface. *f* changes for PPy/*p*TS film at stimulated states will be presented in section 5.4.7.2.

Figure 5.12(a) exhibits the *f* changes as a result of mass absorption to the surface of gold coated quartz crystal. A negative frequency shifts occurred as soon as the -400 mV voltage was applied to the surface which means there was an affinity between fluid and the surface. ACSF shows a very large frequency decrease of approximately 600 Hz. Therefore, there was an interaction between ACSF and the surface of the OCP coated QCM crystal surface although after a period of time an equilibrium state will be achieve as is discussed below in section 4.4.8.2.

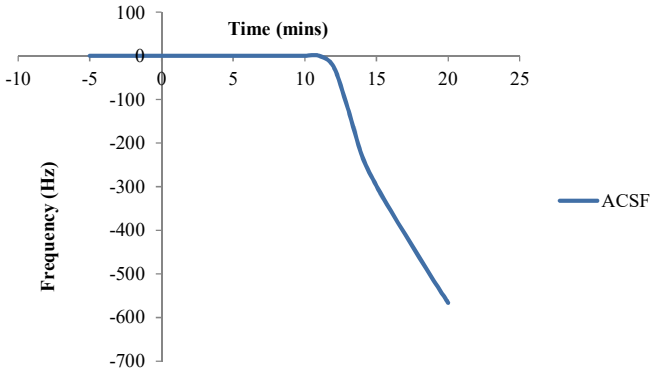

(a)

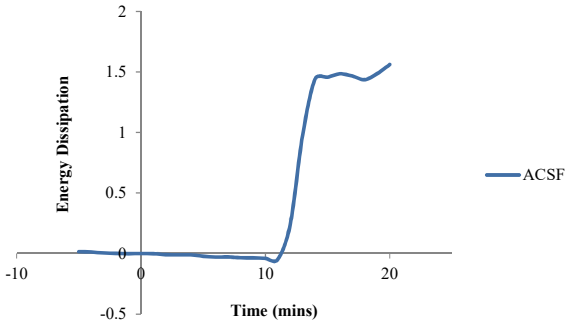

(b)

Figure 5.12 (a): Frequency (*f*) responses to flowing of ACSF on the surface of gold coated quartz crystal; (b): Energy dissipation (D) responses to flowing of ACSF on the surface of gold coated quartz crystal.

Figure 5.12(b) presents the energy dissipation shift due to ACSF introducing to the QCM chamber. As it has been shown in Figure 5.12(b) for negative *f* changes, positive D shifts occurred. However, dissipation change is less than 2 units which means absorption of ACSF makes a rigid and non-viscoelastic layer upon gold coated quartz crystal. According to the literature [35] absorption of small molecules leads to generating non-viscoelastic layer on the surface.

5.4.6 Study the electroactivity of lacosamide molecules

The chemical structure of lacosamide molecule (LCM) has been shown in Figure 5.1 and suggests that LCM does not carry any overall charge[36]. The electrical charge of LCM molecules was studied by flowing a solution of ACSF solution across the surface of Q-sense sensor without any conducting polymer coating. The frequency of the crystal decreased indicating mass adsorption at the surface and after a period of time an equilibrium state was achieved. At this stage a negative voltage (i.e. -400 mV) was applied to the surface of gold coated quartz crystal and after a period of time, a stable state was observed. After second equilibrium state a solution of LCM/ACSF at time ≥ 0 with concentration of 100 mg/ml was introduced upon the surface which is biased at –400mV. As Figure 5.13 presents a negative frequency shift of approximately 800Hz occurred. It has been discussed above that a negative *f* shift is due to mass absorption to the surface of Q-sense sensor[20, 32]. However, in this case this large negative *f* shift did not occur just because of LCM molecule

absorption. LCM molecules had been dissolved in ACSF solution and in the previous section (section 5.4.6) study the interaction of ACSF with quartz crystal surface revealed that there was a noticeable interaction between ACSF and Q-sense surface. In figure 22 a -600 Hz *f* shift resulted due to absorption of ACSF. Therefore, a large proportion of the *f* shift in Figure 5.13 is due to the absorption of ACSF and not LCM molecules. Due to the interactive nature of ACSF ions and LCM it is not possible to determine how much of frequency shift is due to LCM absorption and how much is due to ACSF.

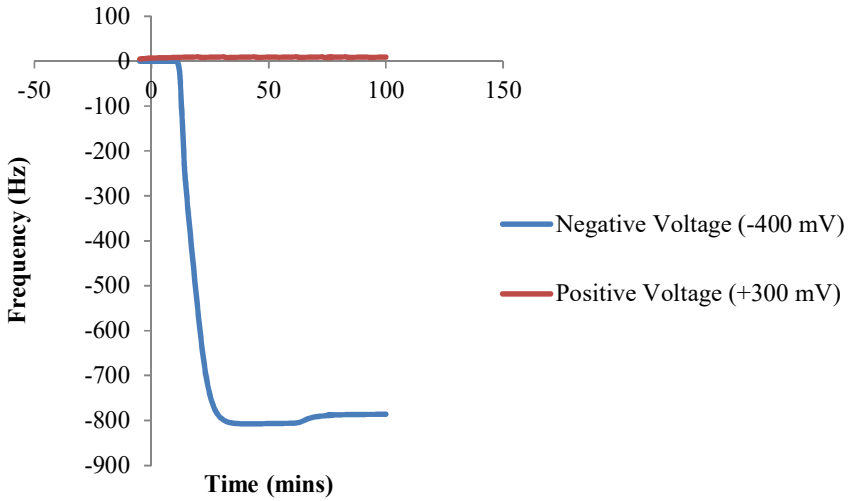

Figure 5.13 Frequency (*f*) of Q-sense sensor due to introducing LCM/ACSF to the chamber with applying a negative (i.e. -400 mV) and a positive (+300 mV).

The affinity of LCM molecules under the influence of a positive surface was assessed by applying positive voltage through the surface of Q-sense sensor. Figure 5.13 shows *f* changes due to application of +300 mV to the surface of gold coated quartz crystal. The *f* alteration is negligible and it suggests there was no noticeable affinity between LCM molecules and the positively charged surface. From this data it appears that there is no considerable affinity between LCM molecules and the surface of gold coated quartz crystal neither in negatively charged state nor in positively charged. Therefore, ionic attraction-repulsion does not have any effect on the interaction of LCM molecules to the surface of quartz crystal, especially at reduced and oxidized state. Because at reduced and oxidized state the surface of conducting polymer is partly carrying a negative or positive charge respectively. In

this case just the surface characteristics of conducting polymer such as surface roughness or wettability played an important role on absorption of LCM molecules.

5.4.7 Lacosamide Adsorption

5.4.7.1 Non-Stimulated State

The Sauerbrey model is applicable only for elastic and rigid adlayers[32]. If this model is employed to calculate the mass of viscoelastic and soft layers; for instance adlayers with considerable ΔD; underestimation of the amount of adsorbed mass could occur as not all of the adsorbed mass contributes to the Δf[15]. That is to say, that in this situation decoupling of the adlayer from the motion of the sensor can affect the mass calculation. Herein, the D shifts demonstrated by the adsorption of LCM molecules to the surface of CP films were negligible. The D shifts for all of CP films were less than 0.4 units and suggests the formation of a non-viscoelastic and rigid layer at the interface and also non-viscoelastic contributions to the f data. Therefore, we utilize the Sauerbrey model to calculate the overall hydrated absorbed mass to the CP surfaces (Figure 5.14(a)). It must be noted that the QCM-D mass measurements contain two mass contributions, one from the drug molecules and the other associated with the water molecules which are hydrodynamically coupled to the drug molecules due to the high water solubility of LCM molecule.

QCM-D frequency (f) measurements are presented in Figure 5.14(a). Drug free ACSF was allowed to flow through the QCM chamber containing the OCP coated crystal until a steady f base line was achieved (i.e., f did not vary by greater than 2%), at this stage the CP surface is considered to possess a stable diffuse electrical double layer (EDL)[37]. Once a steady baseline was achieved, a solution of ACSF containing 100 mg/mL of LCM was introduced into the QCM chamber (at time≥ 0min). Changing to the LCM/ACSF solution was achieved by switching the QCM chamber feed line from a vial containing ACSF to a vial containing the LCM/ACSF solution. A f shift in response to introducing the LCM loaded ACSF solution is observed and is attributed to interactions between the LCM molecules and the PPy/*p*TS, PPy/CS, PPy/PSS and PPy/DBSA film surfaces. This LCM interaction was confirmed by repeating the same experimental only this time changing the feed line to an ACSF solution that did not contain LCM upon which no change in f was

observed. For all of the OCP films investigated there is an overall negative frequency shift indicating an increase in mass upon the crystal which is attributed to drug molecules adsorbing onto the surface of these OCP films[35].

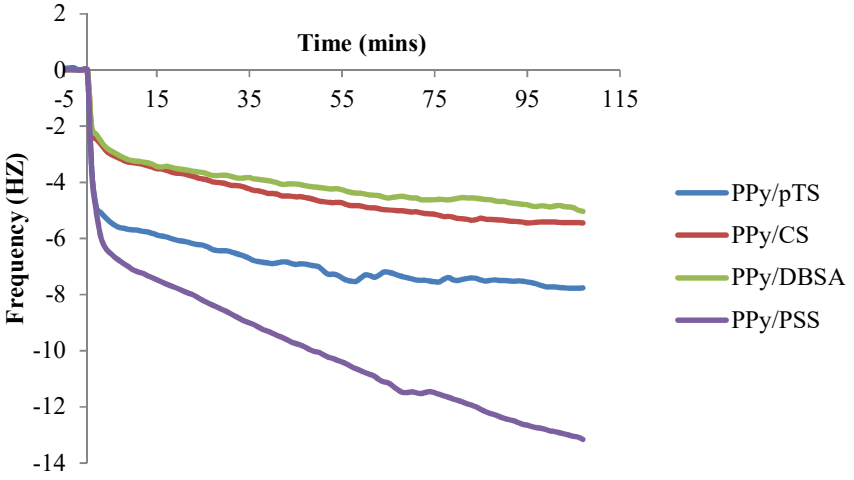

(a)

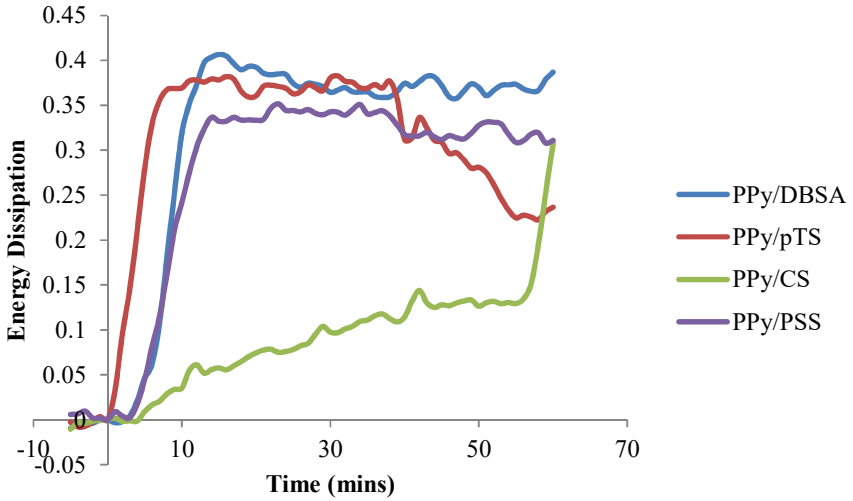

(b)

Figure 5.14 (a) Frequency (f) and (b) energy dissipation (D) responses of LCM mass absorption. The frequency responses are related to the adsorption of LCM from ACSF solution containing 0.1mg/mL LCM to PPy/*p*TS, PPy/CS, PPy/PSS and PPy/DBSA films. The ACSF solution containing the LCM was introduced into the QCM chamber at time = 0min. The mass (ng/cm^2) calculated using the Sauerbrey and the geometric surface area of the QCM crystal is shown.

Given that for all of the CP films the amount of LCM entering the QCM chamber is the same (since the LCM concentration and flow rate is the same for both experiments) this results suggest the rate of interaction with the PPy surface varies based on the physical properties of the PPy film. The frequency decrease can be broken down into two distinct regions, namely rapid decrease (0min>time<5min - PPy/PSS; 10min>time<25min - PPy/*p*TS 2.5min>time<12.0min - PPy/CS; 0min>time<10min – PPy/DBSA) followed by a slower decrease (time>5min – PPy/PSS; time>25min - PPy/*p*TS; time>12.0min - PPy/CS; time> 10min – PPy/DBSA). The rate of the *f* shift for the PPy/PSS at rapid decrease region is the highest one. The trend value of *f* decrease for this polymer is -1.3 Hz/min. the second place belong to PPy/*p*TS by -0.6 Hz/min and then followed by PPy/DBSA with -0.3 Hz/min and finally there is PPy/CS with the value of -0.2 Hz/min. Also, the rate of frequency decrease occurring in the slower region appears approximately 10 times faster for PPy/*p*TS (-0.2 Hz/min) than the other CPs. This frequency decrease rate for PPy/PSS is -0.07 Hz/min, for PPy/CS is -0.03 Hz/min and for PPy/DBSA is -0.015 Hz/min. The appearance of two distinct regions indicates two adsorption processes occurring sequentially. It appears that under non-electrically stimulated conditions LCM has the highest affinity to the PPy/PSS surface and then followed by PPy/*p*TS, PPy/CS and PPy/DBSA. In addition, according to the rapid region of LCM adsorption LCM molecules absorbed to the surface of PPy/PSS with a very high affinity at the very first 5 min of flowing LCM/ACSF solution upon the CP surface. *f* decrease rate at this region for PPy/PSS is 2.2 times higher than PPy/*p*TS and more than 4 times greater than PPy/CS and PPy/DBSA. However, after the first 5 minutes PPy/PSS shows the slowest *f* decrease until to the end of the experiment. At this slow decrease region PPy/*p*TS exhibits the highest trend and then followed by PPy/CS and PPy/DBSA.

LCM molecules are inherently neutral and are also electrochemically inactive (ref to section 5.4.7). Therefore, ionic interactions and chemical binding is unlikely to be the driving force for LCM absorption and the adsorption may be considered as nonspecific. However, surface roughness is an effective factor for drug molecule adsorption[38, 39]. Urbakh *et al[40]* also showed through QCM studies that the frequency shifts decreased rapidly with increasing the surface roughness when fluid interacted with thin layers. PPy/PSS has the roughest surface (Figure 5.8) which

leads to the highest interaction between LCM molecules and CP surface (Figure 5.15) as evidenced by the large decease in frequency (increased mass loading).

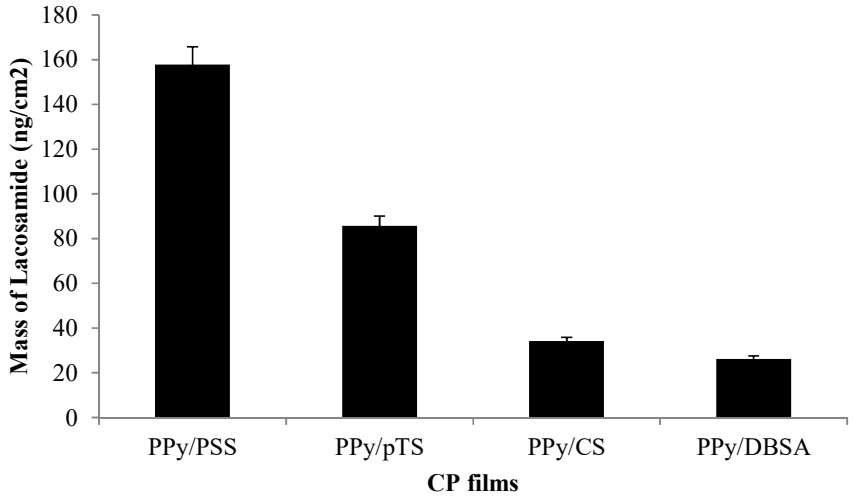

Figure 5.15 Sauerbrey modelled absorbed mass (ng cm^{-2}) for PPy/*p*TS, PSS, CS and DBSA at non-stimulated state.

Figure 5.15 presents values of absorbed LCM molecules to the surface of CPs which calculated by Sauerbrey model. As it has been mentioned before D shifts for all of the CP films are less than 0.4 units (Figure 5.15) therefore, Sauerbrey model is an appropriate method to analysis the amount of absorbed LCM molecules to the surface of CP films and also measuring the thickness of LCM absorbed layer (Figure 5.17). Figure 5.17 exhibits the amount of absorbed drug molecules to the surface of conducting polymers. PPy/PSS possess the maximum amount of absorbed drug molecules (i. e. 157.9±37 ng cm^{-2}). The second place belongs to PPy/*p*TS with the value of 85.8±2.8 ng cm^{-2}. As figure 4.8 shows PPy/CS LCM absorption is higher than PPy/DBSA with the value of 34.2±2.6 ng cm^{-2} however the absorption of this CP is less than PPy/PSS and PPy/*p*TS. Finally PPy/DBSA has the minimum absorption with the value of 26.2±2.6 ng cm^{-2}. In Figure 5.16 PPy/PSS showed the highest negative *f* shift and then followed by PPy/*p*TS, PPy/CS and PPy/DBSA. Results in Figures 4.14 and 4.22 are in a very good agreement. PPy/PSS with the highest *f* shifts possesses the highest amount of absorbed LCM molecules. The roughness of the surface can affect the *f* values in a given experiment. Surface

cavities in rough surfaces can entrap liquids. This phenomenon leads to having *f* decrease and mass increase detection by QCM[35].

Whereas the surface of gold coated quartz crystal is in contact with an aqueous solution, the density and viscosity of that liquid can affect the *f* of oscillating quartz crystal. Therefore, *f* responses of quartz crystal can be because of one of these following reasons or a combination of them;

(a) Firm bounding of an elastic mass to the Q-sense surface
(b) Changing of viscosity-density of the aqueous solution
(c) If the bounded mass in inelastic and dissipates the energy.

When a firm mass bounded to the surface of oscillating quartz crystal the Sauerbrey equation 1 can be utilized to calculate elastic mass just only after it has been experimentally proven that the absorbed mass dose not dissipate any energy. Therefore, the *f* decrease changes due to dried mass absorption will be used to calculate the amount of mass with the assumption of dried mass density is used to calculate film thickness.

To clarify which type of changes can affect the *f* changes, the Δf, ΔR QCM data can be put together. Figure 5.16 shows the plot of changing R versus *f* in a QCM experiment while electrochemical deposition of polypyrrole is carrying out at constant current density. Binding of a pure and elastic mass leaded to *f* decrease and ΔR=0. The horizontal line labelled from B to C is the response behavior of bounding this mass to the surface of quartz crystal. Dotted line labelled from A to D shows the response behavior of *f* and *R* due to absorption of pure liquid viscosity-density. These diagram is a result if viscous coupling of a solution to the quartz crystal.

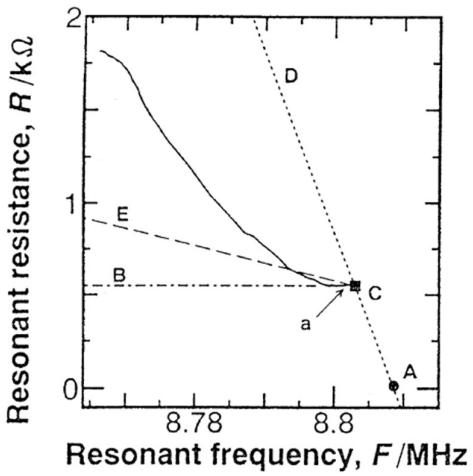

Figure 5.16 *f* and *R* responses for the electrochemical polymerization of polypyrrole with constant current density; Point C is the time zero of starting electropolymerization which continued by a solid line moving forward to the left as polymer deposition proceeds.

Therefore, the solution adds some mass to the surface of oscillating gold coated quartz crystal effectively. With the assumption of no slip existence between solution and surface of quartz crystal, the following relationship can be considered. This equation was first developed by Kanazawa *et al*[41] and it was about the resulting *f* changes.

$$\Delta f = -f^{3/2} (\rho_L \eta / \pi \mu \rho_q)^{1/2} \quad (5.1)$$

Where ρ_L is the liquid density and η is the liquid viscosity. However, it has to be considered when QCM operates in solution; there is no way to distinguish the amount of bounded mass from the amount of mass which has been contributed by solution. Therefore, in this case the earliest studies have been carried out by Muramatsu *et al*[42] as follows:

$$\Delta R = (2\pi f \rho_L \eta)^{1/2} A / K^2 \quad (5.2)$$

K is electromechanical coupling factor. As equation (5.1) and (5.2) exhibit both Δf and ΔR, are proportional to $(\rho_L \eta)^{1/2}$. Therefore, the diagram of Δf versus ΔR is linear for liquids with different densities and viscosities[35]. Considering all of these

equations and dissections, interaction of an elastic mass with surface of oscillating quartz crystal leads to *f* decreasing changes and developed Sauerbrey model is utilized to calculate the amount of bounded mass to the surface.

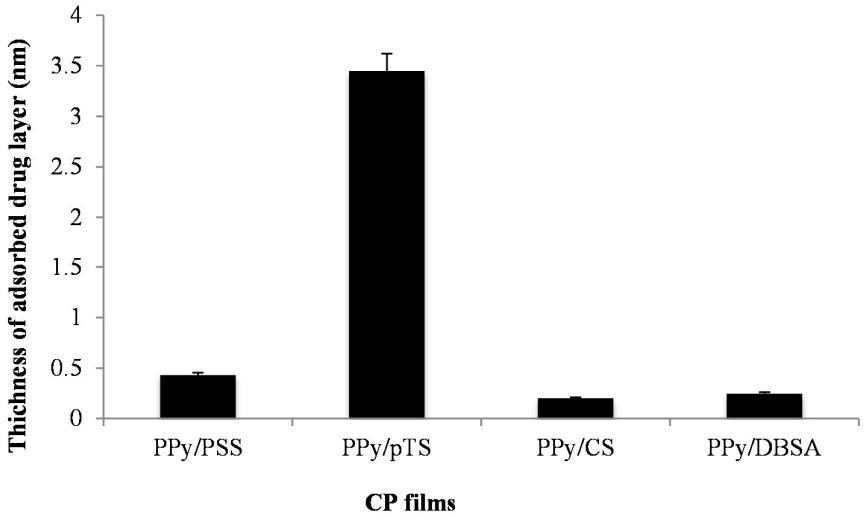

Figure 5.17 Sauerbrey modelled thickness of LCM absorption to the surface of CP films (nm) at non-stimulated state.

Figure 5.17 demonstrates thickness of bounded LCM molecules upon the surface of conducting polymer. Thickness of absorbed LCM molecules has the maximum value for PPy/*p*TS (i.e. 3.4±0.0 nm) and then followed by PPy/PSS (i.e. 0.4±0.0 nm). The thickness of PPy/CS and PPy/DBSA is roughly the same with the value of 0.2 nm. Considering the surface geometric area of CP films which is equals to the surface of gold coated quartz crystal with the value of 1 cm^2 calculation of LCM layer density is possible using equation 4.4;

$$\rho=m/V \qquad (5.3)$$

Where ρ is density, m is mass and V represents the volume. Table 5.2 presents the amount of absorbed LCM molecules, thickness of bounded LCM layer, and volume of LCM layer and density of absorbed LCM layer upon the surface of conducting polymer film.

Table5.2 Mass, thickness, volume and density of absorbed LCM molecules upon the surface of CP films

Conducting polymer film	Absorbed LCM mass (ng)	Thickness of absorbed LCM (nm)	Volume of absorbed LCM (nm^3)	Density of absorbed LCM ($ng\ cm^{-3}$)
PPy/PSS	157.9	0.4	40	3.9
PPy/*p*TS	85.8	3.4	340	0.2
PPy/CS	34.2	0.2	20	1.7
PPy/DBSA	26.2	0.2	20	1.3

As Table 5.2 shows the LCM adlayer with the highest density has been generated upon PPy/PSS film followed by PPy/CS, PPy/DBSA and PPy/*p*TS. According to Figure 4.9 PPy/PSS possesses the most hydrophilic surface among the other conducting polymer films and then followed by PPy/CS, PPy/DBSA and PPy/*p*TS. Conducting polymer surface cavities can entrap liquids if the surface is hydrophilic, and obviously more hydrophilic surfaces can entrap more aqueous liquid and fill out their cavities. On the other hand, air can be entrapped by the more hydrophobic surfaces and they often do not wet[35]. Entrapping more liquid and filling out more cavities can lead to generating denser adlayer upon the surface of PPy/PSS which is the most hydrophilic surface. Conversely, PPy/*p*TS, that has the most hydrophobic surface, (Figure 5.9) has the lowest density. However, the LCM absorbed layer density does not have any effect on the interaction of LCM molecules and the surface of CP films. Density of the absorbed layer can be interesting if removal of absorbed layer from the surface of CP is considered. At this state, the densest adlayer is the hardest choice for drug adlayer removal.

5.4.7.2 Stimulated State

The influence of an applied potential to the CP films on LCM adsorption behavior was investigated. Adsorption of LCM was studied whilst the CP as held at either a reducing or oxidizing potential. These potentials were chosen from the cyclic voltammograms recorded for each CP films (Figures 4.25(a-c)).

5.4.7.2.1 Application of a reducing potential

The main aim of this study is to investigate the release of an anti-epilepsy drug which has been encapsulated within a reservoir upon application of an electrical stimulation. Considering that, the affinity of drug molecules to the surface of conducting polymers has been investigated at reduced and oxidized states. In this section the reduced state will be presented.

Prior to present drug molecules interaction results the processes occurring at the PPy surface a series of mechanisms have been proposed and exhibited in Figure 5.18. ACSF solution was flowed through the QCM chamber and after approximately 30 minutes an equilibrium state, indicated by steady f shifts was achieved (data not shown). Figure 5.18(a) shows the schematic of this equilibrium state. At this stage the conducting polymer surface is considered to be hydrated[35] and to possess a stable diffuse electrical double layer (EDL)[43].

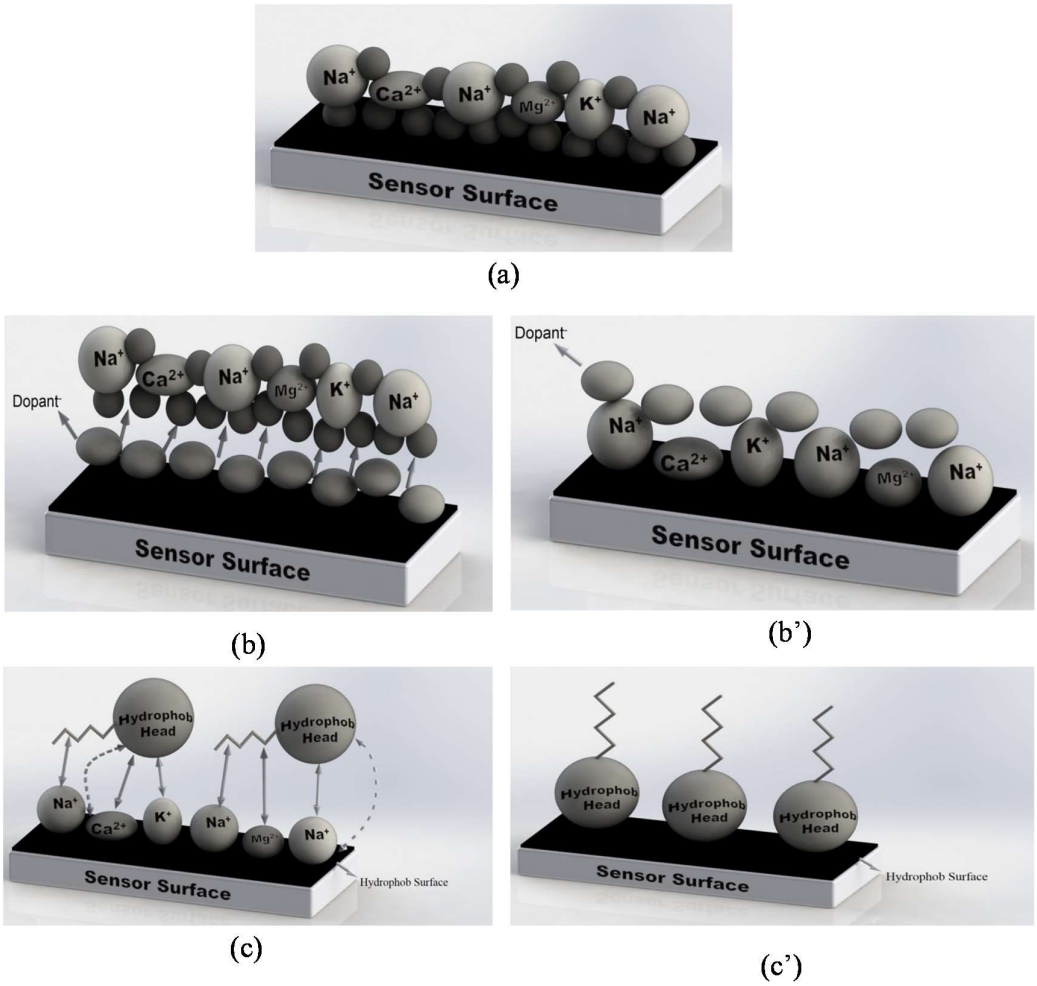

Figure 5.18 (a) Schematic mechanism of LCM absorption to the surface of CP films at reduced state, equilibrium state; (b and b') EDL formation upon QCM sensor surface due to negative charge application; (c and c') LCM molecule absorption to the surface and EDL disruption.

In the reduced state the conducting polymer develops a negative charge which can be balanced by anion exchange with the surrounding media [71, 72] either by anion expulsion from the CP film or cation inclusion, with a combination of both processes likely to be occurring simultaneously as demonstrated by Moulton et al [73]. Figure 5.18(b and b') shows the schematic of EDL formation on the surface of CP films coated QCM sensor.

The insertion/accumulation of positively charged species from the ACSF at the CP film surface has occurred at this stage. The cation accumulation also disrupts the stable EDL and results in mass accumulation at the CP film surface. When the flowing ACSF was changed to contain LCM the frequency started to increase

indicating mass loss from the CP film surface [15]. Encarnacao et al [70] demonstrated that increasing the ionic strength of a solution can cause an increase in frequency, however the ionic strength of the LCM/ACSF solution was the same as the ACSF solution and therefore ionic strength cannot account for this change. It may be possible that the LCM molecules in the ACSF disrupt the stable state. Therefore, according to the literature [74] the surface of CP films became more hydrophobic and therefore interaction between the LCM and the CP film may arise due to hydrophobic interactions between the LCM molecule (Figure 5.18(c and c')) and the film.

The QCM data for the experiment when a reducing voltage is applied to the conducting polymer films is shown in Figure 5.19. Figure 5.125 presents the *f* and *D* shifts due to LCM molecules interaction with the surface of conducting polymer films while a negative voltage is applying to the surface. For all of the conducting polymer films a positive *f* shift has been observed. Considering to Figure 5.19 (a, b and c) and Figures 4.26-4.29 this positive *f* shifts are related to loosing mass from the interface. Flowing of LCM/ACSF through the QCM chamber while a negative voltage is being applied to the surface of conducting polymer interrupted the steady EDL at the interface and hydrophobic-hydrophobic interaction between the surface of conducting polymer and hydrophobic region of LCM molecule leads to ACSF cation removing from the interface and LCM molecules absorption to the surface. The total net of this absorption and desorption leads to positive *f* shifts and mass lost. Considering Figure 5.10(a) *f* decrease shifts can be separated into two parts. One part possesses the higher *f* changes rates and at the other part *f* shifts with slower rate. *f* decrease shifts at the very beginning of the experiment are faster. PPy/DBSA film has the highest *f* decrease rate (i.e. 3.5 Hz/min) which has occurred at 0< time < 6 minutes. *f* shifts for PPy/PSS and PPy/CS are approximately the same (i.e. 3 Hz/min) and has happened at 0< time < 12 minutes for PPy/PSS and 0< time < 23 minutes for PPy/CS film. The lowest *f* changes rate at the faster part of the curves belongs to the PPy/*p*TS film with the value of 2.1 Hz/min and also it has occurred at 0< time < 13 minutes.

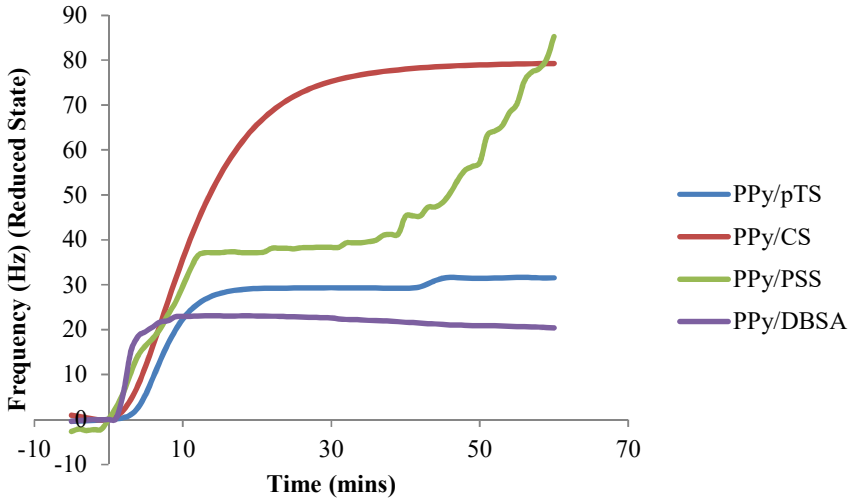

(a)

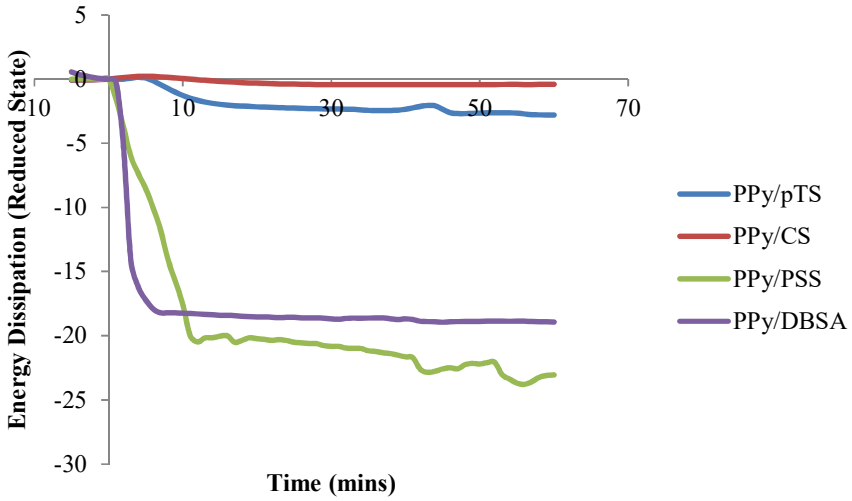

(b)

Figure 5.19 (a): Frequency (f) responses from the adsorption of LCM to PPy/*p*TS and PPy/CS films; and (b) Energy dissipation (D) responses from the adsorption of LCM to PPy/*p*TS and PPy/CS films. A reducing potential was applied to the OCP films during adsorption of LCM.

After the first part of the experiment which has the faster f changes Figure 5.10 shows for all of the conducting polymer films the f increase changes rate has dropped down. At this part the fastest rate belongs to the PPy/PSS film with value of 1.0 Hz/min and was observed at time >12 minutes. The second place belongs to the PPy/CS film which has f increase rate of 0.3 Hz/min for time>23 minutes. PPy/*p*TS

film is in the third place with the rate value of 0.1 Hz/min for time > 13 minutes. Finally, the slowest *f* increase rate was seen for time> 6 minutes of PPy/DBSA film. The *f* increase rate of this conducting polymer film is -6×10^{-3} Hz/min. All of these conducting polymer films exhibits a general increasing trend in the *f* shifts except PPy/DBSA film. The *f* increase rate for this conducting polymer film at time> 6 minutes in negative which means the *f* shift shows a decreasing trend. The *f* increase rate at the faster part is approximately 10 times higher than the *f* increase rate at the slower part of the curves except of PPy/DBSA film. For this conducting polymer film the *f* increase rate at faster part is about 1000 times higher than the slower part and also as it has been mentioned before the trend of the *f* shift has altered from increasing at faster part to decreasing at slower part. Therefore, it seems PPy/DBSA has shown different behavior in absorption of LCM/ACSF at the reduced state.

Contact angles of conducting polymer films were measured to investigate any changes in surface energy of the conducing polymer films during the adsorption experiment (Figure 5.19). Contact angles were measured after a series of treatments of the conducting polymer films to mimic the adsorption experiment shown in Figure 5.19 with the data presented in Figure 5.20. For the first treatment, contact angle of the as grown conducting polymer film was measured (Figure 5.20, PPy/dopant). The same conducting polymer film was the soaked in ACSF solution for 30 minutes and dried followed by measurement of the static contact angle (Figure 5.20, PPy/dopant-ACSF). The next treatment involved applying a reducing voltage to the surface of conducting polymer for 60 minutes immersed in ACSF followed by rinsing with Milli-Q water, drying and static contact angle measurement (Figure 5.20, PPy/dopant-ACSF (mV)). In the final treatment the conducting polymer films were soaked in a solution of LCM/ACSF while the negative voltage was applying to the surface for 30 minutes. At the end of this treatment step, the surface of the conducting polymer was rinsed and dried and the static contact angle was measured (Figure 5.20, PPy/dopant-LAC (mV)).

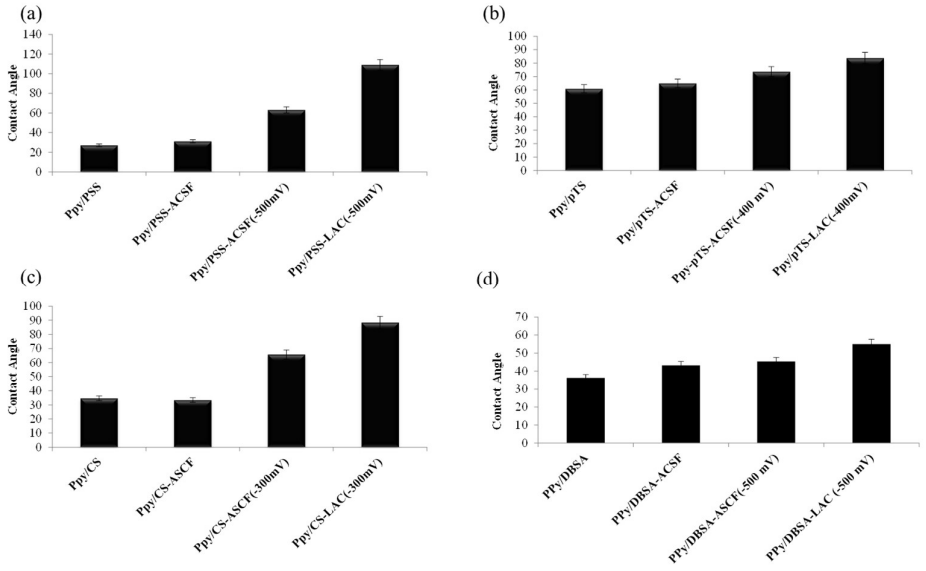

Figure 5.20 Goniometry measurement of conducting polymer coated cover slip films for the four dopants (a) PSS, (b) *p*TS, (c) CS and (d) DBSA. PPy/dopant indicates the contact angle of as-grown film. PPy/dopant-ACSF shows the contact angle of 30 min soaked film in ACSF. PPy/dopant-ACSF (mV) indicated the contact angle of film after 60 min application of reducing voltage in ACSF. PPy/dopant-LAC (mV) shows the contact angle of film after soaking in PPy/dopant in a solution of LCM/ASCF while application of the reducing voltage. Each reducing voltage is different and was obtained from the PPy film CVs shown in Figure 5.5.

Figure 5.20 shows that for all of conducting polymer films the contact angle after the final step is higher than the mean of the untreated film indicating the surface of CP has become more hydrophobic at the final step. As it has been discussed before, an alteration in surface hydrophilicity may lead to large f changes. When a surface become hydrophobic liquids will not be entrapped within surface cavities longer[35] and there is also the possibility that hydrophilic entrapped molecules are expelled out from the surface cavities. This phenomenon leads to a loss in mass from the interface resulting in a f increase indicating mass loss. The relationship between surface hydrophobicity and the attached mass have been investigated and has demonstrated that the more hydrophobic a surface is less mass attachment to the surface occurs[16, 44, 45].

5.4.7.2.2 Application of an oxidizing potential

The oxidizing voltage was determined from CVs shown in Figures 5.12. The *f* shifts observed in Figure 5.24 and 5.28 are in opposite directions for oxidizing and reducing voltages. However, the total net positive *f* shift in the oxidized state (Figure 5.27(a)) is less than total net *f* change in the reduced state (Figure 5.24(a)) and may be due to the more hydrophilic nature of the conducting polymer films in the oxidized state[67] thus absorbing more water molecules. Figure 5.22(c) exhibits the schematic of LCM molecules absorption to the surface of conducting polymer films. The *f* shift for PPy/DBSA is roughly 380 times higher than PPy/PSS (Figure 5.27) and 1000 times higher than PPy/CS and PPy/*p*TS. After a period of time conducting polymer films reached another steady state. After reaching stable state, a solution of 100mg/ml LCM/ACSF was introduced to the QCM chamber. The LCM molecules interact with the surface of conducting polymer films causing a *f* negative shifts indicating LCM molecule absorption. These results indicate the f decrease shown in Figure 5.27(a) is most likely associated with the adsorption of LCM molecules. Because of the very high magnitude of f shift for PPy/DBSA in comparison with the other conducting polymer films, the f shifts for the other films has overlapped. These *f* changes are less than 4 Hz for PPy/*p*TS and 10 Hz for PPy/CS. However, these f changes has become higher for PPy/PSS (about 30 Hz) and PPy/DBSA which is about 10994.1 Hz. The amount of absorbed lacosamide molecules to the surface of PPy/*p*TS is the lowest one with the value of 59.4±0.5 ng cm-2. LCM molecules absorbed for PPy/CS and PPy/PSS is approximately the same with the value of 145.2±0.7 ng cm-2 and 143.6±0.8 ng cm-2 respectively. The highest mass at oxidized state absorbed to the surface of PPy/DBSA coated quartz crystal (i.e. 3.27×105 ng cm-2). Mass absorption results at oxidized state exhibits opposite results from passive state. At the oxidized state the highest LCM absorption belongs to PPy/DBSA while PPy/DBSA coated quartz crystal has the lowest absorbed mass amount among conducting polymer films at the passive state.

At time greater than 10 min the f shift for PPy/DBSA decreased at very fast rate (i.e. 216.5 Hz/min), however, f decrease shift for time before 10 minutes is much slower (i.e. 18.8 Hz/min). f decrease rate for PPy/PSS film is faster at the beginning of the experiment which is from 0<time<46 min. At this part f decrease rate is 0.58 Hz/min and from time >46 min the f decrease rate is lower (i.e. 0.14 Hz/min). At times

greater than 54 minutes the f shift for PPy/CS film is decreasing at a rate of 4.5 × 10-6 Hz/min while the PPy/*p*TS is decreasing at a much faster rate of 3.5 x 10-2 Hz/min. However, f decrease rate for times before 54 minutes is higher for PPy/CS film (i.e. 0.14 Hz/min) than PPy/*p*TS (i.e. 0.06 Hz/min) film.

These results indicate that there is still a greater extent of adsorption occurring at the PPy/DBSA film compared to the other conducting polymer films. Also, after PPy/DBSA the highest affinity between LCM molecules and the surface of conducting polymers belongs to the PPy/PSS. Between PPy/CS and PPy/*p*TS there are two different parts which can be recognizable by f decrease rates. At the first part PPy/CS shows higher f decreases rate and at the final part PPy/*p*TS exhibits much faster affinity to entraps LCM molecules.

Energy dissipation shifts (Figure 5.27(b)) for PPy/PSS, PPy/CS and PPy/*p*TS films was less than 6.5 units and is considered to be negligible indicating the existence of a non-viscoelastic and rigid layer at the interface due to applying positive oxidizing potential. However, the dissipation shifts for PPy/DBSA film is 8423.8 units and it revealed generation a soft and viscoelastic layer at the interface.

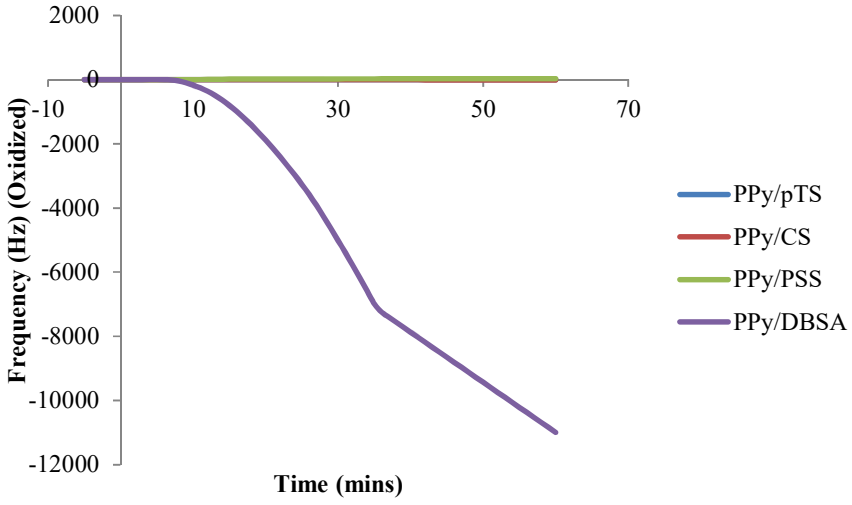

(a)

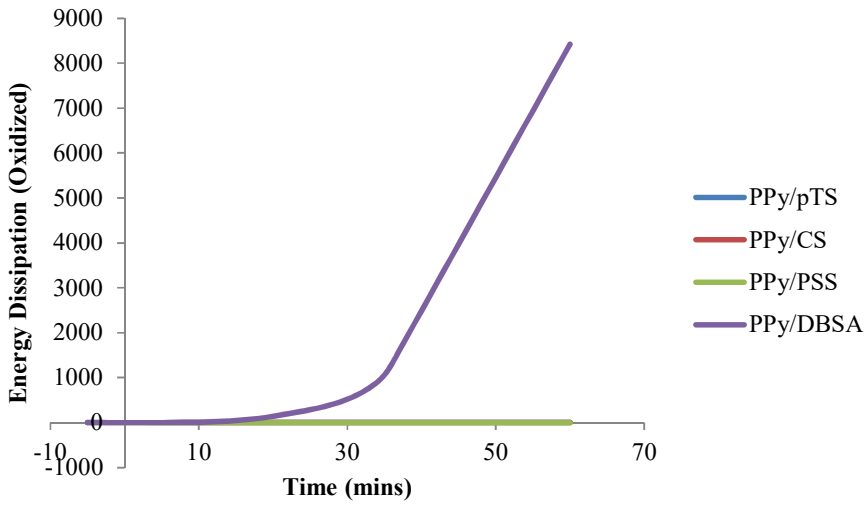

(b)

Figure 5.21 (a) Frequency (*f*) responses from the adsorption of LCM to PPy/*p*TS and PPy/CS films at oxidized state and (b) energy dissipation (D) from the adsorption of LCM to PPy/*p*TS and PPy/CS films at oxidized state; Frequency and dissipation data are from the fifth overtone.

The ACSF solution had been flushed through the QCM chamber and the system reached an equilibrium state after approximately 30 minutes. At the equilibrium state the conducting polymer film has become hydrated and a stable EDL has been formed[46]. Figure 5.22(a) shows a schematic of this equilibrium state.

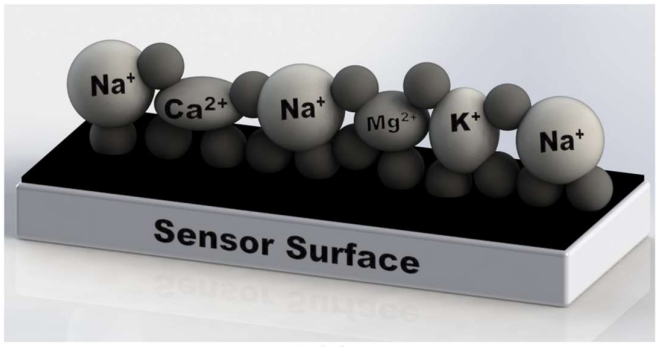

(a)

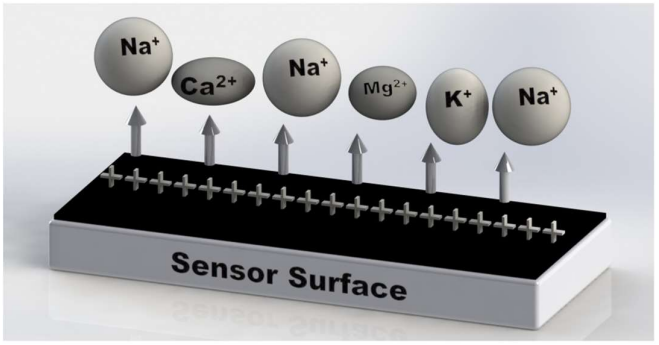

(b)

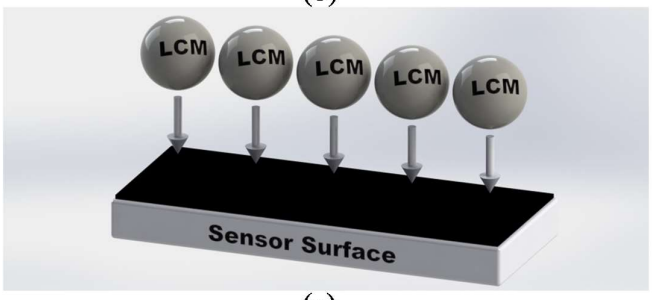

(c)

Figure 5.22 (a) Schematic of first equilibrium state due to absorption of ACSF cations to the surface of conducting polymer; (b) Schematic of cation migration from the EDL which leads to mass lost; (c) Schematic of LCM absorption mechanisms to the surface of conducting polymer films.

After reaching the first steady state oxidizing voltages were applied to the surface of conducting polymer coated QCM sensors. Application of a positive charge to the CP films leads to generation of excess positive charge at the interface. At the oxidized state the CP can balance the excess positive charge by repulse the cations which have been absorbed to the surface before achieving steady state and generating a stable EDL. This phenomenon causes the migration of cations from the EDL and finally lead to positive frequency shifts (data not shown) which means an amount of mass has been lost from the interface. Results from reduced and oxidized states are in a

good agreement with the other researcher's work [3, 55-57]. Figure 5.22(b) demonstrates the schematic of this state.

5.5 Conclusion

Investigation of drug molecules interaction with the surface of conducting polymers has not been fully developed before. Whereas, application of conducting polymers for centralized drug delivery have been enlarged in the recent decades. This study demonstrates the affinity of lacosamide which is an anti-epilepsy drug to the surface of polypyrrole doped with PSS, *p*TS, CS and DBSA counterions. At non-stimulated state the maximum interaction between drug molecules and conducting polymer surface belongs to polypyrrole doped with PSS and then followed by *p*TS, CS and DBSA. Surface roughness and surface wettability of the conducting polymer films are two effective factors on the adsorption of drug molecules to the surface at non-stimulated sate. The roughest surface which was PPy/PSS entrapped much more LCM molecules. The thickness of deposited polymer layer does not have any influence on the interaction of lacosamide molecules to the conducting polymer surfaces.

Applying reducing voltage caused a mass absorption which is due to ion movement between EDL and ACSF as solvent. However, introduction of LCM/ACSF solution leaded to disruption of the stable EDL and a mass lost will happen. The repulsion effect between hydrophobic head of lacosamide molecules and hydrophobic nature of conducting polymer film surfaces at reduced state plays an important role at this stage. Goniometry results approved the more hydrophobic nature of conducting polymer surfaces at the final step of applying negative voltage. Unfortunately, we cannot distinguish the amount of absorbed LCM to the surface and the amount of desorbed ions from the surface using QCM technique. Oxidation state for all of the conducting polymers exhibited lower drug interaction compared to drug interaction at passive state. At oxidized state PPy/DBSA coated quartz crystal shows the highest interaction with LCM molecules and then followed by PPy/CS, PPy/PSS and PPy/*p*TS conducting polymer films. For passive release of LCM molecules, PPy/BDSA seems to be more appropriate conducting polymer to fabricate as a drug delivery device. Although at stimulated state (oxidizing) the PPy/*p*TS illustrated

better functionality. In the other word, at oxidized state PPy/*p*TS shows the lowest interaction and this characteristic makes the PPy/*p*TS conducting polymer film more appropriate to fabricate a drug delivery device.

At the other part of the QCM study, the interaction of ACSF ions with the surface of gold coated quartz crystal at passive state has been revealed that ACSF cations and anions have interactions with the surface. For all of these ions the absorbed amount is between 15 to 35 ng cm^{-2}. Also the electrical activity of ACSF solution has been studied. Results present a hug affinity between ACSF ions and the surface of gold coated quartz crystal while applying negative voltage. Applying positive voltages exhibited a repulsion effect or ions desorption from the generated EDL at the surface of gold coated quartz crystal.

The amount of absorbed and desorbed of LCM molecules at the surface of gold coated quartz crystal is pretty much the same of absorption and desorption of ACSF to the surface. This result means that lacosamide molecules do not have any affinity to the partially charged surface. Therefore, ionic attraction and repulsion force does not play an important role in the lacosamide molecules interaction with the conducting polymer surfaces.

5.6 References

1. F Ho¨o¨k, P Brzezinski, B Kasemo, Langmuir, 1998. **14**: 729-734.
2. F Caruso,P Kingshott, J. Colloid Interface Sci, 1997. **186**: 129-140.
3. F Ho¨o¨k, Anal. Chem, 2001. **73**: 5796-5804.
4. K.K Chittur, Biomater, 1998. **19**(4-5): 357-369.
5. T.C Ta, Anal. Chem, 2000. **72**: 2627-2634.
6. B.A Cavic, M Thompson, Analyst, 1999. **124**: 1405-1420.
7. M.B Johnsson, N Edwards, K Stalgren, Langmuir, 2001. **17**: 3902-3911.
8. A.Y Kugiyama, H Takeuchi, Electroanal, 2000. **2**: 1322-1326.
9. S.K Marx, N Gratzziany, N Barness, I Liron, Biosens. Bioelectron, 2001. **16**: 239-244.
10. H.Z Peng, Y Xie, Q Nie, L Yao, Analyst, 2001. **126**: 189-194.
11. J.E Mark, *Polymer Data Handbook*. 1998: Oxford University Press.
12. Y.P Tan, H Liang, C Yao, Sensor Actuat B, 2001. **73**: 179-184.
13. S. P Yao, H Liang, C Wu, Y Nie, Anal. Sci, 2000. **16**: 211-215.
14. F.R Lack, G.W Fair, Bell Syst. Technol, 1934. **13**: 453-455.
15. M.V Voinova, B Kasemo, Biosens. Bioelectron, 2002. **17**: 835-841.
16. K.A Marx,T Warren, M Braunhut, Biotechnol. Prog, 2003. **19**: 987-999.
17. K.A Marx, Bio Macromol, 2002. **4**(5): 1009-1120.
18. S.M Reddy, J.P Lewis, T.J Vadgama, Anal. Chim. Acta, 1998. **363**: 203-213.
19. L.W Alfonta, I Throckmorton, D.J Singh, Anal. Chem, 2001. **73**: 5287-5295.
20. ZhYue, S.E. Moulton, M.J Cook, S O'Leary, G.G Wallace, Adv. Drug Deliv. Rev, 2013. **65**: 559-569.
21. J.N Barisci, C.O Too, G.G Wallace, JIM, 1998. **9**: 723-731.
22. T.W Lewise, G.G Wallace, A Mazzoldi, D De Rossi, Synt Met, 2001. **122**: 379-385.
23. A.F Quigley, B.C Thompson, S.E Moulton, M Kita, E.L Kennedy, G.M Clark, G.G Wallace, R.M.I Kapsa, Adv. Mat, 2009. **21**(43): 4393-4397.
24. B.C Thompson , S.E Moulton, R.T Richardson, G.G Wallace, Biomat, 2011. **32**: 3822-3831.
25. P.L Haigh, MRB, 1999. **34**(5): 665–672.
26. A Kaynak, MRB, 1997. **32**: 271-285.

27. P Gardner, Expert Opin. Drug Deliv., 2006. **3**(4): 479-487.
28. H Murase, H Kocure, I Fujibayashi, K Tamura, N Haruta, J. Appl. Plym. Sci, 1994. **54**: 2051-2062.
29. M.K Missirlis, J.Appl. Plym. Sci, 2004. **8**: 37-57.
30. A Gelmi, M.J Higgins, G.G Wallace, Biomat, 2010. **31**: 1974–1983.
31. R.A. McAloney, M.C Goh, Langmuir, 2003. **19**: 3947-3952.
32. G Burnie, J. Biomol. Techniques, 2008. **19**: 151-158.
33. B.C Thompson, S.E Moulton, R.T Richardson, G.G Wallace, Biomat, 2011. **32**: 3822-3831.
34. P.J Molino, B Zhang, A Tibbens, X Liu , R.M.I Kapsa , M.J Higgins , G.G Wallace, AMI, 2014. **13**: 1-12.
35. K.A Marx, Bio Macromol, 2003. **4**(5): 1109-1120.
36. K Bettina, J.F Beyreuther, C Heers, N Krebsfanger, U Scharfenecker, T Stohr, CNS Drug Review, 2007. **13**(1): 21-42.
37. M Joao, P.S Encarnacao, N.M Guilherme, Biosens. Bioelectron, 2007. **22**: 1351-1358.
38. K Rechendorff, M Foss, V.P Zhdanov, F Besenbacher, Collo. Surf. B, 2008. **66**: 53-59.
39. K Rechendorff, Langmuir, 2006. **22**: 10885-10888.
40. L.D Urbakh, Langmuir, 1996. **12**: 6354-6360.
41. K.K G Kanazawa, Anal. Chim. Acta, 1985. **175**: 99-105.
42. H.T Muramatsu, E Karube, Anal. Chem, 1988. **60**: 2142-2150.
43. J.M. Encarnacao, P.S Guilherme, N.M Ferreira, Biosens. Bioelectron, 2007. **22**: 1351-1358.
44. C.K Fredriksson, S Rodahl, M Kasemo, Langmuir, 1998. **14**: 248-251.
45. M.H Rodahl, F Krozer, A Brzenzinski, P Kasemo, Rev. Sci. Instrum, 1995. **66**: 3924-3930.
46. T.O Nomura, Anal. Chim. Acta, 1982. **142**: 281-284.

6 CONCLUSION AND FUTURE WORK

6.1 Flat composite membrane fabrication, characterization and drug transport study

The aim of this section of the thesis was investigating transport of anti-epilepsy drug through conducting polymer coated Pt/PVDF flat and tube membranes. Transport study experiments have been conducted at stimulated (constant and pulsed potential), and non-stimulated states.

In Chapter 3 work was undertaken to optimise the transport of the drug lacosamide through a flat PVDF membrane that was coated in polypyrrole (PPy). A variety of dopants including DS, HA, *p*TS, DBSA, PSS and CS were used to synthesise PPy on the surface of platinised PVDF flat membranes. Different electropolymerization conditions were applied to deposit the polymer layer. Cyclic voltammograms (CV) characterisation of these conducting polymer films revealed that PPy/*p*TS, PPy/DBSA, PPy/PSS and PPy/CS exhibited more appropriate redox switching property in comparison with PPy/DS and PPy/HA coated membranes. SEM images and water flux results showed that coating a platinum layer on the surface of PVDF flat membrane decreases the porosity and water flux. In addition, electropolymerization of conducting polymer decreased the porosity and water flux with different dopants having different effects on the porosity and water flux properties. PPy/*p*TS coated Pf/PVDF membrane showed the maximum water flux followed by PPy/CS, PPy/DS, PPy/HA, PPy/DBSA and PPy/PSS. There was no discernible difference in the water flux of PPy/DS and PPy/HA.

After fabrication and characterization of PPy coated flat Pt/PVDF membranes, drug transport studies through these membranes were conducted. All of the composite membranes showed drug transport under passive (at non-stimulated) state. Maximum drug transport at this state was seen for PPy/CS followed by PPy/BDSA. The concentration of drug transport for these two composite membranes is about 8 times higher than the concentration of drug transport for PPy/*p*TS. PPy/PSS did not show any drug transport under non-stimulated state.

For all of these PPy membranes, transport under a stimulated reduced state is higher than drug transport at an oxidized state. Concentration of transported drug at reduced state for PPy/CS coated Pt/PVDF membrane is the highest followed by PPy/*p*TS, PPy/DBSA and PPy/PSS. The PPy/PSS coated membrane demonstrated the greatest difference in transported drug concentration between the reduced and oxidized state. For this composite membrane at oxidized state no drug transport was seen while 10.05±0.65 μg/ml LCM molecule transported through this membrane at reduced state. PPy/CS coated membrane showed 2.5 time difference between concentration of transported drug at reduced and oxidized states. This difference for PPy/*p*TS is 2 times and for PPy/DBSA is 1.5 times.

6.2 Tube composite membrane fabrication, characterization and drug transport study

Chapter 4 presented fabrication and characterization of PPy coted tube membranes. *p*TS, DBSA, CS and PSS were four dopants used in the synthesis of PPy on the surface of Pt/PVDF tube membranes. Cyclic voltammograms of these conducting polymer coted tube membranes showed that PPy/CS and PPy/PSS possessed the more ideal redox properties. SEM images of the surface of these conducting polymer coated membranes exhibited the porous structure. In addition, cross-section images of these membranes showed the formation of PPy layer on the outer surface of these membranes.

After fabrication and characterization studies, drug transport was investigated through tube membranes. The aim of using a tube PVDF membrane was in order to use the inner tube space as a reservoir in which drug could be stored. PPy/*p*TS, PPy/DBSA, PPy/PSS and PPy/CS were deposited on the outer surface of Pt/PVDF tube membranes. Among these conducting polymers, PPy/CS and PPy/PSS exhibited better redox properties. Therefore, PPy/CS and PPy/PSS were chosen for drug release studies. The concentration of release lacosamide at a PPy reduced state was higher than in the oxidized state. In addition, PPy/CS possesses the higher drug release concentration than PPy/PSS at stimulated state.

Pulsed potential drug release studies were investigated for these tube membranes. The aim of conducting this experiment was achieving an on/off drug release profile. Switching between fully reduced and fully oxidized states for each conducting polymer coated tube membrane led to have on/off LCM transport. The fully reduced and fully oxidized voltages were chosen according to the LCM transport studies by applying single voltages. Similar to the stimulated release studies, PPy/CS showed more sufficient results than PPy/PSS at pulsed potential state.

6.3 Interaction of drug molecules with the surface of conducting polymers

The affinity of drug molecules to the surface of conducting polymer has been considered in Chapter 5. The attachment of drug molecules to the surface of conducting polymer coated composite membranes is an effective factor on the amount of drug transport through these membranes. To investigate the interaction of lacosamide molecules and PPy/*p*TS, PPy/DBSA, PPy/CS and PPy/PSS, the QCM technique has been utilized. Interaction studies were conducted at non-stimulated and stimulated states. At non-stimulated state the maximum interaction was observed with PPy/PSS and then followed by PPy/*p*TS, PPy/CS and PPy/DBSA. Surface roughness and wettability are two important properties of conducting polymer films which can effect on the mass of adsorbed lacosamide.

6.4 Future work

Throughout this thesis it has been successfully showed that the release of an anti-epilepsy drug across the polypyrrole coated Pt/PVDF membranes can be controlled upon an external electrical stimulation. The shape of membrane played an important role on having an on/off release profile. The tube shape membrane exhibited the satisfactory response to pulsed potential stimulation. However, the concept of this project is fabricating and characterizing of an implantable device for in-vivo application for the treatment of epilepsy. To achieve this goal, some key issues need to be considered. In this section some suggestion to fabricate an implantable device

which is able to deliver anti-epilepsy drug directly to the brain tissue and also record the EEG signals of the brain will be presented.

Before presenting the idea of fabricating implantable device, it is worthwhile to highlight that there is a potential to investigate release of the mixture of anti-epilepsy drugs across flat and tube polypyrrole coated membranes. A mixture of charged and neutral anti-epilepsy molecules can be encapsulated within tube membranes, and also in the feed side of the transport cell to investigate transport of them through flat membranes. In this case the polarity of applied voltage can interact with the molecule charge and effect on the transport profile of drug molecules.

6.4.1 Two electrode stimulation implantable device

As the last part of the Chapter 4 presented, applying the pulsed facilitated an on/off release profile of lacosamide. However, the three electrode set up which had been utilized to investigate drug release is not implantable. By changing the three electrodes set up to two electrodes set up the aim of implanting this drug carrier into the brain tissue is more possible.

As Figure 6.1 presents the auxiliary electrode is placed inside of the polypyrrole coated Pt/tube. Similar to the PPy coated Pt/PVDF tubes, the outer surface of this tube can be coated by PPy. This device can play the role of drug carrier, and also operates as a gating system.

The surface of this tube which is coated with conducting polymer plays the role of working electrode and CP coated Pt/IrO_2 can be connected to the e-DAQ system as an auxiliary electrode. The stimulation of this system is conducted with similar protocols which have been utilized through this thesis.

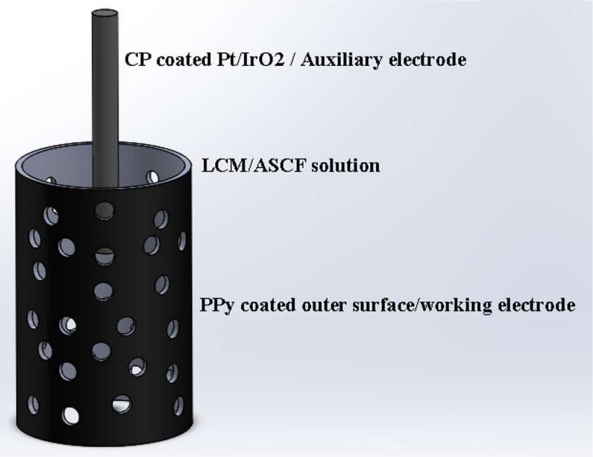

Figure 6.1 Two electrodes system.

The inside electrode can be a Pt/IrO_2 microelectrode. Iridium oxide (IrO_2) is a biocompatible metallic oxide film. According to the literature[1, 2], IrO_2 electrode possesses low impedance and high charge storage capacity. These features of this electrode provide the opportunity to utilized IrO_2 or Pt/IrO_2 as a superior candidate for recording of EEGs. To measure the neural signals, the key strategy is decreasing the impedance[2]. In addition, IrO_2 is suitable in cases when an electrical stimulation is needed due to its electroactivity[3, 4]. The redox kinetics on the surface of this electrode is fast. By fixing the impedance, the electrode will stay at that value until application of a new voltage. This process is fully reversible[4].

6.5 References

1. S.F Cogan, Annu. Rev. Biomed. Eng., 2008. **10**: p. 275–309.
2. M.B.A Fontes, Journal of Physics: Conference Series, 2013. **421**: p. 012019.
3. R.D Meyer, T.H Nguyen, R.D Rauh, Neural Systems Rehab. Eng., 2001. **9**(1): p. 2-11.
4. J.D Weiland, Biomed. Eng, 2000. **47**: p. 911–918.

Appendix A; list of publications currently being prepared arising from this Thesis

1) *"Development and Validation of a Seizure Initiated Drug Delivery System for the Treatment of Epilepsy"* Rikky Muller, Sara Ahmadi, Winston Ng, Zhilian Yue, Willo M. Grosse, Mark J. Cook,Gordon G.Wallace and Simon E. Moulton

2) *"Investigating Drug Interaction with the Conducting Polymer Films using Quartz Crystal Microbalance"* Sara Ahmadi, Paul J. Molino, Mark J. Cook, Gordon G. Wallace and Simon E. Moulton

3) *"Tube PVDF membrane carriers for anti-epilepsy treatment studies"* Sara Ahmadi, Simon E. Moulton, Mark J. Cook, Gordon G. Wallace

4) *"Study Transport of an anti-epilepsy drug through conducting polymer coated platinised PVDF membrane"* Sara Ahmadi, Simon E. Moulton, Mark J. Cook, Gordon G. Wallace